CONANTOKIN PEPTIDES: STRUCTURE, FUNCTION, AND USE TO DEFINE NMDA RECEPTOR SUBTYPES IN LIVE NEURONS

by

Kigen James Curtice

A dissertation submitted to the faculty of
The University of Utah
in partial fulfillment of the requirements for the degree of

Doctor of Philosophy

Department of Biology

The University of Utah

December 2014

The University of Utah Graduate School

STATEMENT OF DISSERTATION APPROVAL

The dissertation of **Kigen James Curtice**

has been approved by the following supervisory committee members:

Martin P. Horvath	, Chair	**8/8/2014** Date Approved
Baldomero M. Olivera	, Member	**8/8/2014** Date Approved
David P. Goldenberg	, Member	**8/8/2014** Date Approved
David F. Blair	, Member	**8/8/2014** Date Approved
Christopher P. Hill	, Member	**8/11/2014** Date Approved

and by **M. Denise Dearing** , Chair/Dean of

the Department/College/School of **Biology**

and by David B. Kieda, Dean of The Graduate School.

ABSTRACT

N-methyl-D-aspartate receptors (NMDARs) are vital components of the mammalian nervous system that intimately contribute to excitatory neurotransmission. Learning, memory formation, synaptic plasticity, and many neurodegenerative diseases are linked with NMDARs. In order to study these processes, there is need for scientific tools that can be used to examine NMDARs.

Cone snail venom is a mixture of neurotoxins with specific targets in the nervous system. Conantokins are a family of conotoxin that inhibit NMDARs and can select for different NMDAR subtypes. Therefore, understanding mechanisms of conantokin selectivity and using selective conantokins as tools to identify NMDAR subtypes in the brain are important advancements for neurobiology.

In this dissertation, Chapters 2 and 3 describe structural studies of conantokin *Bk*-B (con*Bk*-B) and of conantokin *Rl*-B (con*Rl*-B). These conantokins exhibited novel NMDAR subtype selectivities and were consequently of interest for structural characterization. The ultra-short con*Bk*-B was found to adopt helical conformation similar to that observed in other conantokins. Con*Rl*-B was found to be a kinked helix that is unique among structurally characterized conantokins. Comparison of conantokin structures, paired with mutational analysis, highlighted that residues 5, 6, 8, and 10 determine subtype selectivity in conantokins.

Chapter 4 describes biochemical studies of NMDAR ligand-binding domain (LBD) proteins for the NR1-2b, NR2A, NR2B, and NR2C NMDAR subtypes. Limited proteolysis

assays showed agonist binding, indicating LBD proteins were correctly folded. Additional experiments found no strong interactions between LBD proteins and conantokins. The results suggest that additional protein domains, heteromeric NMDARs, or neuronal membranes may be required for conantokin-NMDAR binding.

In Chapter 5, conantokins are used to define the NMDAR subtypes in neurons from mouse cerebellum. Agonist challenge assays revealed diversity in cerebellar neurons, and conantokin *R*-B was used to show NR2B NMDAR subtypes in cerebellar neurons of young mice. In older mice, a population of neurons with non-NR2B NMDARs was discovered. This dissertation demonstrates the first use of conantokins to define NMDAR subtypes in live neurons, provides a foundation for understanding neuronal diversity in the brain, and establishes NMDAR subtype composition in individual neurons of the developing cerebellum.

Dedicated to my friends and family. Thank you for support, encouragement, compassion, understanding, and love.

TABLE OF CONTENTS

LIST OF FIGURES

LIST OF TABLES

ACKNOWLEDGMENTS

The work described herein could not have been realized without aide from numerous faculty and students. Foremost I would like to acknowledge my advisors, Martin P. Horvath and Baldomero M. Olivera, for pushing me to think deeper, providing project guidance, and facilitating opportunities that have allowed me to develop as a scientist and educator. My committee members, David F. Blair, David Goldenberg, and Christopher P. Hill were instrumental in helping me define a research path. I additionally thank David Goldenberg for contributing to my first research experiences and providing me with a solid foundation in biochemistry. Dr. Jack Skalicky taught me practical aspects of NMR and provided assistance with structure determination presented in Chapters 2 and 3. Millie Boyd, Ty Daly, Tiffanie Hales, Dima Hurlbut, Larry Whiting, and Sierra Wilen, performed the majority of cloning work for NMDA receptor derived proteins described in Chapter 4. Tiffani Erickson was tireless in optimizing protein expression conditions described in Chapter 4. Shrinivasan Raghuraman and Russell W. Teichert are acknowledged for the development of constellation pharmacology techniques that are a keystone of Chapter 5. Lee Leavitt and Tyler Harris contributed to data collection and implementation of R programming presented in Chapter 5. Kevin Chase wrote the R programs for analysis of constellation pharmacology data presented in Chapter 5. I recognize my friends for their encouragement in pursuing a doctorate. I thank Viktoriya Kobylkina for her emotional support and for being the greatest companion. And finally, I acknowledge my family for their continuous support and compassion over the last 31 years.

CHAPTER 1

BACKGROUND AND INTRODUCTION

Cone snails and their venom

Cone snails of the genus *Conus* are venomous predators that live throughout oceans of the world. There are over 500 species of cone snail, which are classified into three diverse groups that prey on fish, snails, or worms. Cone snails capture and paralyze prey by injection of venom through a harpoon-like structure called the radula. The venom is a complex mixture of peptide-neurotoxins called conotoxins. In prey, molecular interactions between conotoxins and proteins of the nervous system disrupt communication between neurons and from neurons to muscles. The net result of envenomation by *Conus* snails is rapid and complete paralysis, which allows snails to engulf their prey.

Cone snails can also use their venom defensively, and human envenomation by cone snails has been documented multiple times. Stings from cone snails cause severe neurological effects that include pain, paralysis, visual impairment, difficulty breathing, and sometimes death[1]. The first documented observation of human envenomation by a cone snail was described in 1848[2], and additional occurrences of human envenomation led to interest in understanding cone snail venom. By the middle of the 20th century, cone snail anatomy and mechanisms of venom injection were well understood[3]. However, little was known about the molecular components of *Conus* venom.

Early research into the molecular nature of *Conus* venom examined effects of venom injection on animals and explored experimental treatments of crude venom. In a seminal paper from 1960, Kohn, Saunders, and Wiener noted that *Conus* venom was made of proteins, had multiple components, and that venom composition varied across cone snail species[4]. These findings fueled increased interest in *Conus* venom and by the 1980s several neurotoxic peptides that generated unique behaviors in animal assays had been characterized.

Conotoxins from *Conus geographus* were the first to be purified to homogeneity and characterized both structurally and biochemically[5,6]. The conotoxins were found to act on ion channels of the nervous system and some could discriminate between isoforms of highly similar ion channels[7]. Use of conotoxins to study the nervous system garnered much attention and a systematic approach to classifying new toxins was adopted[8].

Conotoxins

Conotoxins disrupt function of the nervous system via specific interactions with numerous transmembrane proteins that participate in neurotransmission. The potency and selectivity of conotoxins has fostered development of *Conus* peptides as scientific tools and medicines. Many conotoxins are thoroughly characterized, and the major conotoxin families continue to grow as venoms from new *Conus* species are explored[9-11]. An overview of select conotoxin families, known molecular targets, and proposed mechanisms of action are shown in Table 1.1, illustrating the diversity of neurotoxic peptide families found in *Conus* venoms.

Conotoxin composition varies among cone snail species, and collectively the genus *Conus* is believed to produce over 100,000 unique neuro-active peptides[11]. This vast pool of neurotoxins and the observation that many conotoxins are highly selective for targets in the nervous system intimates usefulness to study ion channels of the nervous system and suggests that some conotoxins may have medicinal value[12].

Table 1.1: Major conotoxin families

Conotoxin	Target	Mechanism
α-conotoxins	Nicotinic acetylcholine receptors	Competitive antagonism
μ-conotoxins	Sodium channels	Pore blocker
∂-conotoxins	Sodium channels	Inhibits inactivation
ι-conotoxins	Sodium channels	Enhances inactivation
κM-conotoxins	Potassium channels	Pore blocker
ω-conotoxins	Calcium channels	Pore blocker
Conantokins	N-methyl-D-aspartate receptors	Competitive antagonism

Many conotoxins are shown to have therapeutic benefits in mice and some have reached human clinical trials for the treatment of neuropathologies ranging from pain to epilepsy[11,13-17]. Of note, the ω-conotoxin MVIIA is FDA approved and marketed as Ziconotide, Prialt® for the treatment of severe, neuropathic pain[18,19]. The development of ω-conotoxin MVIIA into a medicine illustrates that exploration of *Conus* venoms can lead to discovery of novel medications.

In addition to medicinal use, conotoxins are suitable tools for examining the molecular, cellular, and functional details of the nervous system. For example, α-conotoxins, which specifically inhibit nicotinic acetylcholine receptors (nAChRs), have played a crucial role in understanding nAChR form and function[20,21]. Many α-conotoxins can distinguish among different nAChR isoforms and, for this reason, can be used to study cholinergic innervation of the nervous system[22-25]. Some examples of α-conotoxin use include mapping of subunit interfaces in nAChRs[26], defining composition of nAChRs in live neurons[27], and examining the physiological role of nAChRs in the mammalian nervous system[28-30]. Additionally, similar progress has been made towards understanding the structure and function of voltage gated sodium channels[31-33] and voltage gated calcium channels[34,35], which can be studied using μ-conotoxins and ω-conotoxins, respectively.

Similar to the examples above, conantokins are a family of conotoxin with tremendous potential for examining molecular and cellular details of the nervous system. Conantokins inhibit N-methyl-D-aspartate (NMDA) type glutamate receptors and can have selectivity for various receptor isoforms[36-38]. Therefore, conantokins can be used to study NMDA receptor (NMDAR) form and function in the nervous system. NMDARs are excitatory ion channels that contribute to various neurological and physiological processes such as long-term potentiation, synaptic plasticity, learning, and memory[39-42]. Additionally, evidence suggests that NMDARs are involved in many neurodegenerative diseases that involve calcium toxicity[42]. Hence, in addition to utility for studying NMDARs, conantokins could be developed into medicines for future treatment of NMDAR-associated nervous system disorders.

NMDARs of the mammalian nervous system

NMDARs are part of the glutamate receptor superfamily of ligand-gated and G protein-coupled transmembrane protein receptors that respond to the neurotransmitter glutamate. Glutamate is the most abundant excitatory neurotransmitter in the mammalian nervous system, and glutamatergic synapses can contain multiple types of glutamate receptors. These include receptors that open an ion channel, the ionotropic glutamate receptors, and receptors that initiate intracellular signaling through G proteins, the metabotropic glutamate receptors [43]. Three families of ionotropic glutamate receptors are well characterized; the α-Amino-3-hydroxy-5-methyl-4-isoxazolepropionic acid receptors (AMPARs); the kainate receptors (KARs); and the NMDARs[43,44]. Although AMPARs, KARs, and NMDARs all respond to the agonist glutamate, they exhibit distinctive kinetic properties, have different requirements for activation, and are likely to have unique

physiological functions[45]. This dissertation focuses on NMDARs, which are of utmost interest due to a central physiological role and an interaction with conantokin peptides from *Conus* venom.

The NMDA type glutamate receptor is a tetrameric, transmembrane protein complex that is assembled from at least two gene products. In mammals, many NMDAR subtypes are found that differ in subunit composition. Diversity in mammalian NMDARs arises from differential assembly of NR1 subunits (with eight splice variants), NR2 subunits (with four homologous genes), and NR3 subunits (with 2 homologous genes)[44,46-48]. The NMDAR subunits found in mammals are shown in Figure 1.1, panel A.

Functional NMDAR tetramers have two obligatory NR1 subunits and a combination of NR2 and/or NR3 subunits[49]. The most commonly studied NMDAR is a diheteromeric assembly consisting of one NR1 variant and one NR2 variant. Examples of diheteromeric NMDARs are shown in Figure 1.1, panel B. However, it is evident that more complex triheteromeric assemblies are present *in vivo* (e.g., $NR1_2$/NR2A/NR2B)[50-53]. Examples of triheteromeric NMDARs are shown in Figure 1.1, panel C. Ultimately, there is extreme diversity in tetrameric NMDAR subtypes that can be generated from differential assembly of NMDAR subunits.

The diversity of possible NMDAR tetramers generates many questions. Which subtypes are present in real neurons? What is the physiological role of each subtype? Do individual neurons express one, or many subtypes? How are these subtypes distributed in the brain? However, technical limitations make identification of exact NMDAR subunit combinations difficult. Nonetheless, a variety of NMDAR subtypes have been positively identified in mammalian neurons.

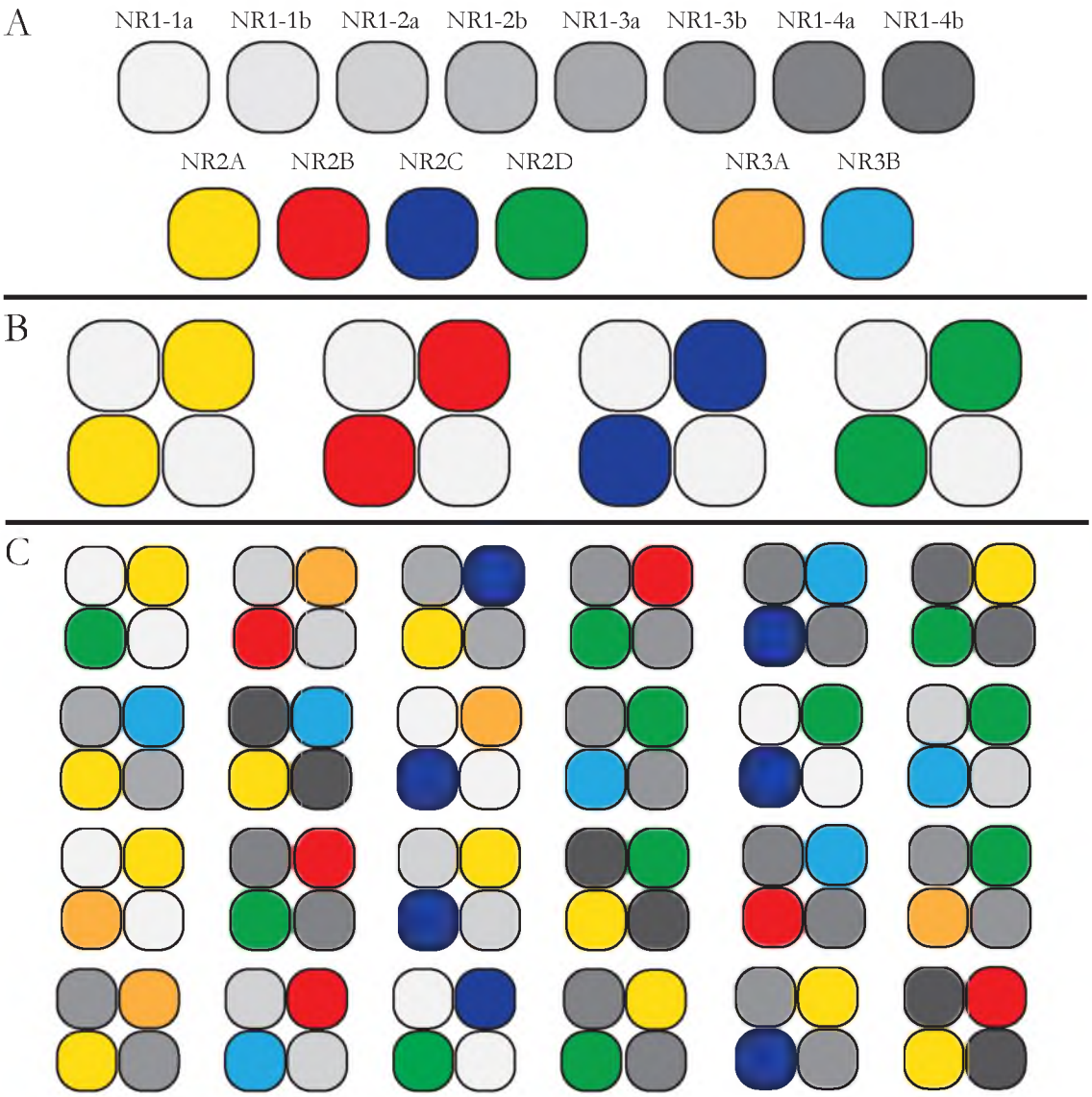

Figure 1.1: Diversity of potential NMDAR subtypes. A: Eight splice variants of NR1, four homologous NR2 genes, and two homologous NR3 genes encode the NMDA receptor subunits in mammals. **B:** Examples of diheteromeric receptors assembled from NR1-1a and the four NR2 gene products. **C:** Examples of triheteromeric receptors assembled from combinations of NR2 and NR3 paired with NR1 splice variants.

Diheteromeric NMDARs are the most intensely studied subtype in heterologous systems due to ease of data analysis. *In vivo,* however, evidence suggests that diheteromeric receptors often coexist with triheteromeric receptors, and in some cases triheteromeric receptors are most prevalent[54-57]. For example, $NR1_2$/NR2A/NR2B triheteromeric receptors are the predominant NMDAR in the hippocampus and other regions of the central nervous system[51-53]. Also, $NR1_2$/NR2B/NR2D triheteromers are found in dopaminergic neurons of the substantia nigra[58]. Intriguingly, the triheteromeric receptors have unique functional properties compared to diheteromeric receptors, which implicates unique physiological roles for each NMDAR subtype[59,60]. Adding to the complexity, NR3 subunits also co-assemble with NR2 or other NR3 subunits, creating yet another set of functionally unique NMDAR subtypes[61-63].

In addition to organizational complexity, NMDARs also have a high degree of complexity for receptor activation and regulation at the molecular level. In $NR1_2$/$NR2_2$ diheteromeric NMDA receptors, opening of the ion-channel requires the co-agonists glutamate and glycine, together with membrane depolarization that removes a magnesium ion block of the ion-channel pore[64,65]. In triheteromeric receptors, such as a $NR1_2$/$NR2_1$/$NR3_1$ combination, activation is influenced more strongly by glycine because glycine is an agonist of the NR3 subunit[61,62]. Beyond basic activation requirements, many molecules modulate NMDAR function, and these generally interact with the extracellular amino-terminal domain (ATD). For example, zinc binds the ATD and is a potent inhibitor of most NMDA receptor subtypes[66-68], especially those containing NR2A[69] and NR2B[70] subunits. Additionally, polyamines such as spermine and spermidine influence NDMAR activation through interaction with the ATD[71-73]. Also, protons can antagonize NMDARs via interactions with the ATD[74-76]. All together, NMDARs are complex assemblies of four

protein subunits that behave in a dynamic and regulated manner, which implies that NMDARs have complex functions in neurotransmission.

Recently, major advances have been made in understanding the atomic structures of NMDA receptors and determining molecular features that confer functions such as voltage sensitivity and regulation of receptor activity. Examples include, a crystal structure of the ligand-binding domain (LBD) from NR1 that revealed a clamshell-like mechanism of ligand binding[77]. The crystal structure of a NR1-NR2A LBD heterodimer, which illustrated a partial subunit interface[78]. The structure of the NR2B ATD that showed binding sites for various regulatory molecules[79]. Finally, the ATD NR1-NR2B dimer, which revealed additional subunit interfaces and regulator binding sites important for NMDAR modulation. Although these and additional structures[80-82] have led to many novel discoveries, the most influential structure will be that of the recently published NMDAR tetramer, which divulged all subunit interfaces and domains of the NMDAR including the ATD, LBD, and transmembrane domain (TMD)[83]. Figure 1.2 depicts this NMDAR tetramer (PDB id: 4PE5) and highlights regions that are important for activation, inhibition, and modulation of NMDARs.

NMDARs have critical roles in nervous system development, synaptic plasticity, learning, and memory, and are implicated in a variety of disease states such as Alzheimer's, Parkinson's, multiple sclerosis, and epilepsy[42,84-89]. The mammalian nervous system contains many NMDAR subtypes and little is understood on how each subtype contributes to nervous system development, function, and disease[39,42,78,85,90,91]. In order to study the form and function of NMDAR subtypes in the mammalian nervous system, pharmacological tools that are selective for the various NMDAR subtypes are necessary. Fortunately, conantokin peptides from *Conus* venoms provide an avenue for that discovery and development of tools that can be used to study NMDARs.

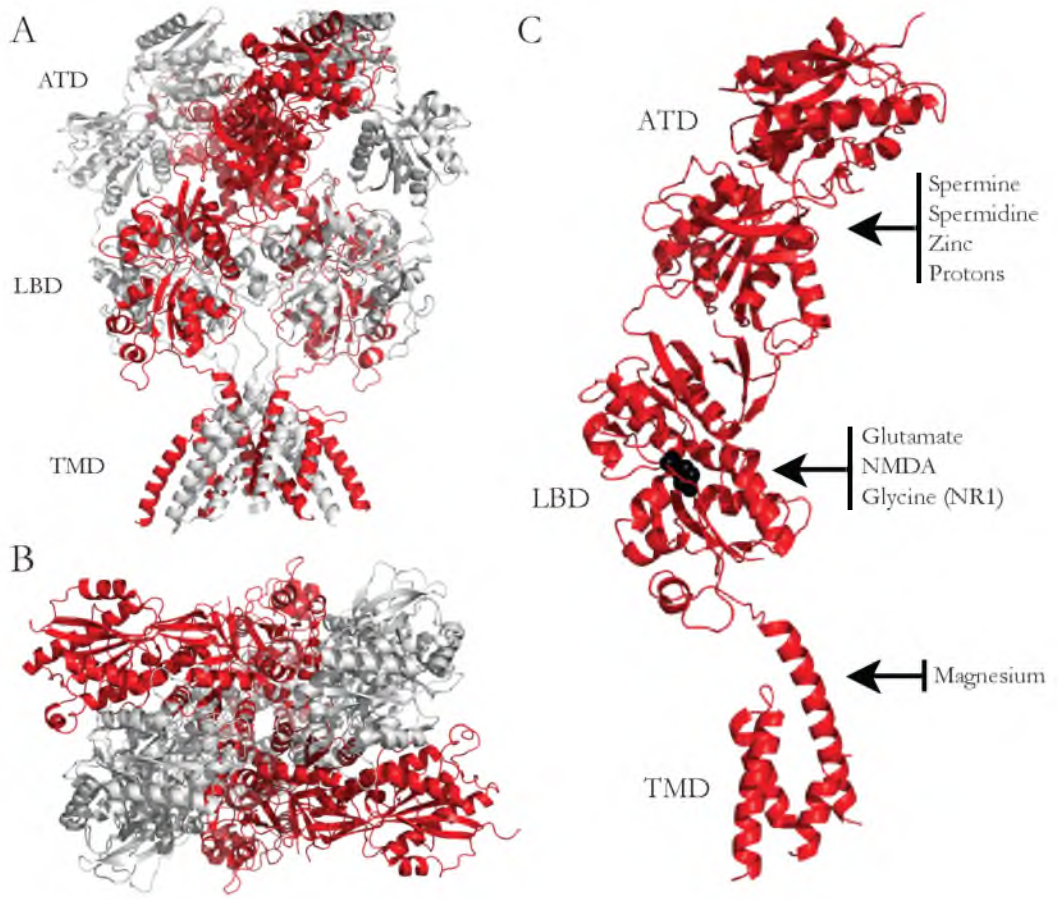

Figure 1.2: NMDAR structure. A: Horizontal view of a NMDAR tetramer containing two NR1 (grey) and two NR2B (red) subunits shown as a cartoon. (PDB id: 4PE5). Locations of the amino-terminal domain (ATD), ligand-binding domain (LBD) and transmembrane domain (TMD) are shown. **B:** Top-down view of the NMDAR tetramer, ATD in foreground, illustrating the central ion-channel pore. **C:** A single NR2B subunit shows domain organization in NMDAR subunits. Biologically relevant modulators and agonists are listed next to the domains that they bind. Glutamate (black spheres) is shown bound to the LBD.

Conantokin peptides

Conantokins are peptide-toxins found in *Conus* venom that inhibit NMDAR activation. Generally 9-30 residues in length and rich in γ-carboxyglutamate (Gla) residues, conantokins adopt a helical conformation by coordination of divalent cations via gla residues. Conantokin-G (conG) from *Conus geographus* was the first conantokin to be discovered and was found to induce sleep in young mice and hyperactivity in old mice upon intracerebral injection[92]. Searches for additional conantokins led to identification of

conantokin-T (conT) from *Conus tulipa*[93], and both conG and conT were found to inhibit activation of NMDARs in cultured neurons from rat[93,94]. Conantokin inhibition of NMDARs was then illustrated in a more controlled setting by using heterologously expressed NMDARs in *Xenopus* oocytes[95]. The selectivity of conantokins for different NMDAR subtypes was revealed by comparison of conG to AP5, which is a broad-spectrum NMDAR NMDA antagonist[96].

Among conotoxins, which are generally cysteine rich and disulfide bond stabilized, conantokins are unique because they contain few cysteine residues, but many gla residues. Because of this, structural analysis has been a priority for conantokin researchers. NMR spectroscopy and circular dichroism (CD) studies indicate that conG and conT interact with calcium ions, which causes increased peptide helicity[97]. Furthermore, calcium-stabilized helical structures of conG and conT have been determined by NMR spectroscopy[98-100]. These studies and others show that gla residues stabilize a helical conformation by coordinating calcium ions, which results in alignment of gla residues on a single helical face[101-105]. Interestingly, calcium-chelating agents have little effect on conantokin inhibition of NMDARs[106,107]. This finding suggests that conantokins do not need helical structure to inhibit NMDARs, or that the conantokin-NMDAR interactions independently stabilize helical structure.

Two mechanisms have been proposed to describe mechanisms for conantokin inhibition of NMDARs. Some evidence indicates that conantokins act competitively near the glutamate-binding site on the LBD[95]. Other observations suggest conantokins interact near the spermine-binding site on the ATD[108,109]. However, neither of these mechanisms has been conclusively proven, and it may be the case that conantokins have more complex interactions with multiple domains of the NMDAR.

Conantokins as tools to study NMDARs

Conantokins that are selective for single NMDAR subtypes can be used as tools to examine the NMDARs in the nervous system. This dissertation aims to advance our understanding of conantokin peptides and NMDA receptors in three major ways. First, novel conantokins with unique subtype selectivities are described, which shows that conantokins with new selective properties can be found through exploration of *Conus* venoms. Second, structural studies on conantokin peptides illustrate the molecular determinants of selectivity, which will enable discovery and development of increasingly selective conantokins. Third, conantokin peptides are used to define NMDAR subtypes in live neurons, which proves that conantokins are useful tools for understanding NMDARs of the nervous system.

Summary of this dissertation

This dissertation examines conantokin peptides at many levels. The experiments described herein include structural studies that reveal atomic details of conantokins, biochemical studies to examine conantokin-NMDAR binding, and calcium imaging studies that use conantokins to define NMDAR subtypes in living neurons.

In Chapter 2, the discovery and characterization of novel conantokins from *Conus bocki* are described. These were the first conantokins to show preference for NMDARs containing the NR2D subunit. Additionally, con*Bk*-B from *bocki* was found to be the shortest naturally occurring conantokin described to date (9 residues) and the NMR solution structure of con*Bk*-B was presented.

Chapter 3 describes the NMR solution structure of con*Rl*-B, a recently discovered and ultra-selective conantokin from *Conus rolani*. Con*Rl*-B shows greater than 100-fold

selectivity for NMDA receptors containing the NR2B subunit[110]. The NMR structure of con*R*I-B showed a distinct kinked-helix conformation that is unique among structurally characterized conantokins.

Chapter 4 describes the cloning, expression, purification, and examination of soluble NMDAR LBD protein constructs. These proteins were analyzed biochemically for ligand binding and conantokin binding. The results show that the LBD proteins bind to cognate ligands, but no evidence was found for conantokin binding. In the context of other work, the results indicate that NMDAR LBD monomers are not sufficient for conantokin binding.

Chapter 5 illustrates the first use of conantokins to define NMDAR composition in live neurons cultured from the cerebellum of mouse. Agonist challenge assays paired with calcium imaging revealed the frequency of glutamatergic and cholinergic neurons in mouse cerebellar neurons. Additionally, conantokin con*R*I-B was used to identify NR2B NMDAR subtypes in all cerebellar neurons of young mice, and a population of non-NR2B NMDAR subtypes in a subset of neurons from older mice.

As a whole, this work takes the appropriate steps towards understanding mechanisms of subtype selectivity in conantokins, shows that conantokins with novel properties can be discovered by examining venoms from new *Conus* species, and illustrates the first use of conantokins to define NMDAR subtypes in neurons of the mammalian nervous system. These advancements will aid future neurobiologists in understanding the physiological role of NMDARs in the mammalian nervous system.

References

1 McIntosh, J. M. & Jones, R. M. Cone venom–from accidental stings to deliberate injection. *Toxicon* **39**, 1447-1451 (2001).

2 Adams, A. Narrative of the Voyage of H.M.S. Samarang. **2**, 356-357 (1848).

3 Hermitte, L. C. D. Venomous marine mollusks of the genus *Conus*. *Transactions of the Royal Society of Tropical Medicine & Hygiene* **39**, 485-512 (1946).

4 Kohn, A. J., Saunders, P. R. & Wiener, S. Preliminary studies on the venom of the marine snail *Conus*. *Annals of the New York Academy of Sciences* **90**, 706-725 (1960).

5 Clark, C., Olivera, B. M. & Cruz, L. J. A toxin from the venom of the marine snail *Conus geographus* which acts on the vertebrate central nervous system. *Toxicon* **19**, 691-699 (1981).

6 Cruz, L. J., Hunkapiller, M. W., Gray, W. R. & Olivera, B. M. Isolation and structure of a peptide toxin from the marine snail *Conus magus*. *Archives of Biochemistry and Biophysics* **218**, 329-334 (1982).

7 Cruz, L. J. *et al.* *Conus geographus* toxins that discriminate between neuronal and muscle sodium channels. *Journal of Biological Chemistry* **5**, 9280-9288 (1985).

8 Gray, W. R., Olivera, B. M. & Cruz, L. J. Peptide toxins from venomous *Conus* snails. *Annual Review of Biochemistry* **57**, 665-700 (1988).

9 Becker, S. & Terlau, H. Toxins from cone snails: properties, applications and biotechnological production. *Applied Microbiology and Biotechnology* **79**, 1-9 (2008).

10 Olivera, B. M. *Conus* peptides: biodiversity-based discovery and exogenomics. *Journal of Biological Chemistry* **281**, 31173-31177 (2006).

11 Olivera, B. M. & Teichert, R. W. Diversity of the neurotoxic *Conus* peptides: a model for concerted pharmacological discovery. *Molecular Interventions* **7**, 251-260 (2007).

12 Lewis, R. J. & Garcia, M. L. Therapeutic potential of venom peptides. *Nature Reviews Drug Discovery* **2**, 790-802 (2003).

13 Barton, M. E. & White, H. S. The effect of CGX-1007 and CI-1041, novel NMDA receptor antagonists, on kindling acquisition and expression. *Epilepsy Research* **59**, 1-12 (2004).

14 Livett, B. G. *et al.* Therapeutic applications of conotoxins that target the neuronal nicotinic acetylcholine receptor. *Toxicon* **48**, 810-829 (2006).

15 Satkunanathan, N. *et al.* Alpha-conotoxin Vc1.1 alleviates neuropathic pain and accelerates functional recovery of injured neurones. *Brain Research* **1059**, 149-158 (2005).

16 Smith, M. T., Cabot, P. J., Ross, F. B., Robertson, A. D. & Lewis, R. J. The novel N-type calcium channel blocker, AM336, produces potent dose-dependent antinociception after intrathecal dosing in rats and inhibits substance P release in rat spinal cord slices. *Pain* **96**, 119-127 (2002).

17 Zhang, M. M., Green, B. R., Catlin, P. & Fiedler, B. Structure/function characterization of μ-conotoxin KIIIA, an analgesic, nearly irreversible blocker of mammalian neuronal sodium channels. *Journal of Biological Chemistry* **282**, 30699-30706 (2007).

18 Mathur, V. S. Ziconotide: a new pharmacological class of drug for the management of pain. *Seminars in Anesthesia, Perioperative Medicine, and Pain* **19**, 67-75 (2000).

19 Miljanich, G. P. Ziconotide: neuronal calcium channel blocker for treating severe chronic pain. *Current Medicinal Chemistry* **11**, 3029-3040 (2004).

20 Azam, L. & McIntosh, J. M. Alpha-conotoxins as pharmacological probes of nicotinic acetylcholine receptors. *Acta Pharmacologica Sinica* **30**, 771-783 (2009).

21 Dutton, J. & Craik, D. Alpha conotoxins nicotinic acetylcholine receptor antagonists as pharmacological tools and potential drug leads. *Current Medicinal Chemistry* **8**, 327-344 (2001).

22 Luo, S. *et al.* Characterization of a novel α-conotoxin TxID from *Conus textile* that potently blocks rat $\alpha 3\beta 4$ nicotinic acetylcholine receptors. *Journal of Medicinal Chemistry* **56**, 9655-9663 (2013).

23 Dowell, C. *et al.* α-Conotoxin PIA is selective for $\alpha 6$ subunit-containing nicotinic acetylcholine receptors. *The Journal of Neuroscience* **23**, 8445-8452 (2003).

24 Martinez, J. S. *et al.* Alpha-conotoxin EI, a new nicotinic acetylcholine receptor antagonist with novel selectivity. *Biochemistry* **34**, 14519-14526 (1995).

25 McIntosh, J. M. *et al.* A nicotinic acetylcholine receptor ligand of unique specificity, alpha-conotoxin ImI. *Journal of Biological Chemistry* **269**, 16733-16739 (1994).

26 Sines, S. M., Kreienkamp, H. J., Bren, N., Maeda, R. & Taylor, P. Molecular dissection of subunit interfaces in the acetylcholine receptor: identification of determinants of α-Conotoxin M1 selectivity. *Neuron* **15**, 205-211 (1995).

27 Nicke, A., Wonnacott, S. & Lewis, R. J. Alpha-conotoxins as tools for the elucidation of structure and function of neuronal nicotinic acetylcholine receptor subtypes. *European Journal of Biochemistry* **271**, 2305-2319 (2004).

28 Schilaty, N. D. *et al.* Acute ethanol inhibits dopamine release in the nucleus accumbens via $\alpha 6$ nicotinic acetylcholine receptors. *The Journal of Pharmacology and Experimental Therapeutics* **349**, 559-567 (2014).

29 Jackson, K. J., Sanjakdar, S. S., Muldoon, P. P., McIntosh, J. M. & Damaj, M. I. The $\alpha 3\beta 4^*$ nicotinic acetylcholine receptor subtype mediates nicotine reward and physical nicotine withdrawal signs independently of the $\alpha 5$ subunit in the mouse. *Neuropharmacology* **70**, 228-235 (2013).

30 Luo, S. *et al.* α-conotoxin AuIB selectively blocks $\alpha 3\beta 4$ nicotinic acetylcholine receptors and nicotine-evoked norepinephrine release. *The Journal of Neuroscience* **18**, 8571-8579 (1998).

31 Essack, M., Bajic, V. B. & Archer, J. A. C. Conotoxins that confer therapeutic possibilities. *Marine Drugs* **10**, 1244-1265 (2012).

32 Fiedler, B., Green, B. R., Catlin, P. & Watkins, M. Structural and functional diversities among μ-conotoxins targeting TTX-resistant sodium channels. *Biochemistry* **45**, 3723-3732 (2006).

33 Li, R. A. & Tomaselli, G. F. Using the deadly μ-conotoxins as probes of voltage-gated sodium channels. *Toxicon* **44**, 117-122 (2004).

34 Sadeghi, M. *et al.* Novel ω-conotoxins from C. catus reverse signs of mouse inflammatory pain after systemic administration. *Molecular Pain* **9**, 51 (2013).

35 Hannon, H. E. & Atchison, W. D. Omega-conotoxins as experimental tools and therapeutics in pain management. *Marine Drugs* **11**, 680-699 (2013).

36 Jimenez, E. C. Conantokins: from "sleeper" activity to drug development. *Phiippline Science Letters* **2**, 59-66 (2009).

37 Sheng, Z., Dai, Q., Prorok, M. & Castellino, F. J. Subtype-selective antagonism of N-methyl-D-aspartate receptor ion channels by synthetic conantokin peptides. *Neuropharmacology* **53**, 145-156 (2007).

38 Layer, R., Wagstaff, J. & White, H. Conantokins: peptide antagonists of NMDA receptors. *Current Medicinal Chemistry* **11**, 3073-3084 (2004).

39 Flores-Soto, M. E. *et al.* Structure and function of NMDA-type glutamate receptor subunits. *Neurología* **27**, 301-310 (2012).

40 Mayer, M. L. & Armstrong, N. Structure and function of glutamate receptor ion channels *Annual Review of Physiology* **66**, 161-181 (2004).

41 Cotman, C. W. & Iversen, L. L. Excitatory amino acids in the brain - focus on NMDA receptors. *Trends in Neurosciences* **10**, 263-265 (1987).

42 Cull-Candy, S., Brickley, S., Farrant, M. NMDA receptor subunits: diversity, development and disease. *Current Opinion in Neurobiology* **11**, 327-335 (2001).

43 Dingledine, R., Borges, K., Bowie, D. & Traynelis, S. F. The glutamate receptor ion channels. *Pharmacological Reviews* **51**, 7-62 (1999).

44 Adelmann, G., Jonas, P. & Monyer, H. *Ionotropic glutamate receptors in the CNS*. (Springer Berlin Heidelberg, 1999).

45 Traynelis, S. F. *et al.* Glutamate receptor ion channels: structure, regulation, and function. *Pharmacological Reviews* **62**, 405-496 (2010).

46 Hollmann, M. in *Ionotropic glutamate receptors in the CNS* Vol. 141 3-98 (Springer Berlin Heidelberg, 1999).

47 Moriyoshi, K. *et al.* Molecular cloning and characterization of the rat NMDA receptor. *Nature* **354**, 31-37 (1991).

48 Sugihara, H., Moriyoshi, K., Ishii, T., Masu, M. & Nakanishi, S. Structures and properties of seven isoforms of the NMDA receptor generated by alternative splicing. *Biochemical and Biophysical Research Communications* **185**, 826-832 (1992).

49 Schüler, T., Mesic, I., Madry, C., Bartholomäus, I. & Laube, B. Formation of NR1/NR2 and NR1/NR3 heterodimers constitutes the initial step in N-methyl-D-aspartate receptor assembly. *The Journal of Biological Chemistry* **283**, 37-46 (2008).

50 Brickley, S. G., Misra, C., Mok, M. H. S., Mishina, M. & Cull-Candy, S. G. NR2B and NR2D subunits coassemble in cerebellar Golgi cells to form a distinct NMDA receptor subtype restricted to extrasynaptic sites. *Journal of Neuroscience* **23**, 4958-4966 (2003).

51 Rauner, C. & Köhr, G. Triheteromeric NR1/NR2A/NR2B receptors constitute the major N-methyl-D-aspartate receptor population in adult hippocampal synapses. *Journal of Biological Chemistry* **286**, 7558-7566 (2011).

52 Soares, C. & Lee, K. F. H. A Prominent role for triheteromeric GluN1/GluN2A/GluN2B NMDARs at central synapses. *The Journal of Neuroscience* **33**, 14975-14977 (2013).

53 Tovar, K. R. & Westbrook, G. L. The incorporation of NMDA receptors with a distinct subunit composition at nascent hippocampal synapses in vitro. *Journal of Neuroscience* **19**, 4180-4188 (1999).

54 Chazot, P. L., Coleman, S. K., Cik, M. & Stephenson, F. A. Molecular characterization of N-methyl-D-aspartate receptors expressed in mammalian cells yields evidence for the coexistence of three subunit types within a discrete receptor molecule. *The Journal of Biological Chemistry* **269**, 24403-24409 (1994).

55 Kew, J. N., Richards, J. G., Mutel, V. & Kemp, J. A. Developmental changes in NMDA receptor glycine affinity and ifenprodil sensitivity reveal three distinct populations of NMDA receptors in individual rat cortical neurons. *The Journal of Neuroscience* **18**, 1935-1943 (1998).

56 Luo, J., Wang, Y., Yasuda, R. P., Dunah, A. W. & Wolfe, B. B. The majority of N-methyl-D-aspartate receptor complexes in adult rat cerebral cortex contain at least three different subunits (NR1/NR2A/NR2B). *Molecular Pharmacology* **51**, 79-86 (1997).

57 Yashiro, K. & Philpot, B. D. Regulation of NMDA receptor subunit expression and its implications for LTD, LTP, and metaplasticity. *Neuropharmacology* **55**, 1081-1094 (2008).

58 Jones, S. & Gibb, A. J. Functional NR2B- and NR2D-containing NMDA receptor channels in rat substantia nigra dopaminergic neurones. *The Journal of Physiology* **569**, 209-221 (2005).

59 Hansen, K. B., Ogden, K. K., Yuan, H. & Traynelis, S. F. Distinct functional and pharmacological properties of triheteromeric GluN1/GluN2A/GluN2B NMDA receptors. *Neuron* **81**, 1084-1096 (2014).

60 Hatton, C. J. & Paoletti, P. Modulation of triheteromeric NMDA receptors by N-terminal domain ligands. *Neuron* **46**, 261-274 (2005).

61 Henson, M. A., Roberts, A. C., Pérez-Otaño, I. & Philpot, B. D. Influence of the NR3A subunit on NMDA receptor functions. *Progress in Neurobiology* **91**, 23-37 (2010).

62 Madry, C., Mesic, I., Bartholomäus, I. & Nicke, A. Principal role of NR3 subunits in NR1/NR3 excitatory glycine receptor function. *Biochemical and Biophysical Research Communications* **354**, 102-108 (2007).

63 Pina-Crespo, J. C. *et al.* Excitatory glycine responses of CNS myelin mediated by NR1/NR3 "NMDA" receptor subunits. *Journal of Neuroscience* **30**, 11501-11505.

64 Nowak, L., Bregestovski, P., Ascher, P. & Herbet, A. Magnesium gates glutamate-activated channels in mouse central neurones. *Nature* **307**, 462-465 (1984).

65 Mayer, M. L., Westbrook, G. L. & Guthrie, P. B. Voltage-dependent block by Mg2+ of NMDA responses in spinal cord neurones. *Nature* **309**, 261-263 (1984).

66 Westbrook, G. L. & Mayer, M. L. Micromolar concentrations of Zn2+ antagonize NMDA and GABA responses of hippocampal neurons. *Nature* **328**, 640-643 (1987).

67 Madry, C., Mesic, I., Betz, H. & Laube, B. The N-terminal domains of both NR1 and NR2 subunits determine allosteric Zn2+ inhibition and glycine affinity of N-methyl-D-aspartate receptors. *Molecular Pharmacology* **72**, 1535-1544 (2007).

68 Rassendren, F. A., Lory, P., Pin, J. P. & Nargeot, J. Zinc has opposite effects on NMDA and non-NMDA receptors expressed in *Xenopus* oocytes. *Neuron* **4**, 733-740 (1990).

69 Paoletti, P., Ascher, P. & Neyton, J. High-affinity zinc inhibition of NMDA NR1-NR2A receptors. *The Journal of Neuroscience* **17**, 5711-5725 (1997).

70 Rachline, J., Perin-Dureau, F., Le Goff, A., Neyton, J. & Paoletti, P. The micromolar zinc-binding domain on the NMDA receptor subunit NR2B. *Journal of Neuroscience* **25**, 308-317 (2005).

71 McGurk, J. F., Bennett, M. V. & Zukin, R. S. Polyamines potentiate responses of N-methyl-D-aspartate receptors expressed in *Xenopus* oocytes. *Proceedings of the National Academy of Sciences* **87**, 9971-9974 (1990).

72 Rock, D. M. & Macdonald, R. L. Polyamine regulation of N-methyl-D-aspartate receptor channels. *Annual Review of Pharmacology and Toxicology* **35**, 463-482 (1995).

73 Williams, K., Dawson, V. L., Romano, C., Dichter, M. A. & Molinoff, P. B. Characterization of polyamines having agonist, antagonist, and inverse agonist effects at the polyamine recognition site of the NMDA receptor. *Neuron* **5**, 199-208 (1990).

74 Banke, T. G., Dravid, S. M. & Traynelis, S. F. Protons trap NR1/NR2B NMDA receptors in a nonconducting state. *Journal of Neuroscience* **25**, 42-51 (2005).

75 Traynelis, S. F. & Cull-Candy, S. G. Proton inhibition of N-methyl-D-aspartate receptors in cerebellar neurons. *Nature* **345**, 347-350 (1990).

76 Traynelis, S. F., Hartley, M. & Heinemann, S. F. Control of proton sensitivity of the NMDA receptor by RNA splicing and polyamines. *Science* **268**, 873-876 (1995).

77 Furukawa, H. Mechanisms of activation, inhibition and specificity: crystal structures of the NMDA receptor NR1 ligand-binding core. *The European Molecular Biology Organization Journal* **22**, 2873-2885 (2003).

78 Furukawa, H., Singh, S. K., Mancusso, R. & Gouaux, E. Subunit arrangement and function in NMDA receptors. *Nature* **438**, 185-192 (2005).

79 Karakas, E., Simorowski, N. & Furukawa, H. Structure of the zinc-bound amino-terminal domain of the NMDA receptor NR2B subunit. *The European Molecular Biology Organization Journal* **28**, 3910-3920 (2009).

80 Yao, Y., Belcher, J., Berger, A. J., Mayer, M. L. & Lau, A. Y. Conformational analysis of NMDA receptor GluN1, GluN2, and GluN3 ligand-binding domains reveals subtype-specific characteristics. *Structure* **21**, 1788-1799 (2013).

81 Jespersen, A., Tajima, N. & Fernandez-Cuervo, G. Structural insights into competitive antagonism in NMDA receptors. *Neuron* **81**, 366-378 (2014).

82 Farina, A. N. *et al.* Separation of domain contacts is required for heterotetrameric assembly of functional NMDA receptors. *Journal of Neuroscience* **31**, 3565-3579 (2011).

83 Karakas, E. & Furukawa, H. Crystal structure of a heterotetrameric NMDA receptor ion channel. *Science* **344**, 992-997 (2014).

84 Bisaga, A., Popik, P., Bespalov, A. Y. & Danysz, W. Therapeutic potential of NMDA receptor antagonists in the treatment of alcohol and substance use disorders. *Expert Opinion on Investigational Drugs* **9**, 2233-2248 (2000).

85 Chaffey, H. & Chazot, P. L. NMDA receptor subtypes: structure, function and therapeutics. *Current Anaesthesia and Critical Care* **19**, 183-201 (2008).

86 Hrabetova, S. *et al.* Distinct NMDA receptor subpopulations contribute to long-term potentiation and long-term depression induction. *The Journal of Neuroscience* **20**, RC81 (2000).

87 Meldrum, B. S. The role of glutamate in epilepsy and other CNS disorders. *Neurology* **44**, 14-23 (1994).

88 Micu, I. *et al.* NMDA receptors mediate calcium accumulation in myelin during chemical ischaemia. *Nature* **439**, 988-992 (2006).

89 Paoletti, P., Bellone, C. & Zhou, Q. NMDA receptor subunit diversity: impact on receptor properties, synaptic plasticity and disease. *Nature Reviews: Neuroscience* **14**, 383-400 (2013).

90 Akazawa, C., Shigemoto, R., Bessho, Y., Nakanishi, S. & Mizuno, N. Differential expression of five N-methyl-D-aspartate receptor subunit mRNAs in the cerebellum of developing and adult rats. *The Journal of Comparative Neurology* **347**, 150-160 (1994).

91 Cathala, L., Misra, C. & Cull-Candy, S. Developmental profile of the changing properties of NMDA receptors at cerebellar mossy fiber–granule cell synapses. *The Journal of Neuroscience* **20**, 5899-5905 (2000).

92 Olivera, B. M. *et al.* A sleep-inducing peptide from *Conus geographus* venom. *Toxicon* **23**, 277-282 (1985).

93 Haack, J. A. *et al.* Conantokin-T. A gamma-carboxyglutamate containing peptide with N-methyl-D-aspartate antagonist activity. *The Journal of Biological Chemistry* **265**, 6025-6029 (1990).

94 Mena, E. E. *et al.* Conantokin-G: A novel peptide antagonist to the N-methyl-D aspartic acid (NMDA) receptor. *Neuroscience Letters* **118**, 241-244 (1990).

95 Hammerland, L. Conantokin-G selectively inhibits N-methyl-D-aspartate-induced currents in *Xenopus* oocytes injected with mouse brain mRNA. *European Journal of Pharmacology: Molecular Pharmacology* **226**, 239-244 (1992).

96 Haack, J. A., Parks, T. N. & Olivera, B. M. Conantokin-G antagonism of the NMDA receptor subtype expressed in cultured cerebellar granule cells. *Neuroscience Letters* **163**, 63-66 (1993).

97 Prorok, M., Warder, S. E., Blandl, T. & Castellino, F. J. Calcium binding properties of synthetic gamma-carboxyglutamic acid-containing marine cone snail "sleeper" peptides, conantokin-G and conantokin-T. *Biochemistry* **35**, 16528-16534 (1996).

98 Rigby, A. C., Baleja, J. D., Furie, B. C. & Furie, B. Three-dimensional structure of a gamma-carboxyglutamic acid-containing conotoxin, conantokin G, from the marine snail *Conus geographus*: the metal-free conformer. *Biochemistry* **36**, 6906-6914 (1997).

99 Skjaerbaek, N., Nielsen, K. J., Lewis, R. J., Alewood, P. & Craik, D. J. Determination of the solution structures of conantokin-G and conantokin-T by CD and NMR spectroscopy. *The Journal of Biological Chemistry* **272**, 2291-2299 (1997).

100 Warder, S. E. *et al.* The NMR solution structure of the NMDA receptor antagonist, conantokin-T, in the absence of divalent metal ions. *Federation of European Biochemical Sciences Letters* **411**, 19-26 (1997).

101 Lin, C. H., Chen, C. S., Hsu, K. S., King, D. S. & Lyu, P. C. Role of modified glutamic acid in the helical structure of conantokin-T. *Federation of European Biochemical Sciences Letters* **407**, 243-248 (1997).

102 Rigby, A. C. *et al.* Role of gamma-carboxyglutamic acid in the calcium-induced structural transition of conantokin G, a conotoxin from the marine snail *Conus geographus*. *Biochemistry* **36**, 15677-15684 (1997).

103 Chen, Z. *et al.* Conformational changes in conantokin-G induced upon binding of calcium and magnesium as revealed by NMR structural analysis. *Journal of Biological Chemistry* **273**, 16248 (1998).

104 Warder, S. E. *et al.* The roles of individual gamma-carboxyglutamate residues in the solution structure and cation-dependent properties of conantokin-T. *The Journal of Biological Chemistry* **273**, 7512-7522 (1998).

105 Lin, C. H., Chan, F. C., Hwang, J. K. & Lyu, P. C. Calcium binding mode of gamma-carboxyglutamic acids in conantokins. *Protein Engineering* **12**, 589-595 (1999).

106 Klein, R. C. & Castellino, F. J. Inhibition of MK801 binding in adult rat brain sections by conantokin-G and conantokin-T. *Neuroscience Letters* **273**, 171-174 (1999).

107 Klein, R. C., Prorok, M. & Castellino, F. J. Direct binding properties of conantokins to native N-methyl-D-aspartate receptors. *The Journal of Peptide Research* **61**, 307-317 (2003).

108 Skolnick, P., Boje, K., Miller, R., Pennington, M. & Maccecchini, M. L. Noncompetitive inhibition of N-methyl-D-aspartate by conantokin-G: evidence for an allosteric interaction at polyamine sites. *Journal of Neurochemistry* **59**, 1516-1521 (1992).

109 Chandler, P., Pennington, M. & Maccecchini, M. Polyamine-like actions of peptides derived from conantokin-G, an N-methyl-D-aspartate (NMDA) antagonist. *Journal of Biological Chemistry* **268**, 17173-17178 (1993).

110 Gowd, K. H. *et al.* Conantokins derived from the Asprella clade impart conRl-B, an N-methyl d-aspartate receptor antagonist with a unique selectivity profile for NR2B subunits. *Biochemistry* **51**, 4685-4692 (2012).

CHAPTER 2

FROM MOLECULAR PHYLOGENY TOWARDS DIFFERENTIATING PHARMACOLOGY FOR NMDA RECEPTOR SUBTYPES

Originally published as: Platt, R. J. & Curtice, K. J. *et al.* (2014) From molecular phylogeny towards differentiating pharmacology for NMDA receptor subtypes. Toxicon. 81: 67-79

Contributions: Nuclear magnetic resonance spectroscopy and structure determination for conantokin *Bk*-B, electrophysiology with conantokin *Bk*-B, writing, editing, and submission of manuscript.

Toxicon 81 (2014) 67–79

Contents lists available at ScienceDirect

Toxicon

journal homepage: www.elsevier.com/locate/toxicon

From molecular phylogeny towards differentiating pharmacology for NMDA receptor subtypes

Randall J. Platt [a,1], Kigen J. Curtice [a,*,1], Vernon D. Twede [a], Maren Watkins [a], Paweł Gruszczyński [b,c,d], Grzegorz Bulaj [b], Martin P. Horvath [a], Baldomero M. Olivera [a]

[a] Department of Biology, University of Utah, Salt Lake City, UT 84112, USA
[b] Medicinal Chemistry, University of Utah, Salt Lake City, UT 84112, USA
[c] Intercollegiate Faculty of Biotechnology and Chemistry, University of Gdańsk, 80-952 Gdańsk, Poland
[d] Medical University of Gdańsk, 80-822 Gdańsk, Poland

ARTICLE INFO

Article history:
Received 15 August 2013
Received in revised form 11 January 2014
Accepted 29 January 2014
Available online 7 February 2014

Keywords:
NMDA receptor antagonist
Conus peptides
NMR structure
Molecular modeling
Subtype-selective antagonist
Glutamate receptors

ABSTRACT

In order to decode the roles that *N*-methyl-D-aspartate (NMDA) receptors play in excitatory neurotransmission, synaptic plasticity, and neuropathologies, there is need for ligands that differ in their subtype selectivity. The conantokin family of *Conus* peptides is the only group of peptidic natural products known to target NMDA receptors. Using a search that was guided by phylogeny, we identified new conantokins from the marine snail *Conus bocki* that complement the current repertoire of NMDA receptor pharmacology. Channel currents measured in *Xenopus* oocytes demonstrate conantokins con*Bk*-A, con*Bk*-B, and con*Bk*-C have highest potencies for NR2D containing receptors, in contrast to previously characterized conantokins that preferentially block NR2B containing NMDA receptors. Conantokins are rich in γ-carboxyglutamate, typically 17–34 residues, and adopt helical structure in a calcium-dependent manner. As judged by CD spectroscopy, con*Bk*-C adopts significant helical structure in a calcium ion-dependent manner, while calcium, on its own, appears insufficient to stabilize helical conformations of con*Bk*-A or con*Bk*-B. Molecular dynamics simulations help explain the differences in calcium-stabilized structures. Two-dimensional NMR spectroscopy shows that the 9-residue con*Bk*-B is relatively unstructured but forms a helix in the presence of TFE and calcium ions that is similar to other conantokin structures. These newly discovered conantokins hold promise that further exploration of small peptidic antagonists will lead to a set of pharmacological tools that can be used to characterize the role of NMDA receptors in nervous system function and disease.
Published by Elsevier Ltd.

1. Introduction

Glutamate receptors are broadly classified into two groups, the metabotropic receptors that transduce ligand binding via G protein-coupled signaling cascades and the ionotropic receptors that report ligand binding by opening an ion channel. Ionotropic glutamate receptors of the mammalian central nervous system are further divided into two subclasses, N-methyl-D-aspartate (NMDA) and

Abbreviations: Gla, γ, gamma-carboxyglutamate; NMDA, N-methyl-D-aspartate; Fmoc, N-(9-fluorenyl) methoxycarbonyl; MTBE, methyl-tert-butyl ether; ACN, acetonitrile; TFA, trifluoroacetic acid; ESI, electrospray ionization; NMR, nuclear magnetic resonance; BSA, bovine serum albumin; TFE, 2,2,2-trifluoroethanol; MD, molecular dynamics; DSSP, define secondary structure of protein.

* Corresponding author. 257 South 1400 East, Rm. 201, Salt Lake City, UT 84112, USA. Tel.: +1 801 585 1868; fax: +1 801 585 5010.
E-mail address: kigen.curtice@utah.edu (K.J. Curtice).

[1] These authors contributed equally to this manuscript.

http://dx.doi.org/10.1016/j.toxicon.2014.01.016
0041-0101/Published by Elsevier Ltd.

non-NMDA receptors. NMDA receptors are heterotetrameric cation channels formed from two obligatory NR1 subunits and two NR2 or NR3 subunits (Schüler et al., 2008). In mammals, seven NMDA receptor subunit genes (NR1, NR2A, NR2B, NR2C, NR2D, NR3A, and NR3B) combined with splice variants for NR1, NR2C, NR2D, and NR3A gene products create multiple molecular isoforms (Cull-Candy et al., 2001; Dingledine et al., 1999; Hollmann and Heinemann, 1994; Simeone et al., 2004). Each isoform likely contributes uniquely to processes such as synaptic plasticity, learning, memory, and nervous system pathologies (Cull-Candy et al., 2001); however, the precise role of each isoform is not well understood.

In combination with gene knockouts, pharmacological reagents provide useful tools for defining the roles of individual NMDA receptor isoforms. To this end, small molecule discovery and design have provided several antagonists that preferentially block NMDA receptors, including N-terminal domain-binding allosteric modulators, such as zinc, which targets NR2A (Choi and Lipton, 1999; Low et al., 2000; Paoletti et al., 1997; Rachline et al., 2005), and ifenprodil derivatives that target NR2B (Acklin et al., 1998; Ametamey et al., 2000; Auberson et al., 1999, 2002; Kinarsky et al., 2005; Morley et al., 2005; Mosley et al., 2009). In addition, non-competitive quinazolin-4-one derivatives, and competitive piperazine-2,3-dicarboxylate derivatives show moderate selectivity for the NR2C and/or NR2D subunits (Costa et al., 2009; Feng et al., 2004; Mosley et al., 2010). However, a reliable differentiating pharmacology for NMDA receptor subtypes is not currently available.

Conantokins are peptide inhibitors of NMDA receptors that are rich in gamma-carboxyglutamate (Gla) residues and are thought to act competitively at or near the glutamate-binding site on NR2 subunits (Donevan and McCabe, 2000; Hammerland, 1992; Sheng et al., 2009; Tsai et al., 2005; Wittekindt et al., 2001). Post-translationally modified Gla residues in conantokins are generally spaced every three to four amino acid residues and coordinate with divalent cations to stabilize an α-helical conformation (Blandl et al., 2000; Chandler et al., 1993; Rigby et al., 1997; Warder et al., 1998). Some conantokins contain appropriately positioned positive residues that help maintain helicity in the absence of metal ions (Blandl et al., 1999; Lin et al., 1997; Teichert et al., 2007; Warder et al., 1997). All conantokins characterized to date either mildly or strongly prefer the NR2B subtype (Layer et al., 2004; Twede et al., 2009a). These NR2B-selective peptides, including the well-characterized con*G*, have shown significant potential in the treatment of epilepsy, chronic pain, ischemic stroke, and probing the mechanisms of drug addiction (Layer et al., 2004; Twede et al., 2009a).

Recently, con*Br* from *Conus brettinghami* was characterized as a conantokin that, though having highest potency for NR2B-containing receptors, exhibited relatively high potency for NMDA receptors containing NR2D subunits (Twede et al., 2009b). Analogs of con*Br* highlighted the importance of tyrosine at position five for NR2D subtype inhibition (Twede et al., 2009b). We hypothesized that additional examples of NR2D inhibitors might exist within the venoms of closely related *Conus* species and tested this by searching cDNA libraries. Several contantokins were identified from species in the same clade as *C. brettinghami*. In this report, we describe our results characterizing conantokins from *Conus bocki* (Fig. 1), particularly focusing on cDNA clones with the tyrosine-at-position-five character.

The phylogeny-directed search yielded eleven conantokin sequences, five of which were chemically synthesized and characterized. While two of these conantokins (con*Bk*-D and con*Bk*-E) were inactive on all NMDA receptors tested, the other three (con*Bk*-A, con*Bk*-B, and con*Bk*-C) blocked NMDA receptor ion currents. Different from previously described conantokins, these *C. bocki* conantokins are the first identified that show a preference for NR2D-containing NMDA receptors. The NMDA receptor-inhibiting toxins are additionally distinctive in that one (con*Bk*-B) is exceptionally short. These peptides provide proof-of-principle, showing that NR2D-blocking NMDA receptor antagonists exist in cone snail venom and that phylogeny-guided searches can facilitate identification of novel peptides with desirable pharmacological activity.

2. Materials and methods

2.1. Isolation of conantokin clones from C. bocki

C. bocki cDNA was used as a template for polymerase chain reactions (PCRs) with oligonucleotides corresponding

Fig. 1. The shells of four specimens of *Conus bocki* from various localities in the Central Philippines. Specimens are generally collected using tangle nets at depths of ~100 m.

to conserved regions of the signal sequence and 3′ UTR sequences of conantokin prepropeptides. Resulting PCR products were purified using the High Pure PCR Product Purification Kit (Roche Diagnostics, Indianapolis, IN) following the manufacturer's protocol. DNA fragments were annealed to pAMP1 vector DNA and the resulting products were transformed into competent DH5α cells using the CloneAmp pAMP System for Rapid Cloning of Amplification Products (Life Technologies/Gibco BRL, Grand Island, NY). Nucleic acid sequences of resulting conantokin toxin-encoding clones were determined using ABI (Applied Biosystems) automated sequencing (Core DNA Facility, University of Utah).

2.2. Peptide synthesis

Peptide sequences encoded by *C. bocki* cDNA were synthesized using N-(9-fluorenyl) methoxycarbonyl (Fmoc)-protected amino acids. After synthesis, peptides were cleaved from 20 mg of resin by suspension in a 1-ml mixture of TFA/H_2O/1,2-ethanedithiol/phenol/thioanisole (82.5%/5%/2.5%/5%/5% by volume) for 1.5 h at room temperature. The resulting mixture was filtered under vacuum into methyl-tert-butyl ether (MTBE) at −20 °C. Peptide was collected by centrifugation at 5000 × *g* for 8 min and washed with MTBE; centrifugation and wash steps were repeated three times. The resulting pellet was dissolved in 0.1% trifluoroacetic acid (TFA)/20% acetonitrile (ACN). The peptide solution was applied to a Vydac C18 semi-preparative column (10 mm × 250 mm, 5 μm particle size) for purification. Elution was carried out at 4 ml/min with use of 0.1%-TFA/10–40%ACN/H_2O. Electrospray ionization (ESI) mass spectra were obtained using a Voyager GE STR mass spectrometer at the Mass Spectrometry and Proteomic Core Facility of the University of Utah.

2.3. Heterologous NMDA receptor expression in Xenopus oocytes

Rat NMDA receptor cDNA clones of NR1-3b, NR2A, NR2B, NR2C, and NR2D contained in a pSGEM vector were provided by Dr. Michael Hollmann from Ruhr-Universität Bochum (GenBank IDs U08266, AF001423, U11419, U08259, and U08260, respectively). cRNA was prepared and purified using in-vitro RNA transcription kits (Ambion, Inc., St. Louis, MO) according to the manufacturer's protocol. For each NMDA receptor subunit cRNA, 2–5 ng was injected into an oocyte using a nanoinjector. Injected oocytes were incubated at 17 °C in ND-96/Pen/Strep/Ami/Septra buffer (96 mM NaCl, 2 mM KCl, 1.8 mM $CaCl_2$, 1 mM $MgCl_2$) for 1–6 days containing 100 units/ml penicillin G, 100 μg/ml streptomycin, 100 μg/ml amikacin sulfate, 160 μg/ml sulfamethoxazole, and 32 μg/ml trimethoprim.

2.4. Electrophysiology

Voltage clamp electrophysiology was performed as previously described (*36*). Briefly, oocytes were voltage-clamped at −70 mV and gravity perfused with magnesium ion-free ND-96 buffer (96.0 mM NaCl, 2.0 mM KCl, 1.8 mM $CaCl_2$, 5 mM HEPES, pH 7.2–7.5) with 0.1 mg/ml bovine serum albumin (BSA). Currents were elicited by one-second pulses of gravity-perfused agonist solution (200 μM glutamate and 20 μM glycine in magnesium ion-free ND96 with 0.1 mg/ml BSA). In order to determine appropriate agonist concentrations, glutamate concentration–response relationships were independently determined for all four NR2 subtypes using saturating glycine (20 μM) (Fig. S3), and these showed that 200 μM glutamate elicits greater than 90% maximal response for all subtypes. Calcium ions were used in all ND-96 buffers to establish conditions similar to those thought to be important for the structure of conantokins under physiological conditions (Chandler et al., 1993; Rigby et al., 1997; Warder et al., 1998). To rule out the possibility that Ca^{2+}-activated chloride channels were indirectly affecting current inhibition by peptides, control experiments were performed with 1.8 mM Ba^{2+}, and these demonstrated no difference in inhibition (Gowd et al. unpublished data). During experiments, oocytes were continuously perfused in buffer with the exception of static bath periods during peptide administration. Since on- (and off-) rates of some conantokins are relatively slow (Donevan and McCabe, 2000), static bath durations were a minimum of 5 min and were determined empirically by the time point at which maximal inhibition was achieved at a given peptide concentration. Qualitatively, the longer peptides con*Bk*-A and con*Bk*-C had slower kinetics than the ultra-short con*Bk*-B. Analyses of current recovery following removal of toxin provided estimates of dissociation constants (k_{off}) ranging from 0.8 to 2 min^{-1} (see Fig. S1), meaning that a 5-min static bath period would be sufficient to reach at least 97% of equilibrium even at the lowest ligand concentration for the slowest dissociating peptide.

NMDA receptor response at a given peptide concentration was calculated by measuring the first agonist-elicited response after the static bath period and then normalizing to baseline agonist response without peptide. For con*Bk*-B, complete inhibition of NR2D-type receptors was not achieved at maximum peptide concentration. This is likely an experimental artifact that arises from fast off-rate kinetics of con*Bk*-B paired with slow desensitization of NR2D receptors. Thus, percent response was calculated by comparing equivalent time points in control and test responses. Previous work has shown no significant difference in conantokin inhibition when measured by peak (initial) response compared to plateau response (>10 s agonist exposure) (Wittekindt et al., 2001). Concentration-response data were plotted using Prism software (GraphPad Software, Inc., La Jolla, CA) and model curves were generated by fitting the normalized data to the Hill equation ($\%\ response = 100/\{1+([conantokin]/IC_{50})^{nH}\}$). To test whether receptor subtype preferences were statistically significant, we applied a two-tailed, unpaired Student's *t*-test comparing IC_{50} values determined from multiple trials with no assumption concerning the equivalence of variance.

2.5. Circular dichroism (CD)

Conantokins were dissolved in 10 mM HEPES buffer (pH 7.4) with or without 2 mM $CaCl_2$ and with or without 60%

2,2,2-trifluoroethanol (TFE) to a final peptide concentration of 100 μM. CD spectra were obtained from an average of five scans measured on an Aviv 62DS (Biomedical Inc., Lakewood, NJ) from 250 to 190 nm at room temperature. The molar ellipticity (θ) was calculated by the following equation: $\theta = [100^*(\text{CD signal at 222 nm})]/[(n-1)^*L^*(\text{peptide concentration in mM})]$ where n is the number of residues, L is the cuvette path length in cm, and the CD signal is given in millidegrees. Helical content was calculated according to the following equation: % α helix $= 100^*(\theta_{222}/\theta_{max})$, with the theoretical maximum, $\theta_{max} = -39{,}500^*(1-(2.75/n))$.

2.6. Molecular modeling

Models of con*Bk*-A and con*Bk*-C were built using PyMOL (DeLano, 2002) with a secondary structure as predicted by PSIPRED (Jones, 1999). Initial models were optimized using the LEaP module of the AmberTools package. Topology and coordinates of both models, con*Bk*-A and con*Bk*-C, were built with and without Ca^{2+} (data not shown). The resulting coordinates were submitted to molecular dynamics (MD) simulation with AMBER 9.0 (Case et al., 2005) applying the ff99SB AMBER force field. Simulations were carried out using the implicit solvent model, namely the Generalized Born (GB) solvation model developed by Onufriev, Bashford and Case (GBOBC) (Bashford and Case, 2000). To monitor conformational changes for all amino acid residues, the DSSP method (Kabsch and Sander, 1983) from the Ptraj program was used. Energy minimization involved 5000 steps of the steepest descent (Arfken, 1985) (SD) method and 15,000 steps of the conjugate gradient (CG) method (Fletcher and Reeves, 1964). To heat up the system, a 50-ps MD simulation was carried out using an initial temperature of 250 K and a final temperature of 298 K. Neither restraints nor constraints were applied during the heating step. Next, a 1.25-ns MD simulation with 2-fs time steps was performed. The temperature was maintained at 298 K with Berendsen coupling (Berendsen et al., 1984) and a 10-Å cutoff was applied.

2.7. NMR spectroscopy

HPLC-purified con*Bk*-B peptide was resuspended in NMR buffer to yield final concentrations of 10 mM MES (13D) pH 6.1, 40% TFE, and 1.13 mM peptide. Peptide concentration was determined by absorbance measurement at 280 nm, using an extinction coefficient for the single tyrosine residue of 1280 cm^{-1} M^{-1}. Calcium ion titrations were performed by adding small volumes of 0.1 M calcium chloride dissolved in NMR buffer at early titration points and 1 M calcium chloride dissolved in NMR buffer at later titration points. A mock titration using identical solutions, but without con*Bk*-B peptide, showed that pH was altered less than 0.1 pH unit from start to end points of the calcium titration, indicating chemical shift changes are a result of Ca^{2+} binding and not changes in pH. Following titration, the sample was used for 2D NMR experiments with final solution conditions: 10 mM MES (13D) pH 6.1, 11 mM $CaCl_2$, 40% TFE, and 1.10 mM peptide. Additional Ca^{2+} ion titrations were measured in the absence of TFE, but otherwise similar conditions.

One dimensional [^{1}H] proton spectra and two-dimensional [^{13}C, ^{1}H] HSQC, [^{1}H, ^{1}H] COSY, [^{1}H, ^{1}H] TOCSY, and [^{1}H, ^{1}H] NOESY spectra were recorded at 20 °C on a Varian Inova 600 MHz spectrometer with a cryogenic probe. Data were processed with FELIX2004 and analyzed using SPARKY (T. D. Goddard and D. G. Kneller, University of California, San Francisco). The solution structure of calcium ion-bound con*Bk*-B was determined from 82 NOE distance constraints using NIH-XPLOR (Schwieters and Clore, 2001; Schwieters et al., 2003). Starting with a linear template, simulated annealing generated 100 structures with convergence in backbone architecture and variation in side chain rotamers. To control for potential effects of side chain rotamer in subsequent steps, four low-energy structures that sampled all side chain rotamers were selected to seed refinement in NIH-XPLOR. Each of these four structures seeded a separate refinement protocol in NIH-XPLOR to generate a total of 1000 structures. The five lowest-energy structures from each of the four refinements were combined to create the final 20-structure ensemble. Atomic coordinates and NMR data were deposited with the Protein Data Bank as entry *2m7r*.

Mathematical modeling of Ca^{2+} ion titration data was accomplished with *CALCIUM04*, a C language program (M.P.H.) which implements the least-squares Marquardt algorithm (Marquardt, 1963) to fit parameter values. Adjustable parameters describing the system were the intrinsic dissociation constant at each of two binding sites (K_{D1} and K_{D2}), a cooperativity parameter ($K_{cooperativity}$), and changes in chemical shift values for binding Ca^{2+} at site 1 ($\Delta\delta_1$) and at site 2 ($\Delta\delta_2$). All data were fit with global values for K_{D1}, K_{D2}, and $K_{cooperativity}$, and nuclei-specific values for $\Delta\delta_1$ and $\Delta\delta_2$. To avoid over-parameterization, changes in chemical shift were assumed to be additive, meaning that the final change in chemical shift observed with both sites occupied was taken as $\Delta\delta_1 + \Delta\delta_2$. Con*Bk*-B was described as a partition with four possible states: no Ca^{2+} ions bound (p_{00}), site 1 occupied (p_{01}), site 2 occupied (p_{10}), and both sites occupied (p_{11}). Partition values and fraction of free Ca^{2+} ions ($c = [Ca^{2+}_{free}]/[Ca^{2+}_{total}]$) were obtained by numerical methods so as to satisfy the following system of equations:

$$n = nc + p_{01} + p_{10} + 2p_{11} \quad (1.1)$$

$$1 = p_{00} + p_{01} + p_{10} + p_{11} \quad (1.2)$$

$$K_{D1}/P_{total} = ncp_{00}/p_{01} \quad (1.3)$$

$$K_{D2}/P_{total} = ncp_{00}/p_{10} \quad (1.4)$$

$$K_{D1}K_{D2}K_{cooperativity}/P^2_{total} = n^2c^2p_{00}/p_{11} \quad (1.5)$$

where P_{total} is the total peptide concentration, and n is the ratio $[Ca^{2+}_{total}]/P_{total}$, which is a known quantity. Equations (1.1) and (1.2) describe conservation of mass for calcium ions and peptide respectively. Equations (1.3)–(1.5) describe

three equilibria: dissociation at site 1, dissociation at site 2, and simultaneous dissociation at both sites. Uncertainties in parameter values were estimated with a bootstrap method that repeated curve-fitting analysis for several simulated data sets, with each simulated data set derived by sampling from the experimental data with replacement.

3. Results

3.1. Identification of C. bocki clones encoding conantokins

Conantokin sequences were identified from cDNA clones of mRNAs isolated from the venom duct of *C. bocki* (Fig. 1). This species belongs to the clade *Asprella* that also comprises *C. brettinghami*, *Conus sulcatus*, *Conus rolani*, and *Conus samiae*. Since previous work established that a tyrosine residue at position five was important for high potency towards NMDA receptors with NR2D subunits (Twede et al., 2009b), we focused on such examples found for *C. bocki* conantokins, although additional sequences not containing tyrosine at position five were also cloned. The nucleotide sequences, predicted translation products, and mature peptide sequences of five *C. bocki* peptides are shown in Table 1. Post-translational modification of glutamate residues to γ-carboxyglutamate is well established for the conantokin family (Jimenez, 2009). Five glutamate residues in con*Bk*-A, con*Bk*-C, and con*Bk*-D and three of the glutamate residues in con*Bk*-B and con*Bk*-E were predicted to be modified to γ-carboxyglutamate. Predicted mature peptide sequences were synthesized for con*Bk*-A (22 AA), con*Bk*-B (9 AA), con*Bk*-C (18 AA), con*Bk*-D (19 AA) and con*Bk*-E (9 AA). Interestingly, the predicated mature sequences for con*Bk*-B and con*Bk*-*E* are only 9 residues in length and represent the shortest conantokin sequences identified to date. Of course, it remains to be demonstrated that these peptides are present in injected venom, but this

Table 1
Nucleotide and amino acid sequences of cloned *Conus bocki* conantokins.

Conantokin	Nucleotide and predicted amino acid sequences [a]
con*Bk*-A	CACAGAGGCGATGAAGAATATTCAGAGTTTATAGAGAGAGAACGCGAACTCGTCAGTTCTAAAATCCCCAGATAG H R G D E E Y S E F I E R E R E L V S S K I P R
con*Bk*-B	GCCAGAGGCGAAGAAGAATATTCAGAGGCTATAGGAAGAAAATAA A R G E E E Y S E A I G R K
con*Bk*-C	GCCAGAGACGATGAAGAATATGCAGAGTTTATAGAGCAACAACGCGAAGCAGGATTAGTGTAA A R D D E E Y A E F I E Q Q R E A G L V
con*Bk*-D	GCCAGAGGCAAAGAAGAACTTGCAGAGAACGCGCCGGAGTTTGCCAGAGAACTAGCTACAAATGGAAAAAGATAA A R G K E E L A E N A P E F A R E L A T N G K R
con*Bk*-E	GCCAGAGGCGAAGAAGAATGTTCAGAGGCTATAGGAAGAAAATAA A R G E E E C S E A I G R K
Conantokin	Predicted mature amino acid sequences [b]
con*Bk*-A	G D γ γ Y S γ F I γ R E R γ L V S S K I P R ^
con*Bk*-B	G E γ γ Y S γ A I *
con*Bk*-C	D D γ γ Y A γ F I γ Q Q R γ A G L V ^
con*Bk*-D	G K γ γ L A γ N A P γ F A R γ L A T N *
con*Bk*-E	G E γ γ C S γ A I *
con*Br*[c]	G D γ γ Y S K F I γ R E R γ A G R L D L S K F P ^
con*G*[d]	G E γ γ L Q γ N Q γ L I R γ K S N *
con*T*[e]	G E γ γ Y Q K M L γ N L R γ A E V K K N A *

γ Gla residues.

^, COOH; *, $CONH_2$

[a] predicted cleavage site for mature toxins are shown in bold and stop codons are underlined

[b] conserved and predicted gla residues are highlighted

[c] *Twede et al., 2009*

[d] *Mena et al., 1990*

[e] *Haack et al., 1990*

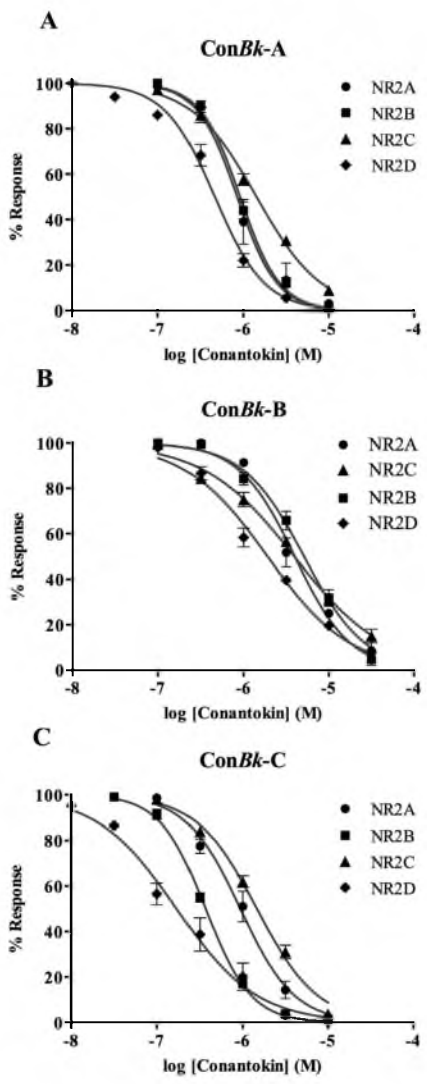

Fig. 2. Relative potencies of conantokins from *Conus bocki* tested on NMDA receptors. One of the four NR2 subunits was co-expressed with NR1-3b in *Xenopus oocytes*. Concentration–response relationships obtained utilizing two-electrode voltage clamp electrophysiology are shown for con*Bk*-A (A), con*Bk*-B (B) and con*Bk*-C (C). Each data point represents the average peak current response from a minimum of three independent oocytes. Error bars represent ± SEM. These three conantokins from C. *bocki* showed the highest potency on receptors with the NR1-3b/NR2D subunit combination (diamonds).

seems likely to be the case as the clones were derived from mRNA isolated from the venom duct.

3.2. *Functional characterization of conantokins from* C. bocki

Peptides were functionally assessed using two-electrode voltage-clamp electrophysiology in *Xenopus oocytes* coexpressing a single NR2 subunit with the NR1-3b subunit. Example recordings from these experiments are provided in the supplementary information, Fig. S1. Dose-response curves are shown in Fig. 2, and IC_{50} values are summarized in Table 2. Con*Bk*-D and con*Bk*-E were inactive at all concentrations tested. Con*Bk*-A, con*Bk*-B, and con*Bk*-C were active and interestingly, exhibited highest potency for NR2D subunits. Con*Bk*-A and con*Bk*-C blocked NR2D-containing NMDA receptors with IC_{50} values of 0.46 (±0.04) μM and 0.17 (±0.02) μM, respectively. The shorter peptide, con*Bk*-B, was 10-fold less potent on all NMDA receptor subtypes compared to the larger counterparts, yet retained NR2D preference with an IC_{50} value of 1.9 μM. Though the preference for NR2D over other receptors was modest, differences in IC_{50} values were statistically significant ($p < 0.05$) for both con*Bk*-B and con*Bk*-C (Table S1).

3.3. *Sequence determinants of NMDA receptor inhibition by con*Bk-*B*

The short length of con*Bk*-B and its preference for NMDA receptor subtypes containing the NR2D subunit motivated experiments to elucidate determinants of subtype selectivity. Con*Bk*-E differs from con*Bk*-B by substitution of tyrosine 5 with cysteine and is thus a naturally occurring single amino acid substitution variant. Inactivity observed for con*Bk*-E demonstrates the importance of position five. We also considered the possibility that con*Bk*-E may covalently form a homodimer via cys-5; however, no activity was subsequently observed in a dimerized form of con*Bk*-E (not shown). We designed and synthesized additional sequence analogs of con*Bk*-B and con*Bk*-C to test the importance of other sequence determinants. Table 3 shows amino-acid sequences for con*Bk*-B, con*Bk*-E, and designed analogs; Table 4 shows the corresponding IC_{50} values. Removing C-terminal amidation from the naturally occurring con*Bk*-B sequence (con*Bk*-B[COOH]) rendered the peptide inactive, suggesting amidation may stabilize the active conformation or interact with NMDA receptors. The analog constructed with the first nine residues of con*Bk*-C (con*Bk*-C [1-9]) was not active on any of the NMDA receptor subtypes tested, indicating only certain amino acid combinations are tolerated in a nine residue scaffold.

To test sequence permutations we constructed nine-residue chimeric conantokins with amino acids derived from con*Bk*-B and con*Bk*-C. The first nine residues of these two conantokins differ at positions 1, 2, 6, and 8. Chimera*Bk*-BC [1-9] contains amino-acid residues derived from con*Bk*-B at positions 1–2 and amino-acid residues derived from con*Bk*-C at positions 6 and 8, and showed inverted preferences for NR2B and NR2D, meaning that this chimera is more similar to previously characterized conantokins in its preference for NR2B over NR2D. Note that this chimera terminates with a free carboxylic-acid functional group and retains activity, indicating an amide protecting group is not absolutely required for NMDA receptor inhibition. Chimera*Bk*-CB [1-9] swaps con*Bk*-B and con*Bk*-C derived amino acids in the converse manner, with con*Bk*-C residues at positions 1–2 and con*Bk*-B at positions 6 and 8, and resulted in an inactive peptide. A point mutation at position eight (con*Bk*-B [A8F]) resulted in loss of preference for NR2D containing receptors, suggesting that residue 8 may

Table 2
Comparison of IC_{50} values measured for *Conus bocki* conantokins and others.

	NMDA receptor subtype IC_{50} value ± SEM (μM) [hill coefficient]				IC_{50} ratio		
	NR2A	NR2B	NR2C	NR2D	D/B	A/B	C/B
con*Bk*-A	0.9 ± 0.3 [−1.9]	0.92 ± 0.07 [−1.9]	1.4 ± 0.2 [−1.1]	0.46 ± 0.04 [−1.5]	0.50	0.92	1.5
con*Bk*-B	3.9 ± 0.2 [−1.3]	5.1 ± 0.2 [−1.2]	3.9 ± 0.1 [−0.8]	1.91 ± 0.06 [−0.9]	**0.37**	**0.76**	**0.76**
con*Bk*-C	0.9 ± 0.1 [−1.4]	0.37 ± 0.07 [−1.6]	1.5 ± 0.07 [−1.2]	0.17 ± 0.02 [−0.93]	0.46	2.5	4.1
con*Rl*-A	0.52[b]	0.11[b]	6.1[b]	0.48[b]	4.4	4.7	**55**
con*G*	>10[c]	0.1[c]	1[c]	1[c]	10	**~100**	10
con*R*	0.53[a]	0.35[a]	~10[a]	~10[a]	**~30**	1.5	~29

Ratios in bold are the extremes; in combination, two conantokins with extreme ratios may help discriminate between NR2 subtypes specified in each column. IC_{50} values were determined using a curve fit of data from $n = 3–6$ oocytes. Standard error of mean (SEM) was determined by analysis of IC_{50} values calculated from individual experimental trials. Con*Bk*-D and con*Bk*-E were inactive at concentrations tested.
[a] Twede et al., 2009a,b.
[b] Gowd et al., 2010.
[c] Teichert et al., 2007.

Table 3
Amino acid sequences of con*Bk*-B and analogs.

Conantokin	Amino acid sequence
con*Bk*-B	GEγγYSγAI[a]
con*Bk*-E	GEγγCSγAI[a]
con*Bk*-B[COOH]	GEγγYSγAI[b]
con*Bk*-C [1-9]	DDγγYAγFI[a]
con*Bk*-B[A8F]	GEγγYSγFI[a]
chimera*Bk*-BC [1-9]	GEγγYAγFI[b]
chimera*Bk*-CB [1-9]	DDγγYSγAI[a]

γ Gla residues.
[a] C-terminal amidation.
[b] C-terminal carboxyl.

contact a region that differs between NMDA receptor subtypes. In summary, short conantokin analogs require con*Bk*-B-like sequences in the amino-terminal portion for activity, and changes in carboxy-terminal residues strongly affect either activity or subtype selectivity.

3.4. Circular dichroism

Conantokins are relatively unstructured yet acquire helicity in the presence of divalent metal ions (Blandl et al., 2000; Chandler et al., 1993; Rigby et al., 1997; Warder et al., 1998). Helical content of *C. bocki* conantokins was assessed by circular dichroism spectroscopy in both the presence and in the absence of Ca^{2+} (Fig. 3). In the absence of Ca^{2+} all three peptides had no apparent helical structure, a result consistent with other conantokins. In the presence of Ca^{2+}, however, con*Bk*-A and con*Bk*-B retained low helical content, whereas con*Bk*-C adopted significant helicity.

Con*Bk*-A and con*Bk*-B appear to be the first NMDA receptor-inhibiting conantokins to exhibit little or no helicity in the presence of Ca^{2+} ions. To test if the shortest conantokin, con*Bk*-B, can acquire helical structure in a stabilizing solvent, the effect of 2,2,2-trifluoroethanol (TFE) was examined (Fig. 3). Upon addition of 60% TFE to peptide in a Ca^{2+}-free solution the helical content of con*Bk*-B increased from 2 to 24 percent and upon addition of 60% TFE to peptide in solution containing Ca^{2+}, helical content increased from 5 to 43 percent. The results suggest that con*Bk*-B can coordinate Ca^{2+} ions to adopt a helical structure, albeit more weakly or with faster exchange kinetics than other conantokins.

3.5. Molecular modeling

To explain the differences of Ca^{2+}-stabilized helical content between con*Bk*-A and con*Bk*-C, we applied molecular modeling (see Fig. S2). Molecular dynamics simulations show the secondary structure of con*Bk*-C without Ca^{2+} ions was a short helix between residues 6–9 with a percentage occurrence of 7%. The presence of Ca^{2+} changed this observation and resulted in two helices spanning residues 2–5 and 12–15 with a percentage occurrence of 70%. In the case of the con*Bk*-A, we observed one helical region between residues 13–17, which did not change in location but did increase in percent occurrence from 4% to 50% upon addition of Ca^{2+} in the MD simulations. We quantified helix-stabilizing interactions as Ca^{2+} bridges between negatively charged groups. For con*Bk*-C these are Asp1-Ca^{2+}-Tyr5 (via π-electrons of the Tyr), Asp1-Ca^{2+}-Gla4,

Table 4
IC_{50} values measured for con*Bk*-B analogs.

	NMDA receptor subtype IC_{50} values ± SEM (uM) [hill coefficient]				NR2D/NR2B IC_{50} ratios
	NR2A	NR2B	NR2C	NR2D	
con*Bk*-B	3.9 ± 0.2 [−1.3]	5.1 ± 0.2 [−1.2]	3.9 ± 0.1 [−0.8]	1.91 ± 0.06 [−0.9]	0.37
con*Bk*-E	>10	>10	>10	>10	ND
con*Bk*-B[COOH]	>10	>10	–	>10	ND
con*Bk*-C [1-9]	>10	>10	>10	>10	ND
con*Bk*-B[A8F]	>10	2.1 ± 0.6 [−1.0]	–	2.9 ± 0.3 [−1.3]	1.4
chimera*Bk*-BC [1-9]	>10	3.3 ± 0.6 [−0.7]	–	6.2 ± 0.2 [−1.0]	1.9
chimera*Bk*-CB [1-9]	>10	>10	–	>10	ND

Each IC_{50} value represents the average from $n = 3–6$ oocytes.

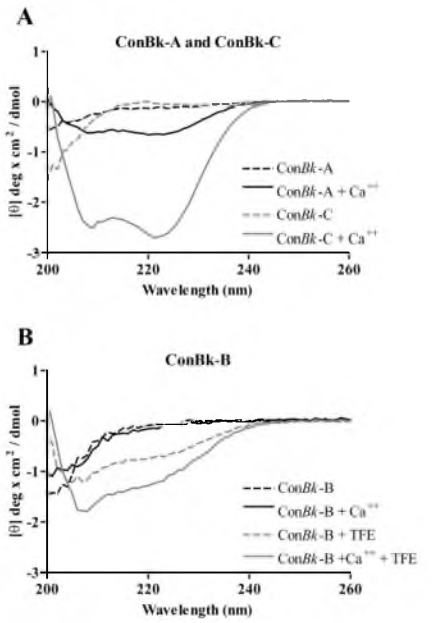

Fig. 3. CD spectra of con*Bk*-A, con*Bk*-B, and con*Bk*-C. A. CD spectra for con*Bk*-A and con*Bk*-C in the presence and absence of 2 mM $CaCl_2$. B. CD spectra for con*Bk*-B without $CaCl_2$, with 2 mM $CaCl_2$, 60% TFE, or both 2 mM $CaCl_2$ and 60% TFE. The dual minima at 208 and 222 nm are characteristic of an α-helical conformation. Ellipticity is plotted on a per-peptide bond basis to simplify comparison of these conantokins that vary in length. Data points represent the average of 5 independent scans.

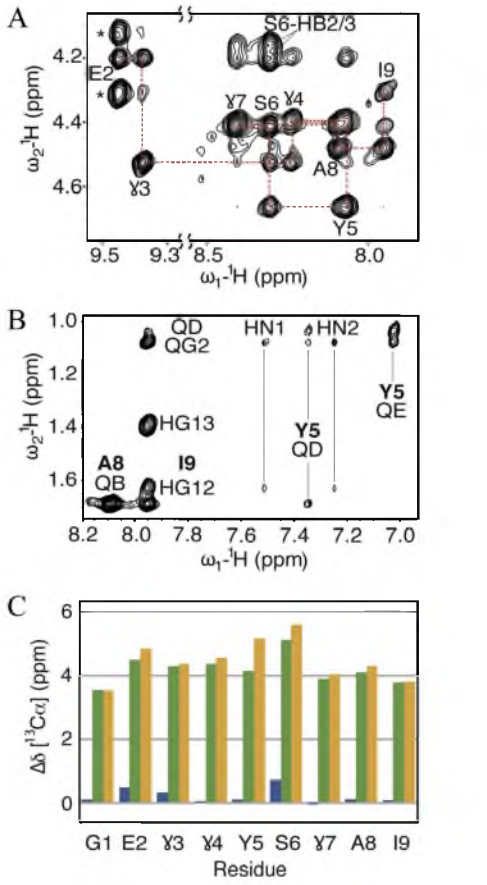

Fig. 4. NMR data for con*Bk*-B. (A) Amide-alpha proton (HN–HA) region of the 2D NOESY spectra recorded for con*Bk*-B shows complete residue connectivity (red dotted lines). NOEs from HA atoms of Gly-1 are indicated by asterisk (*). Multiple i to i+3 HA/HN NOEs can be seen, consistent with an α helix. (B) Amide-aliphatic-aromatic proton region of the 2D NOESY spectra shows NOEs between Tyr-5 and Ile-9, indicating proximity for these side chains within the structure of con*Bk*-B. (C) Effects of calcium ions and TFE on con*Bk*-B structure. Changes in $^{13}C\alpha$ chemical shifts ($\Delta\delta$) were obtained by subtracting the chemical shift values observed in buffer with no added calcium salt and no added TFE. Positive values of $\Delta\delta$ indicate increased helical content due to addition of 10 mM $CaCl_2$ (blue), 40% TFE (green), and both calcium and TFE (yellow). (For interpretation of the references to color in this figure legend, the reader is referred to the web version of this article.)

Gla4-Ca^{2+}-Tyr5, Gla4-Ca^{2+}-Gla7, Gla3-Ca^{2+}-Gla4, Gla3-Ca^{2+}-Gla7, Asp2-Ca^{2+}-Gla10, Asp2-Ca^{2+}-Gla14, and Gla10-Ca^{2+}-Gla14. And for con*Bk*-A these are Gla3-Ca^{2+}-Gla4, Gla7-Ca^{2+}-Gla14, Gla7-Ca^{2+}-Gla10, and Gla10-Ca^{2+}-Gla14. More numerous calcium ion-bridging interactions observed for con*Bk*-C is consistent with higher helicity observed by CD spectroscopy. The sequence alignment presented in Table 1 shows an Arg-Glu-Arg structural motif (residues 11–13) in con*Bk*-A. In the case of con*Bk*-C, corresponding residues are Gln-Gln-Arg. The MD simulations suggest the presence of positively charged Arg11 situated adjacent to negatively charged Gla10 interrupts helical structure in con*Bk*-A. Presumably, the mutation con*Bk*-A [R11Q] would increase helicity of the peptide in the presence of calcium ions, however this prediction is yet to be tested.

3.6. *NMR spectroscopy of con*Bk-*B*

To date, con*Bk*-B is the shortest conantokin to be detected in cDNA libraries and also selects for NR2D over NR2B more so than any other known conantokin. For these reasons, we were motivated to characterize the structural behavior of this ultra-short conantokin. Resonances from ^{1}H and ^{13}C nuclear spins were assigned from 2D NMR spectra obtained with natural abundance samples (Fig. 4(A) and (B)). To determine the relative contributions of calcium ions and TFE for helical structure in con*Bk*-B, we examined $^{13}C\alpha$ chemical shifts in 2D CHSQC spectra. Fig. 4(C) shows differences in con*Bk*-B $^{13}C\alpha$ chemical shifts measured upon addition of 11 mM calcium chloride (10 peptide equivalents), addition of 40% TFE, and the combination of adding both calcium chloride and TFE. Calcium ion addition moved chemical shifts downfield by 0.07–0.48 ppm for all residues except Gla-7, which was essentially unperturbed. Downfield perturbations for $^{13}C\alpha$ nuclei are consistent with a shift in structural equilibrium towards an α helix. TFE produced significantly larger downfield shift changes ranging from 3.56 to 5.14 ppm. The combined effect of calcium ions and TFE generally resulted in larger downfield chemical shift changes ranging from 3.54 to 5.6. The data

indicate that calcium weakly promotes helical structure and its effects are additive to those of TFE, which strongly promotes helical structure in con*Bk*-B.

Calcium ion binding of con*Bk*-B was assessed by tracking proton chemical shift changes from 1D NMR spectra during a titration. Fig. 5 shows proton chemical shift plotted as a function of Ca^{2+} concentration for amide and gamma protons of con*Bk*-B dissolved in 40% TFE. Many protons showed a simple monophasic response to titration with calcium ions, but Gla-4 and Tyr-5 amide protons responded in a biphasic manner, moving upfield with initial increases in calcium ion concentration and moving downfield at later stages of the titration, suggesting there are two Ca^{2+}-binding sites with differing affinities.

We considered several versions of a two-site binding model. One model assumed no interaction between sites, and other models assumed either positive or negative

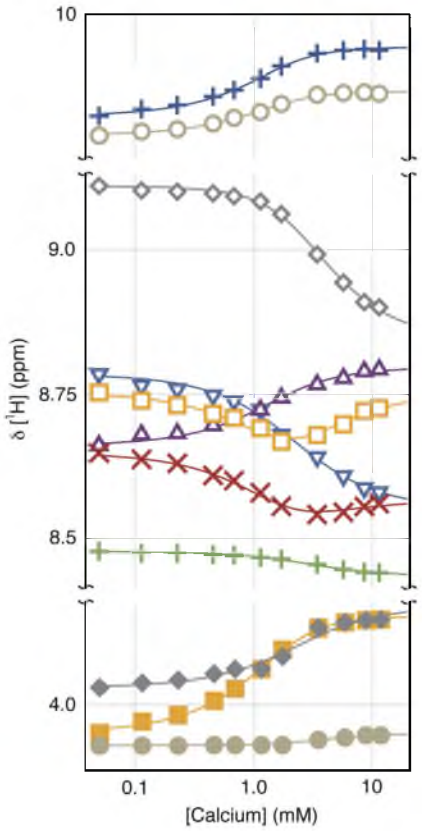

Fig. 5. Calcium binding to con*Bk*-B monitored by NMR. Chemical shifts were obtained from 1D NMR spectra measured for con*Bk*-B peptide solutions at 20 °C containing 40% TFE and varying concentrations of calcium chloride. Response of each amide proton is plotted with the following symbols: + Glu 2, ○ Gla-3, □ Gla-4, × Tyr-5, △ Ser-6, ◇ Gla-7, ▽ Ala-8, + Ile-9. Gamma proton chemical shifts for the three Gla residues in con*Bk*-B are plotted with symbols: ● Gla-3, ■ Gla-4, and ◆ Gla-7. Model curves depict the result of non-linear least-squares fitting of these data (and other data not shown) with global parameters that define a system of two calcium-binding sites with differing intrinsic affinities and modest positive cooperativity between sites.

interaction. The independent sites model adequately accounted for all of the data, but had larger residuals than a model with positive cooperativity. A model with negative cooperativity did not fit data well and was not considered further. The independent sites model and the positively interacting sites model yielded the same intrinsic dissociation constant for the high-affinity binding site [K_{D1} – 0.31(±0.03) mM] and comparable values for the low-affinity binding site [K_{D2} = 2.8(±0.5) mM for independent sites; K_{D2} = 4(±1) mM for cooperative sites]. Interaction between Ca^{2+}-binding sites was described by a parameter ($K_{cooperativity}$) that is the ratio of apparent dissociation constants for a given site with the second site occupied (numerator) and unoccupied (denominator). This parameter refined to a value of $K_{cooperativity}$ = 0.6(±0.2), indicating the affinity at each binding site appeared to increase 1.67-fold with occupancy at the other site. This corresponds to −1.4(+0.7) kJ mol ^{1} of binding energy that is realized when both sites are occupied. Two homogeneous sites with a similar degree of interaction would exhibit a Hill coefficient of n = 1.14. Comparable calcium ion titrations, with similar midpoints and biphasic responses, were also measured without TFE. Curve fitting analyses of these titrations obtained in the absence of TFE could be accomplished with the same dissociation constants defined by data measured with TFE.

3.7. NMR structure determination

The calcium ion-bound structure of con*Bk*-B stabilized with the cosolvent trifluoroethanol was determined by 2D NMR spectroscopy using natural abundance ^{1}H and ^{13}C nuclear spins. Complete resonance assignments were obtained through examination of NOESY, TOCSY, and CHSQC spectra. The NOESY spectra had 82 NOE resonances with signal to noise greater than 10, and these contained 63 short-range [i:i, i:i + 1] and 19 medium-range [i:i + 2, i:i + 3, or i:i+4] distance constraints. The fingerprint region of the NOESY spectra (Fig. 4(A)) showed sequential HN-Hα connectivity and contained i:i+3 cross peaks (Hα-HN) consistent with an α helix. Additional evidence of α-helical structure was seen in 16 of the 19 medium range NOEs between residue side chains. For example, side chain protons of Tyr-5 and Ile-9 had cross peaks indicating proximity (see Fig. 4(B)).

Fig. 6(A) shows the ensemble of energy minimized con*Bk*-B structures as short α helices. Ensemble members were aligned with main chain atoms (Cα, N, HN, C, O) of residues 3–9, since these adopted more consistent positions than those of residues 1 and 2. The alignment yielded a root-mean-squared deviation of 1.6 Å for all atoms of all residues, 1.1 Å for all main chain atoms of all residues, and 0.5 Å for main chain atoms of residues 3–9. The three Gla residues of con*Bk*-B cluster along one face of the helix, apparently poised to coordinate Ca^{2+} ions (Fig. 6(B) and (C)). A glutamate residue at position 2 (Glu-2) is on the opposite face of the helix and is therefore unlikely to contribute directly to high-affinity Ca^{2+} binding. Hydrophobic residues Tyr-5 and Ile-9 are grouped at the C-terminal half of the helix and are found on the face opposite to the Gla residues. The hydrophobic contacts involving Tyr-5

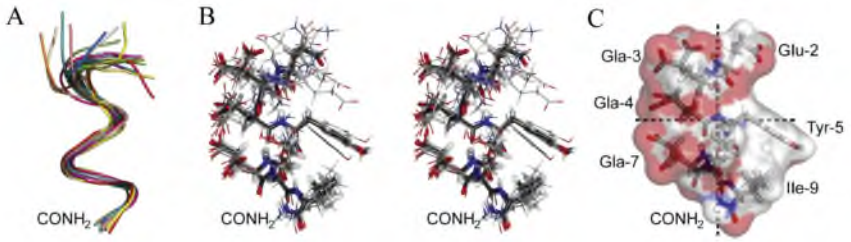

Fig. 6. Con*Bk*-B NMR structure. (A) Twenty energy-minimized structures, shown with colored tubes, highlight the helical conformation of con*Bk*-B. (B) An ensemble of energy-minimized con*Bk*-B structures is shown with all-atom stick models in stereo. Atoms are color coded as follows: H white, C charcoal, O red, N blue. For clarity, only ten (of twenty available) randomly selected models are shown. A representative model, selected because it most closely resembles the ensemble average, is highlighted with thicker sticks. (C) Con*Bk*-B is approximately amphipathic with respect to two perpendicular axes (dotted lines). Charged Gla and other polar moieties are clustered at the N-terminal half of con*Bk*-B and along one face of the helix, while more hydrophobic residues are grouped together at the C-terminal half of the opposite face. (For interpretation of the references to color in this figure legend, the reader is referred to the web version of this article.)

probably augment helix stabilization provided by salt bridges between carboxylate groups and calcium ions.

We compared the con*Bk*-B structure to structures of con*G* and con*T*, two longer conantokin toxins previously characterized by NMR structure determination (Skjaerbaek et al., 1997). Representative models of each conantokin are shown in Fig. 7. The three structures share identical N-terminal residues 1–4 and the structures align fairly well in this region. The most striking difference between the three structures is overall length, with con*Bk*-B shortest (9 residues), con*T* longest (21 residues), and con*G* in the middle (17 residues). Con*Bk*-B and con*G* have very similar orientations for Gla-3, Gla-4 and Gla-7 (highlighted in Fig. 7 with red dots), suggesting these two peptides coordinate calcium ions in a similar manner. Con*Bk*-B and con*T* have highly comparable orientations for Tyr-5, which makes hydrophobic contacts with residue nine in both structures. In the structural comparison, amino-acid position 8 (highlighted in Fig. 7 with black dots) stands out as having the largest variation in volume and shape while located in an otherwise conserved region. Amino-acid identity at position eight is an important determinant of selectivity in conantokins as shown by the A8F replacement variant (see Table 4) and by previous studies (Sheng et al., 2007, 2010). The structural differences highlighted here additionally corroborate the idea that this residue position may hold the key for future design of increasingly selective conantokins.

4. Discussion

A discovery strategy incorporating inferences based on phylogenetics and previous structure-function studies led us to the identification of con*Bk*-A, con*Bk*-B, con*Bk*-C, con*Bk*-D and con*Bk*-E from *C. bocki*. Molecular phylogeny as a means to targeted drug discovery, also known as exogenomics, has been described and successfully applied to discover *Conus* toxins with novel pharmacological properties (Bulaj, 2008; Olivera, 2006; Olivera and Teichert, 2007; Teichert et al., 2007). In the present case we were searching for conantokins that were potentially active on NR2D-containing NMDA receptors and identified *C. bocki* as a possible source because of its close phylogenetic relation to

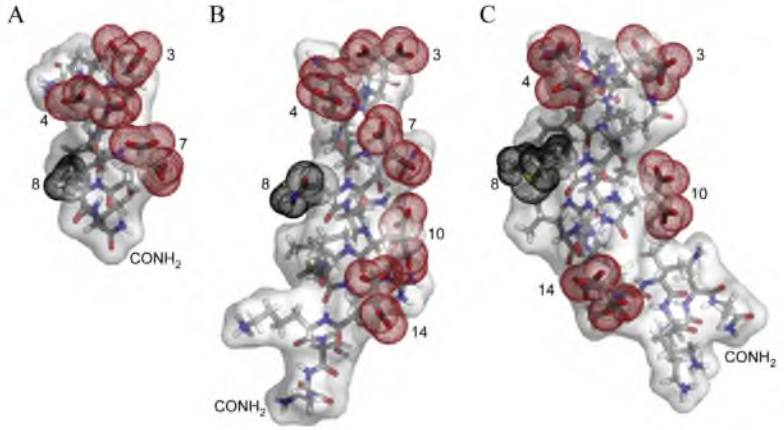

Fig. 7. Comparison of conantokin structures determined by NMR. Representative models of con*Bk*-B (A) [9 residues, pdb id *2m7r*], con*G* (B) [17 residues, pdb id *1onu*], and con*T* (C) [21 residues, pdb id *1ont*] were aligned by superposition of residues 3–9. All three structures are α-helices, depicted here as stick models inside semi-transparent accessible surfaces. Gla residues (highlighted with red dots) are positioned along a nearly contiguous ridge for con*Bk*-B and con*G* and appear more distributed for con*T*. Differences in side chain volume at position 8 (highlighted with black dots) may contribute to NMDA receptor subtype selectivity. (For interpretation of the references to color in this figure legend, the reader is referred to the web version of this article.)

C. brettinghami, previously the source of the most NR2D-potent conantokin (con*Br*) (Twede et al., 2009b). As could be predicted from structure-function studies of con*Br* analogs (Twede et al., 2009b), the three peptides derived from *C. bocki* that contained tyrosine at position five showed inhibition of NMDA receptors with NR2D subunits. Unexpectedly, all three peptides additionally had decreased inhibitory activity for NMDA receptors with NR2B subunits compared to previously described conantokins. Discovery of peptides with decreased potency in block of NR2B containing receptors was, in a sense, a bonus that could not have been predicted *a priori*, and is sure to guide future iterations of the exogenomics approach.

Con*Bk*-D and con*Bk*-E, although inactive in our assays, provide insights into sequence determinants for NMDA receptor inhibition that complement previous insights derived from structure activity work. For instance, alanine scanning in con*G*, con*T*, and con*R* highlighted the importance of residues at positions two and five for activity (Blandl et al., 1998, 2001; Warder et al., 2001). Data obtained in the present study suggests that the positive charge on lysine at position two, of con*Bk*-D, abolishes antagonist activity for NMDA receptors tested here. Also, comparison of con*Bk*-E with con*Bk*-B shows that substitution of a cysteine side chain at position five renders the short peptide scaffold inactive.

Previous work showed that native conantokins can lose biological activity as they are shortened (Blandl et al., 1998, 2001; Warder et al., 2001). The discovery of con*Bk*-B encoding mRNAs in venom ducts strongly suggests that ultra-short conantokin peptides with NMDA receptor inhibitory activity exist in the natural world. Sequence permutations evaluated in this study showed that only certain combinations of amino acids in the nine-residue scaffold retain activity. Surprisingly, some permutations switched peptide preference for receptors between NR2B and NR2D subtypes, suggesting that a few contacts provide distinction between these NMDA receptor homologs. Most critical for selectivity are residues at positions 5, 6, and 8, as previously identified in other conantokins (Sheng et al., 2007, 2009, 2010). Thus, this ultra-short peptide likely interacts with receptors utilizing the same mechanism as its larger counterparts. Interestingly, the structural comparison of con*Bk*-B to con*G* and con*T* independently highlighted position 8 as a possible determinant of subtype selectivity (see Fig. 7).

Our structural analysis suggests that a calcium ion-stabilized helical conformation is not necessary for receptor inhibition, consistent with the observation that con*G* and con*T* inhibition of MK-801 binding in rat brain is not hindered by the addition of EDTA (Klein and Castellino, 1999). In our analysis, Con*Bk*-A and con*Bk*-B showed little helical content in the presence of calcium ions, yet had inhibitory activity comparable to other, more helical conantokins. NMR spectroscopy verified the unstructured state of con*Bk*-B through absence of mid-range NOEs for peptide in the presence of calcium ions. These mid-range NOE's were, however, present when the co-solvent TFE was included. Conantokins likely adopt a unique conformation upon receptor binding so as to maximize contacts between peptide and receptor. This receptor-bound state may be similar to helical structures of con*G*, con*T*, and con*Bk*-B in solution, but is probably a structurally distinct conformation that may or may not require calcium ions. Thus, a major focus of our future research is to determine the receptor interface and conformation of a receptor-bound conantokin.

An important achievement of this work was to demonstrate a measure of NR2D preference for peptide based NMDA receptor antagonists, which makes investigation of the role of these subunits in physiological systems using a pharmacological approach more feasible. The NR2D subunit has a relatively restricted expression pattern that is enriched in midbrain, spinal, and peripheral structures, such as the substantia nigra, striatum, dorsal horn, and dorsal root ganglia (Counihan et al., 1998; Hummel et al., 2008; Karlsson et al., 2002; Kosinski et al., 1998). Thus, NR2D may play a functional role in pathological conditions that affect these regions, such as Parkinson's disease and chronic pain. Although limited work has been done, NR2D knockout studies support this hypothesis (Micu et al., 2006; Minami et al., 2001).

NR2D-containing NMDA receptors additionally have unique physiological properties, including decreased sensitivity to magnesium blockade and prolonged deactivation kinetics (Cull-Candy et al., 2001), which implicates involvement of the NR2D subunit in excitotoxicity. Recent work suggests that NR2D (or NR2C) is involved in excitotoxic damage to myelin sheaths following ischemia (Micu et al., 2006), and may participate in the underlying mechanistic basis for excitotoxic neuronal loss in prion diseases (Khosravani et al., 2008). Subsequently, selective blockage or modulation of NMDA receptor activity should promote neuron survival in these patients if the hypotheses are correct. Motivated by these potential applications, we can now initiate structure-function studies to enhance NR2D selectivity of conantokin peptides through modification of the newly discovered NR2D-preferring *C. bocki* toxins.

In order to investigate the role of NMDA receptor subtypes, we envision use of peptide combinations that can provide a measure of pharmacological differentiation between pairs of NMDA receptor subtypes. Such a strategy of using pairs of conopeptides has recently been used for differentiating between different voltage-gated sodium channel subtypes (Wilson et al., 2011). To take a particular example in the context of NMDA receptor discrimination, the combination of con*Bk*-B and con*R* could, in principle, discriminate between NR2B and NR2D containing receptors. Con*R* is similarly active on NR2B and NR2A containing receptors and inactive on NR2C and NR2D (Table 2). Con*Bk*-B is most active on NR2D containing receptors with varying but lower activity on NR2C $>$ NR2A $>$ NR2B. The contrasting effects of these peptides could therefore be compared in experimental paradigms to provide insight into the relative abundance of NR2B and NR2D NMDA receptor subunit combinations present in various physiological contexts. Similarly, combining con*Bk*-B with con*G* would be expected to provide more than a two order of magnitude difference in selectivity between the NR2A and NR2D subtypes. Even NR2C versus NR2B containing NMDA receptors might be distinguished by using con*Bk*-B together with con*Rl*-A. Although single pharmacological

agents to discriminate between the different NMDA receptor subtypes are preferable, the discovery of con*Bk*-A, con*Bk*-B, and con*Bk*-C provides an initial basis for developing peptide-based differentiating pharmacology for the NMDA receptor receptor family.

Ethical statement

On behalf of all the contributing authors of this manuscript, Kigen Curtice declares that: (a) The work provided herein is original and described accurately, (b) this work is not being considered for publication elsewhere, (c) all authors listed have made significant contribution to the work described, and (d) the highest ethical standards have been used in any experimentation involving animals.

Acknowledgments

We thank Dr. Doju Yoshikami for his insightful discussions regarding electrophysiology and expert consultation. We thank K. H. Gowd and Tiffany Han for their assistance with some of the assays, and acknowledge Cognetix for synthesis of peptides for experiments. We also thank Dr. Jack Skalicky, whose helpfulness with NMR data collection and analysis was invaluable.

This work was supported by the National Institutes of General Medical Sciences, National Institutes of Health [Grant GM48677].

Conflict of interest

The authors declare that there are no conflicts of interest.

Appendix A. Supplementary data

Supplementary data related to this article can be found at http://dx.doi.org/10.1016/j.toxicon.2014.01.016.

References

Acklin, P., Allgeier, H., Auberson, Y.P., Bischoff, S., Ofner, S., Sauer, D., Schmutz, M., 1998. 5-Aminomethylquinoxaline-2,3-diones, part III: arylamide derivatives as highly potent and selective glycine-site NMDA receptor antagonists. Bioorg. Med. Chem. Lett. 8, 493–498.

Ametamey, S.M., Kokic, M., Carrey-Rémey, N., Bläuenstein, P., Willmann, M., Bischoff, S., Scmutz, M., Schubiger, P.A., Auberson, Y.P., 2000. Synthesis, radiolabelling and biological characterization of (D)-7-iodo-N-(1-phosphonoethyl)-5-aminomethylquinoxaline-2, 3-dione, a glycine-binding site antagonist of NMDA receptors. Bioorg. Med. Chem. Lett. 10, 75–78.

Arfken, G., 1985. The method of steepest descents. In: Mathematical Methods for Physicists.

Auberson, Y.P., Acklin, P., Bischoff, S., Moretti, R., Ofner, S., Schmutz, M., Veenstra, S.J., 1999. N-phosphonoalkyl-5-aminomethylquinoxaline-2,3-diones: in vivo active AMPA and NMDA(glycine) antagonists. Bioorg. Med. Chem. Lett. 9, 249–254.

Auberson, Y.P., Allgeier, H., Bischoff, S., Lingenhoehl, K., Moretti, R., Schmutz, M., 2002. 5-Phosphonomethylquinoxalinediones as competitive NMDA receptor antagonists with a preference for the human 1A/2A, rather than 1A/2B receptor composition. Bioorg. Med. Chem. Lett. 12, 1099–1102.

Bashford, D., Case, D.A., 2000. Generalized born models of macromolecular solvation effects. Annu. Rev. Phys. Chem. 51, 129–152.

Berendsen, H.J., Postma, J.P.M., Vangunsteren, W.F., Dinola, A., Haak, J.R., 1984. Molecular dynamics with coupling to an external bath. J. Chem. Phys. 81, 7.

Blandl, T., Prorok, M., Castellino, F.J., 1998. NMDA-receptor antagonist requirements in conantokin-G. FEBS Lett. 435, 257–262.

Blandl, T., Warder, S.E., Prorok, M., Castellino, F.J., 1999. Binding of cations to individual gamma-carboxyglutamate residues of conantokin-G and conantokin-T. J. Pept. Res.: Off. J. Am. Pept. Soc. 53, 453–464.

Blandl, T., Warder, S.E., Prorok, M., Castellino, F.J., 2000. Structure-function relationships of the NMDA receptor antagonist peptide, conantokin-R. FEBS Lett. 470, 139–146.

Blandl, T., Zajicek, J., Prorok, M., Castellino, F.J., 2001. Sequence requirements for the N-methyl-D-aspartate receptor antagonist activity of conantokin-R. J. Biol. Chem. 276, 7391–7396.

Bulaj, G., 2008. Integrating the discovery pipeline for novel compounds targeting ion channels. Curr. Opin. Chem. Biol. 12, 441–447.

Case, D.A., Cheatham, T.E., Darden, T., Gohlke, H., Luo, R., Merz, K.M., Onufriev, A., Simmerling, C., Wang, B., Woods, R.J., 2005. The Amber biomolecular simulation programs. J. Comput. Chem. 26, 1668–1688.

Chandler, P., Pennington, M., Maccecchini, M., Nashed, N.T., Skolnick, P., 1993. Polyamine-like actions of peptides derived from conantokin-G, an N-methyl-D-aspartate (NMDA) antagonist. J. Biol. Chem. 268, 17173–17178.

Choi, Y.B., Lipton, S.A., 1999. Identification and mechanism of action of two histidine residues underlying high-affinity Zn2+ inhibition of the NMDA receptor. Neuron 23, 171–180.

Costa, B.M., Feng, B., Tsintsadze, T.S., Morley, R.M., Irvine, M.W., Tsintsadze, V., Lozovaya, N.A., Jane, D.E., Monaghan, D.T., 2009. N-methyl-D-aspartate (NMDA) receptor NR2 subunit selectivity of a series of novel piperazine-2,3-dicarboxylate derivatives: preferential blockade of extrasynaptic NMDA receptors in the rat hippocampal CA3-CA1 synapse. J. Pharmacol. Exp. Ther. 331, 618–626.

Counihan, T.J., Landwehrmeyer, G.B., Standaert, D.G., Kosinski, C.M., Scherzer, C.R., Daggett, L.P., Veliçelebi, G., Young, A.B., Penney, J.B., 1998. Expression of N-methyl-D-aspartate receptor subunit mRNA in the human brain: mesencephalic dopaminergic neurons. J. Comp. Neurol. 390, 91–101.

Cull-Candy, S., Brickley, S., Farrant, M., 2001. NMDA receptor subunits: diversity, development and disease. Curr. Opin. Neurobiol. 11, 327–335.

DeLano, W., 2002. The PyMOL Molecular Graphics System. DeLano Scientific, Palo Alto, CA.

Dingledine, R., Borges, K., Bowie, D., Traynelis, S., 1999. The glutamate receptor ion channels. Pharmacol. Rev. 50, 7–61.

Donevan, S.D., McCabe, R.T., 2000. Conantokin G is an NR2B-selective competitive antagonist of N-methyl-D-aspartate receptors. Mol. Pharmacol. 58, 614–623.

Feng, B., Tse, H.W., Skifter, D.A., Morley, R., Jane, D.E., Monaghan, D.T., 2004. Structure-activity analysis of a novel NR2C/NR2D-preferring NMDA receptor antagonist: 1-(phenanthrene-2-carbonyl) piperazine-2,3-dicarboxylic acid. Br. J. Pharmacol. 141, 508–516.

Fletcher, R., Reeves, C.M., 1964. Function minimization by conjugate gradients. Comput. J. 7, 149–154.

Haack, J.A., Rivier, J., Parks, T.N., Mena, E.E., Lourdes, J.C., Olivera, B.M., 1990. A gamma-carboxyglutamate containing peptide with N-methyl-d-aspartate antagonist activity. J. Biol. Chem. 265, 6025–6029.

Gowd, K.H., Watkins, M., Twede, V.D., Bulaj, G.W., Olivera, B.M., 2010. Characterization of conantokin Rl-A: molecular phylogeny as structure/function study. J. Pept. Sci. 16, 375–382.

Hammerland, L., 1992. Conantokin-G selectively inhibits N-methyl-D-aspartate-induced currents in Xenopus oocytes injected with mouse brain mRNA. Eur. J. Pharmacol. Mol. Pharmacol. 226, 239–244.

Hollmann, M., Heinemann, S., 1994. Cloned glutamate receptors. Annu. Rev. Neurosci. 17, 31–108.

Hummel, M., Strassle, B., Miller, S., Kaftan, E., Whiteside, G., 2008. Anatomical localization and expression pattern for the NMDA-2D receptor subunit in a rat model of neuropathic pain. Neuroscience 155, 492–502.

Jimenez, E., 2009. Conantokins: from "sleeper" activity to drug development. Philipp. Sci. Lett. 2, 60–66.

Jones, D.T., 1999. Protein secondary structure prediction based on position-specific scoring matrices. J. Mol. Biol. 292, 195–202.

Kabsch, W., Sander, C., 1983. Dictionary of protein secondary structure: pattern recognition of hydrogen-bonded and geometrical features. Biopolymers 22, 2577–2637.

Karlsson, U., Sjödin, J., Angeby Möller, K., Johansson, S., Wikström, L., Näsström, J., 2002. Glutamate-induced currents reveal three functionally distinct NMDA receptor populations in rat dorsal horn – effects of peripheral nerve lesion and inflammation. Neuroscience 112, 861–868.

Khosravani, H., Zhang, Y., Tsutsui, S., Hameed, S., Altier, C., Hamid, J., Chen, L., Villemaire, M., Ali, Z., Jirik, F.R., Zamponi, G.W., 2008. Prion protein attenuates excitotoxicity by inhibiting NMDA receptors. J. Cell. Biol. 181, 551–565.

Kinarsky, L., Feng, B., Skifter, D.A., Morley, R.M., Sherman, S., Jane, D.E., Monaghan, D.T., 2005. Identification of subunit- and antagonist-specific amino acid residues in the N-Methyl-D-aspartate receptor glutamate-binding pocket. J. Pharmacol. Exp. Ther. 313, 1066–1074.

Klein, R.C., Castellino, F.J., 1999. Inhibition of MK801 binding in adult rat brain sections by conantokin-G and conantokin-T. Neurosci. Lett. 273, 171–174.

Kosinski, C.M., Standaert, D.G., Counihan, T.J., Scherzer, C.R., Kerner, J.A., Daggett, L.P., Veliçelebi, G., Penney, J.B., Young, A.B., Landwehrmeyer, G.B., 1998. Expression of N-methyl-D-aspartate receptor subunit mRNAs in the human brain: striatum and globus pallidus. J. Comp. Neurol. 390, 63–74.

Layer, R.T., Wagstaff, J.D., White, H.S., 2004. Conantokins: peptide antagonists of NMDA receptors. Curr. Med. Chem. 11, 3073–3084.

Lin, C.H., Chen, C.S., Hsu, K.S., King, D.S., Lyu, P.C., 1997. Role of modified glutamic acid in the helical structure of conantokin-T. FEBS Lett. 407, 243–248.

Low, C.M., Zheng, F., Lyuboslavsky, P., Traynelis, S.F., 2000. Molecular determinants of coordinated proton and zinc inhibition of N-methyl-D-aspartate NR1/NR2A receptors. Proc. Natl. Acad. Sci. U. S. A. 97, 11062–11067.

Marquardt, D.W., 1963. An algorithm for least-squares estimation of nonlinear parameters. SIAM J. Appl. Math. 11, 431–441.

Mena, E.E., Gullak, M.F., Pagnozzi, M.J., Richter, K.E., Rivier, J., Cruz, L.J., Olivera, B.M., 1990. Conantokin-G: a novel peptide antagonist to the N-methyl-D-aspartic acid (NMDA) receptor. Neurosci. Lett. 118, 241–244.

Micu, I., Jiang, Q., Coderre, E., Ridsdale, A., Zhang, L., Woulfe, J., Yin, X., Trapp, B.D., McRory, J.E., Rehak, R., Zamponi, G.W., Wang, W., Stys, P.K., 2006. NMDA receptors mediate calcium accumulation in myelin during chemical ischaemia. Nature 439, 988–992.

Minami, T., Matsumura, S., Okuda-Ashitaka, E., Shimamoto, K., Sakimura, K., Mishina, M., Mori, H., Ito, S., 2001. Characterization of the glutamatergic system for induction and maintenance of allodynia. Brain Res. 895, 178–185.

Morley, R.M., Tse, H.-W., Feng, B., Miller, J.C., Monaghan, D.T., Jane, D.E., 2005. Synthesis and pharmacology of N1-substituted piperazine-2,3-dicarboxylic acid derivatives acting as NMDA receptor antagonists. J. Med. Chem. 48, 2627–2637.

Mosley, C.A., Acker, T.M., Hansen, K.B., Mullasseril, P., Andersen, K.T., Le, P., Vellano, K.M., Bräuner-Osborne, H., Liotta, D.C., Traynelis, S.F., 2010. Quinazolin-4-one derivatives: a novel class of noncompetitive NR2C/D subunit-selective N-methyl-D-aspartate receptor antagonists. J. Med. Chem. 53, 5476–5490.

Mosley, C.A., Myers, S.J., Murray, E.E., Santangelo, R., Tahirovic, Y.A., Kurtkaya, N., Mullasseril, P., Yuan, H., Lyuboslavsky, P., Le, P., Wilson, L.J., Yepes, M., Dingledine, R., Traynelis, S.F., Liotta, D.C., 2009. Synthesis, structural activity-relationships, and biological evaluation of novel amide-based allosteric binding site antagonists in NR1A/NR2B N-methyl-D-aspartate receptors. Bioorg. Med. Chem. 17, 6463–6480.

Olivera, B.M., 2006. Conus peptides: biodiversity-based discovery and exogenomics. J. Biol. Chem. 281, 31173–31177.

Olivera, B.M., Teichert, R.W., 2007. Diversity of the neurotoxic Conus peptides: a model for concerted pharmacological discovery. Mol. Interv. 7, 251–260.

Paoletti, P., Ascher, P., Neyton, J., 1997. High-affinity zinc inhibition of NMDA NR1-NR2A receptors. J. Neurosci. 17, 5711–5725.

Rachline, J., Perin-Dureau, F., Le Goff, A., Neyton, J., Paoletti, P., 2005. The micromolar zinc-binding domain on the NMDA receptor subunit NR2B. J. Neurosci. 25, 308–317.

Rigby, A.C., Baleja, J.D., Li, L., Pedersen, L.G., Furie, B.C., Furie, B., 1997. Role of gamma-carboxyglutamic acid in the calcium-induced structural transition of conantokin G, a conotoxin from the marine snail Conus geographus. Biochemistry 36, 15677–15684.

Schüler, T., Mesic, I., Madry, C., Bartholomaus, I., Laube, B., 2008. Formation of NR1/NR2 and NR1/NR3 heterodimers constitutes the initial step in N-methyl-D-aspartate receptor assembly. J. Biol. Chem. 283, 37–46.

Schwieters, C.D., Clore, G.M., 2001. Internal coordinates for molecular dynamics and minimization in structure determination and refinement. J. Magn. Reson. 152, 288–302.

Schwieters, C.D., Kuszewski, J.J., Tjandra, N., Clore, G.M., 2003. The Xplor-NIH NMR molecular structure determination package. J. Magn. Reson. 160, 65–73.

Sheng, Z., Dai, Q., Prorok, M., Castellino, F.J., 2007. Subtype-selective antagonism of N-methyl-D-aspartate receptor ion channels by synthetic conantokin peptides. Neuropharmacology 53, 145–156.

Sheng, Z., Liang, Z., Geiger, J.H., Prorok, M., Castellino, F.J., 2009. The selectivity of conantokin-G for ion channel inhibition of NR2B subunit-containing NMDA receptors is regulated by amino acid residues in the S2 region of NR2B. Neuropharmacology 57, 127–136.

Sheng, Z., Prorok, M., Castellino, F.J., 2010. Specific determinants of conantokins that dictate their selectivity for the NR2B subunit of N-methyl-D-aspartate receptors. Neuroscience 170, 703–710.

Simeone, T.A., Sanchez, R.M., Rho, J.M., 2004. Molecular biology and ontogeny of glutamate receptors in the mammalian central nervous system. J. Child. Neurol. 19, 343–360 discussion 361.

Skjaerbaek, N., Nielsen, K.J., Lewis, R.J., Alewood, P., Craik, D.J., 1997. Determination of the solution structures of conantokin-G and conantokin-T by CD and NMR spectroscopy. J. Biol. Chem. 272, 2291–2299.

Teichert, R.W., Jimenez, E.C., Twede, V., Watkins, M., Hollmann, M., Bulaj, G., Olivera, B.M., 2007. Novel conantokins from Conus parius venom are specific antagonists of N-methyl-D-aspartate receptors. J. Biol. Chem. 282, 36905–36913.

Tsai, V.W.-W., Dodd, P.R., Lewis, R.J., 2005. The effects of alanine-substituted conantokin-G and ifenprodil on the human spermine-activated N-methyl-D-aspartate receptor. Neuroscience 130, 457–464.

Twede, V.D., Miljanich, G., Olivera, B.M., Bulaj, G., 2009a. Neuroprotective and cardioprotective conopeptides: an emerging class of drug leads. Curr. Opin. Drug. Discov. Dev. 12, 231–239.

Twede, V.D., Teichert, R.W., Walker, C.S., Gruszczynski, P., Kazmierkiewicz, R., Bulaj, G., Olivera, B.M., 2009b. Conantokin-Br from Conus brettinghami and selectivity determinants for the NR2D subunit of the NMDA receptor. Biochemistry 48, 4063–4073.

Warder, S.E., Blandl, T., Klein, R.C., Castellino, F.J., Prorok, M., 2001. Amino acid determinants for NMDA receptor inhibition by conantokin-T. J. Neurochem. 77, 812–822.

Warder, S.E., Chen, Z., Zhu, Y., Prorok, M., Castellino, F.J., Ni, F., 1997. The NMR solution structure of the NMDA receptor antagonist, conantokin-T, in the absence of divalent metal ions. FEBS Lett. 411, 19–26.

Warder, S.E., Prorok, M., Chen, Z., Li, L., Zhu, Y., Pedersen, L.G., Ni, F., Castellino, F.J., 1998. The roles of individual gamma-carboxyglutamate residues in the solution structure and cation-dependent properties of conantokin-T. J. Biol. Chem. 273, 7512–7522.

Wilson, M.J., Yoshikami, D., Azam, L., Gajewiak, J., Olivera, B.M., Bulaj, G., Zhang, M., 2011. μ-Conotoxins that differentially block sodium channels NaV1.1 through 1.8 identify those responsible for action potentials in sciatic nerve. Proc. Natl. Acad. Sci. 108, 10302–10307.

Wittekindt, B., Malany, S., Schemm, R., Otvos, L., Maccecchini, M.L., Laube, B., Betz, H., 2001. Point mutations identify the glutamate binding pocket of the N-methyl-D-aspartate receptor as major site of conantokin-G inhibition. Neuropharmacology 41, 753–761.

CHAPTER 3

THE NMR SOLUTION STRUCTURE OF CONANTOKIN *RL*-B

Introduction

Conantokins are unique among conotoxins in sequence, structure, and function. Most conotoxins are rich in cysteine residues, have tertiary structures stabilized through disulfide bonds, and are effectors of various voltage- and ligand-gated ion channels. In contrast, conantokins are rich in γ-carboxyglutamate (gla) residues, have tertiary structures stabilized by coordination of calcium ions, and are the only conotoxins discovered to date that inhibit N-methyl-D-aspartate receptors (NMDARs)[1-3]. In the absence of calcium, most conantokins are unstructured as evidenced by circular dichroism (CD) and nuclear magnetic resonance (NMR) experiments[4-7]. Addition of calcium results in conformational changes in conantokins as gla residues align along a single face to coordinate calcium ions. Alignment of gla residues drives conantokins to adopt a helical conformation. The degree to which helicity increases with calcium varies among conantokins, and is dependent on sequence characteristics such as gla residue spacing and the presence of positively charged residues that appear to augment helix stability[8,9]. Figure 3.1 illustrates the calcium-driven unstructured-to-helical transition by comparing NMR structures of conantokin-G (conG), determined in the absence and presence of calcium ions[10,11].

Structure-function studies on conantokins indicate that residues on the amino-terminal half are essential for NMDAR inhibition, and that these residues contribute to

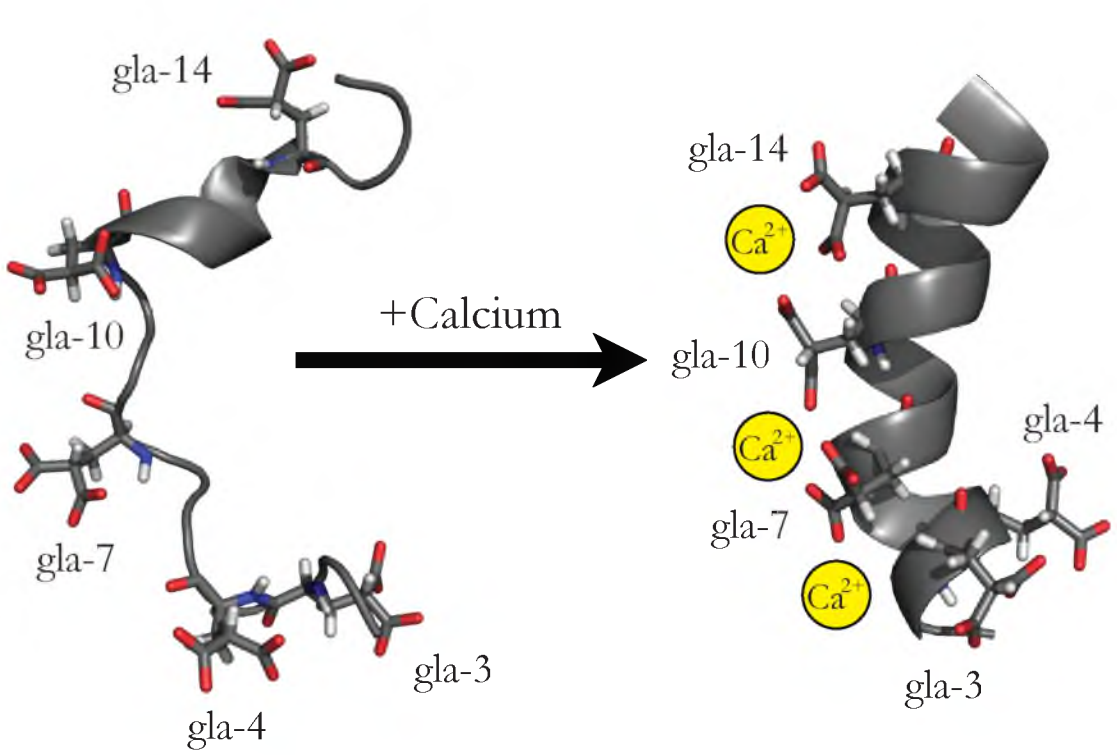

Figure 3.1: Conantokins adopt helical structure in the presence of calcium. NMR solution structures of ConG that were calculated from data collected in the absence (pdb: 1AD7, left) and presence (pdb: 1ONU, right) of calcium ions. Structures are shown as cartoons representations with gla residues shown as sticks. The inferred positions of calcium ions are indicated, even though these are NMR silent.

NMDAR selectivity. For example, ConT is 21 residues yet retains micromolar inhibitory activity with C-terminal truncation down to nine residues[12]. Interestingly, the shortest naturally occurring and active conantokin known, con*Bk*-B, is also nine residues in length[13].

The first five residues in conantokins are most important, which is indicated by mutational scanning experiments that show loss of NMDAR inhibitory activity when any of these are substituted with alanine[14-16]. Also, certain substitutions at residue 5 alter subtype selectivity, or cause inactivity in conantokins[17,18]. However, residue 5 is not the sole determinant of selectivity; additional residues contribute to conantokin function[19].

The recently discovered conantokin *R*-B (con*R*-B) from *Conus rolani* is an ultra-selective conantokin that potently inhibits NR2B NMDA receptor subtypes[20]. The potency

of con*R*-B on NR2B receptor subtypes is similar to that of conG, which was previously the most selective conantokin known. However, con*R*-B has a lower potency for NR2A containing receptors than does conG, making it a superior pharmacological tool. In addition to its selectivity, con*R*-B contains a hydroxyproline residue, which is uncommon among structurally characterized conantokins. The amino-acid sequences for con*R*-B and other representative conantokins are provided in Table 3.1.

In this chapter, the NMR solution structure of con*R*-B is presented. The con*R*-B structure is of particular interest because it is the first structure of a hydroxyproline-containing conantokin. Through structure comparisons and mutational analyses, the con*R*-B structure provides insights into determinants of subtype selectivity. Con*R*-B was found to be a helix-kink-helix, with two short helices interrupted a hydroxyproline residue. This structure, taken in context of other work on conantokins, provides insights into mechanisms of NMDAR inhibition by conantokins.

Methods

Methods for peptide synthesis and NMR spectroscopy for con*R*-B were similar to those described previously for con*Bk*-B[13] with the exception that tri-fluoro-ethanol (TFE) was not needed to stabilize a helical conformation. A summary of major steps in peptide synthesis, data collection, and structure calculation are described below.

Peptide synthesis

The mature peptide sequence for con*R*-B was predicted after analysis of a cDNA library from *Conus rolani* venom glands. Con*R*-B was synthesized using N-(9-fluorenyl) methoxycarbonyl (Fmoc) protected amino acids and purified using high-performance liquid chromatography (HPLC) on a Vydac C18 semipreparative column. Verification of peptide

Table 3.1: Conantokin sequences

Name	Sequence	Ref.
ConG	GEγγLQγNQγLIRγKSN$_{CONH2}$	21
ConT	GEγγYQKMLγNLRγAEVKKNA$_{CONH2}$	1
ConR	GEγγVAKMAAγLARγNIAKGCKVNCYP$_{COOH}$	22
ConL	GEγγVAKMAAγLARγDAV$_{CONH2}$	23
Con*Pr*-A	GEDγYAγGIRγYQLIHGKI$_{COOH}$	24
Con*R*/-B	**GEγγLAγKAOγFARγLAN$_{CONH2}$**	20

mass was performed with electrospray ionization (ESI) mass spectrometry on a Voyager GE STR instrument at the University of Utah mass spectrometry core facility.

NMR spectroscopy

HPLC-purified con*R*/-B peptide (1000 nmol) was resuspended in NMR buffer to yield final concentrations of 1.5 mM peptide, 10 mM MES (13D) pH 6.0, and 15 mM $CaCl_2$. One-dimensional proton NMR spectra and two-dimensional NMR spectra including heteronuclear single quantum coherence (HSQC), total correlations spectroscopy (TOCSY), correlated spectroscopy (COSY), and nuclear Overhauser effect spectroscopy (NOESY) spectra were recorded. All data were collected at 20°C on a Varian Inova 600 Mhz spectrometer with cryogenic probe. Data were processed with FELIX2004 (Accelrys Inc., San Diego, CA) and analyzed using SPARKY (T.D. Goddard and D.G. Kneller, University of California, San Francisco). Residue assignments were performed manually through examination of HSQC, TOCSY, and NOESY spectra using a sequential residue assignment approach. The ensemble of solution structures for con*R*/-B was calculated with CYANA (P. Güntert, University of Frankfurt, Germany) from 196 inter- and intraresidue NOE distance constraints found in the NOESY spectra.

Results

NMR spectroscopy of conRl-B

Analysis of NOESY, TOCSY, COSY, and CHSQC spectra resulted in assignments for nuclei of all residues in con*Rl*-B. The NMR data was of high quality, as evidenced by well defined and dispersed resonances. The CHSQC spectrum for con*Rl*-B is shown in Figure 3.2 and illustrates the quality of data collected for the con*Rl*-B peptide. The fingerprint region of the NOESY spectrum for con*Rl*-B and assignments of the amide-proton to alpha-proton (NH-HA) resonances are shown in Figure 3.3.

In the NOESY spectra, 196 inter- and intraresidue NOE peaks (NOEs) were assigned and subsequently used for structure calculations. The number of NOEs for each residue of con*Rl*-B and the distribution of NOEs by distance are shown in Figure 3.4. NOEs were most abundant from residue 5 to 16, with fewer constraints found at the amino- and carboxyl- termini. Interestingly, medium range distance constraints were most prominent near gla residues (grey bars, Figure 3.4 left panel). This may suggest that the helical structure of conantokins is most constrained near calcium-coordinating gla residues.

Of note, NOE constraints were not observed for residues more than four positions apart, which is consistent with an α-helix (Figure 3.4 right panel). The Ramachandran plot showing phi (ϕ) and psi (ψ) angle combinations for con*Rl*-B is presented in Figure 3.5. All ϕ/ψ angle combinations were found to be in optimal regions for an α-helix. Thus, con*Rl*-B is predominantly helical, as has been observed for other conantokin structures.

Consistent with other conantokin structures, con*Rl*-B has significant helical chatacter and gla residues are aligned on a single helical face (Figure 3.6). However, the con*Rl*-B helix is interrupted by a hydroxyproline at position 10, resulting in a helix-kink-helix motif that is distinct from previously characterized members of this family. In the NMR-calculated

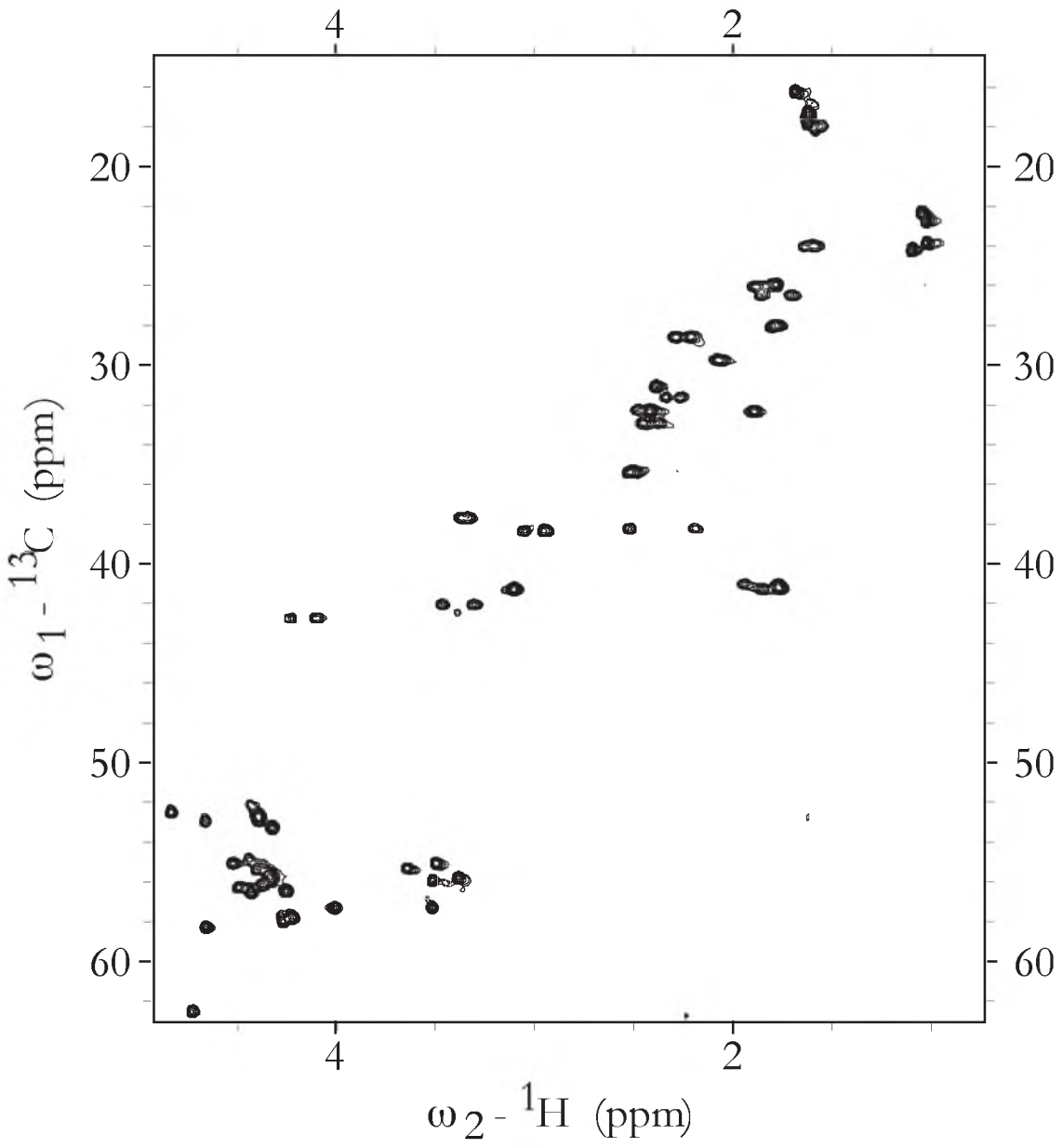

Figure 3.2: CHSQC spectra from con*R*-B. The CHSQC spectrum for con*R*-B illustrates clear resonance peaks for carbon-hydrogen pairs within the polypeptide. These data were used to aid with resonance assignments.

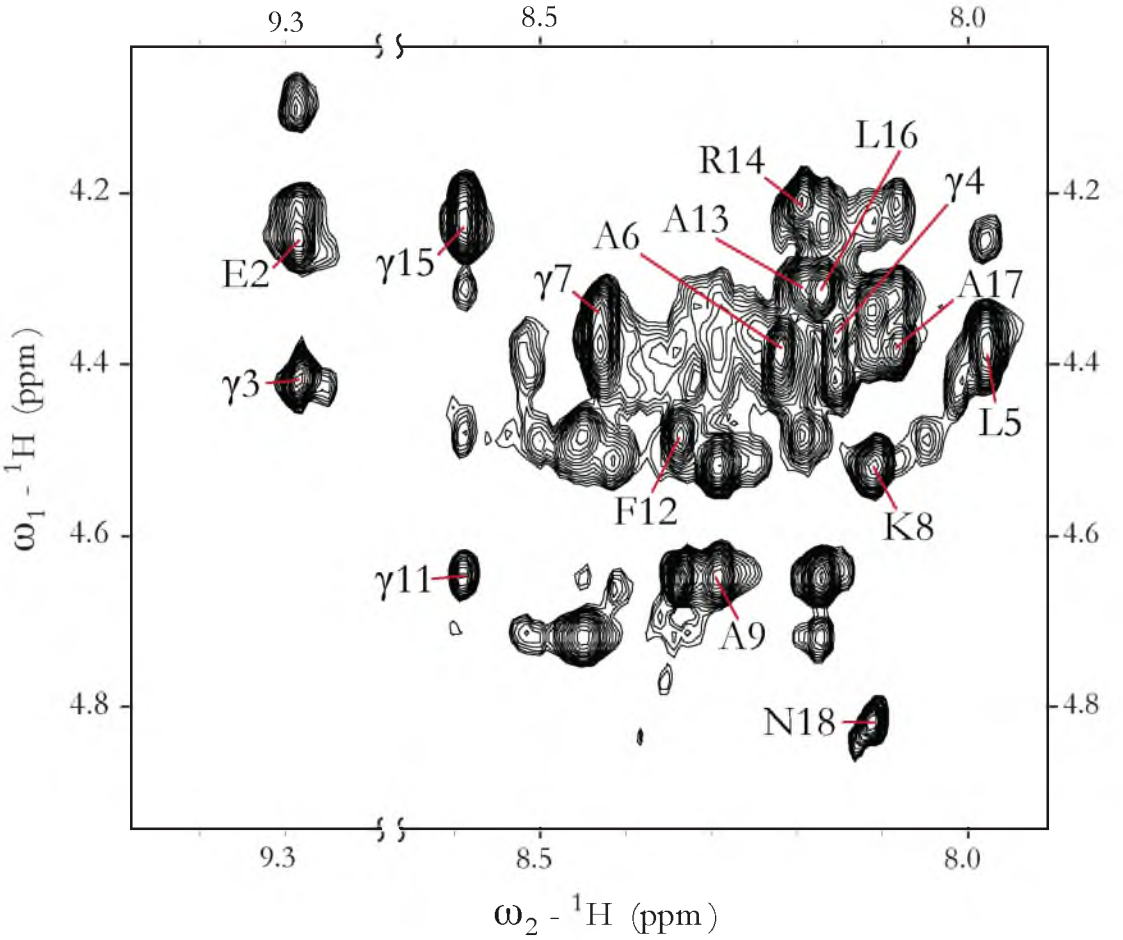

Figure 3.3. NOESY spectra and resonance assignments for con*R*/-B. The fingerprint region of the NOESY spectra for con*R*/-B is depicted with assignments of amide-alpha protons for residues 2-9 and 11-18.

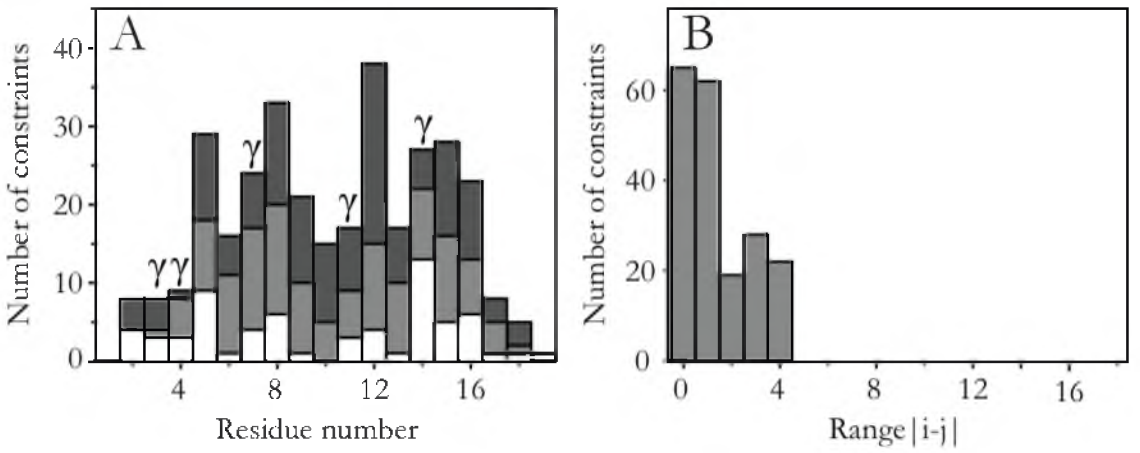

Figure 3.4: Distribution of NOE constraints for con*R*/-B. A: NOE constraints by residue for con*R*/-B structure determination. White bars are intra-residue NOEs (i:i), medium-grey are short range (i:i+1-2) and dark-grey are mid-range (i:i+3-4). **B:** number of NOE constrains by range.

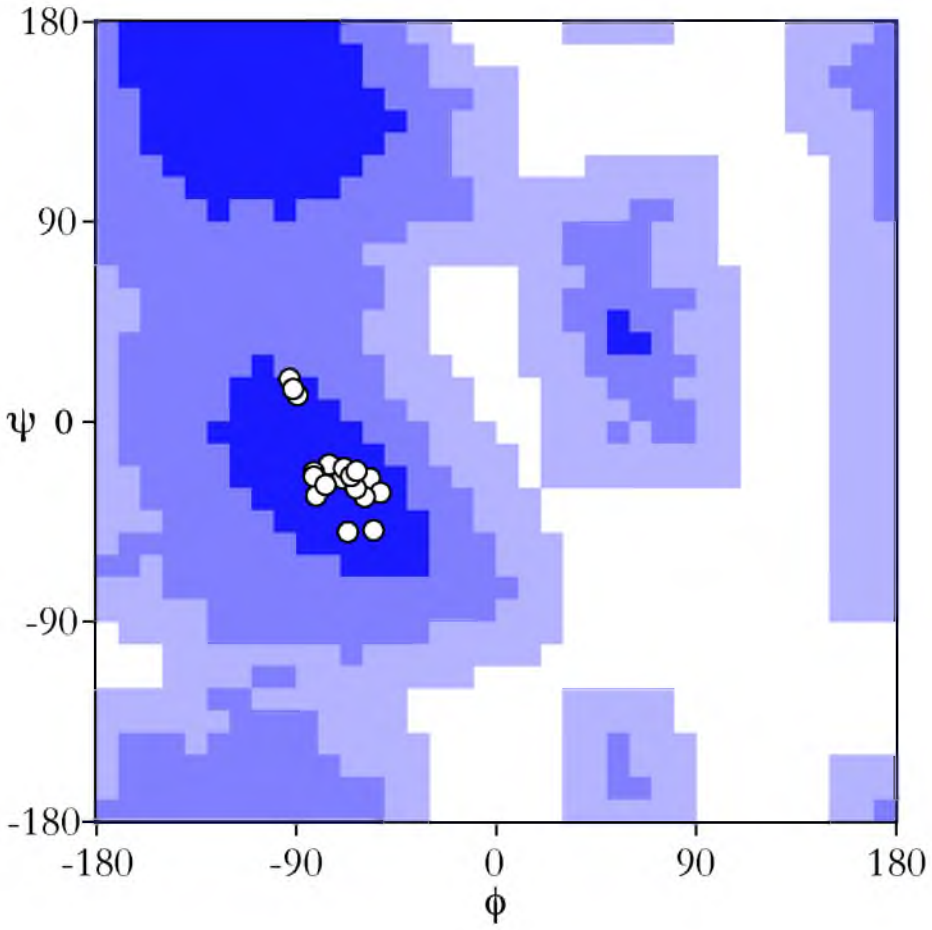

Figure 3.5: Ramachandran diagram for con*R*/-B structures calculated in CYANA. The ϕ-ψ angle combinations for con*R*/-B are found in the optimal region for a α-helix.

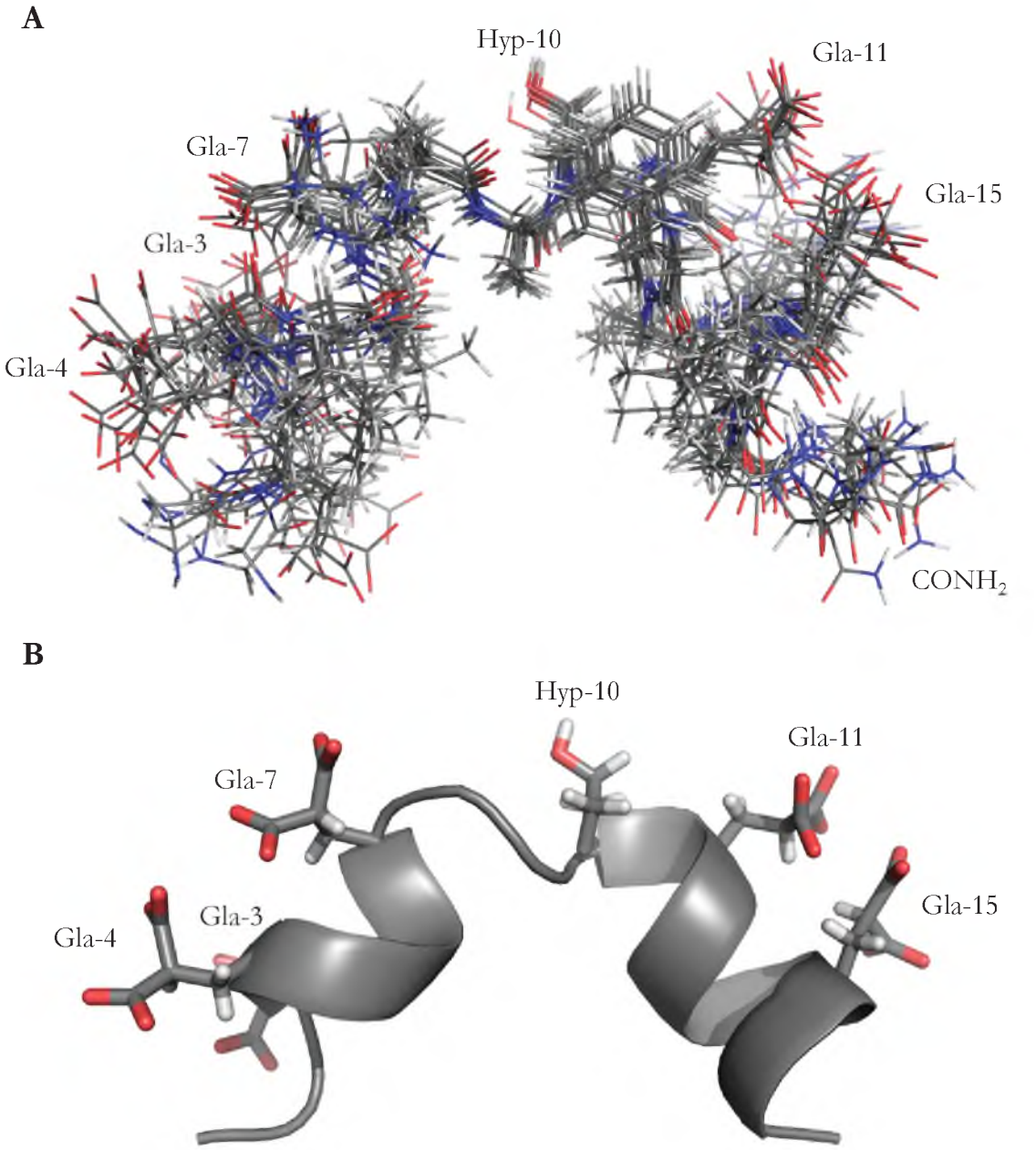

Figure 3.6: The NMR solution structure of con*R*-B. Panel A: The 10-structure ensemble of calculated solution structures for con*R*-B is shown as lines. Panel B: A single representative structure of con*R*-B is shown in cartoon representation with hydroxyproline-10 and gla residues shown as sticks. This view highlights the helix-kink-helix motif, which is a unique feature of con*R*-B.

ensemble, backbone atom positions are consistent and have an average root-mean square deviation of (RMSD) of 0.91 ± 0.16 Å. The positions of side chain atoms from leu-5 to gla-11 are also highly consistent. However, amino and carboxyl terminal residue side chains exhibit higher conformational variability and the RMSD for all atoms of the peptide is 1.45 ± 0.17 Å.

Discussion

Con*R*/-B is the most NR2B-selective conantokin known to date, and because of this was an important target for structural characterization. Additionally, con*R*/-B has a hydroxyproline residue that is uncommon among structurally characterized conantokins and would be expected to alter the standard helical conformation observed in other conantokin structures. NMR spectroscopy revealed that con*R*/-B had significant helical character, similar to other conantokins. Consistent with predictions, the helix was interrupted by the hydroxyproline residue at position 10. The NMR ensemble of con*R*/-B revealed a helix-kink-helix motif that is unique among structurally characterized conantokins.

The helix-kink-helix of con*R*/-B differs from straighter helices observed for conantokins G and T. A comparison of representative NMR structures for con*R*/-B, ConG[11], and ConT[11] is shown in Figure 3.7. The kinked conformation of con*R*/-B suggests that a straight α-helix is not the only conantokin conformation that confers NMDAR inhibition. Since con*R*/-B cannot form a straightened helix, yet retains high potency and selectivity for NMDARs, the inference can be drawn that receptor-bound con*R*/-B is not an idealized, straight helix. This interpretation suggests that other conantokins may adopt non-helical conformations upon receptor binding.

Previous structure-function studies on conantokins have shown that amino terminal residues are crucial for activity and selectivity. For example, alanine scanning mutagenesis of

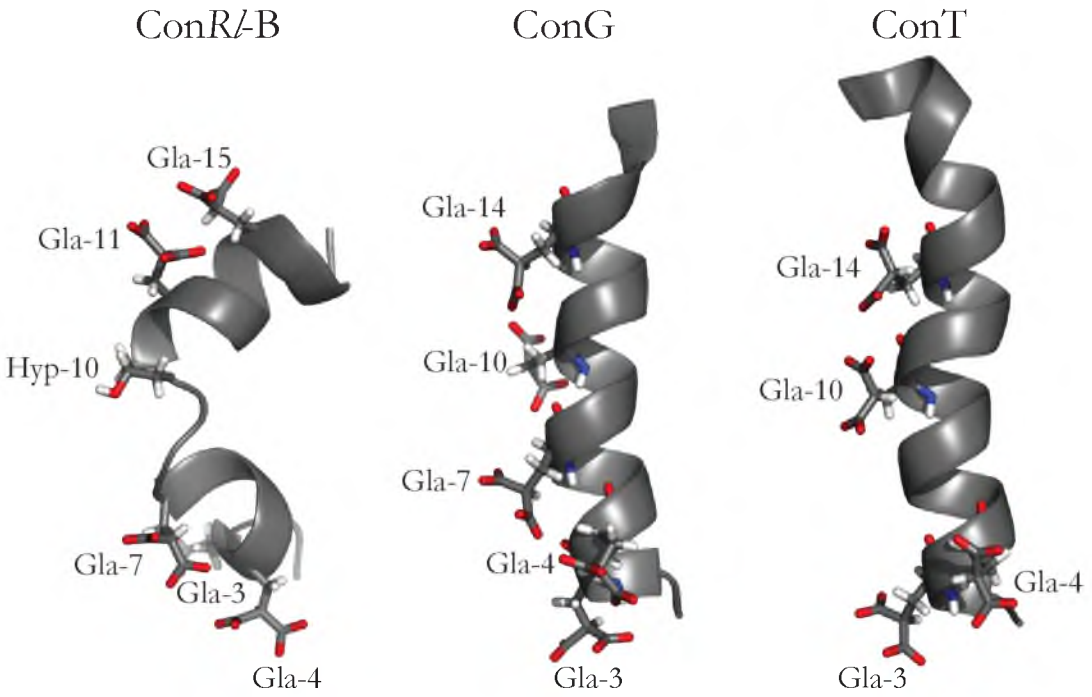

Figure 3.7: Comparison of con*Rl*-B, conG, and ConT structures. Single representative structures are shown from NMR calculated ensembles of con*Rl*-B, conG (pdb:1ONU), and ConT (pdb:1ONT). Most striking is this kinked conformation of con*Rl*-B compared to the straight helices of conG and conT.

conG shows that residues 2-5, 9, and 12 are important determinants of NMDAR inhibitor activity[14]. Similar observations have been made for ConT, where residues 1-5, 8, and 12 are important for activity, with residues 2, 4, and 5, particularly important since any change at these positions disables NMDAR inhibition[12]. Among other conantokins, whose structures have not yet been determined, amino-terminal residues are also the primary determinants of antagonist activity and selectivity[15,18,25]. These observations suggest that, as with other conantokins, the activity and specificity of con*Rl*-B are defined by amino acids presented on the amino terminal half of the kinked helix. Thus, the structural kink itself should not have a dominant influence on activity con*Rl*-B. Consistent with this hypothesis, mutation of hydroxyproline to alanine has small effects on both specificity and affinity of con*Rl*-B for NR2B NMDAR subtypes[20].

Calcium-dependent, straight helical conformations are consistently observed for conantokin peptides. However, con*R*-B was found to be a kinked-helix that, even upon receptor binding, cannot be forced into a straight helix because of conformational constraints imposed by hydroxyproline. If other conantokins use the same binding mechanism as con*R*-B, it may be that other conantokins are nonhelical during binding.

Support for the hypothesis that conantokins adopt nonhelical structure during receptor binding is found in studies that show calcium ions are not required for inhibition of NMDARs, and that conantokins retain inhibitory activity in presence of calcium chelating agents[12,26,27]. These studies suggest that either a helical conformation is not required for inhibition of NMDARs or that binding of the NMDAR independently stabilizes the helical conformation. Another interesting observation is that conantokin-P, which is active in inhibiting NMDARs, contains a long disulfide loop that could make maintenance of a helical conformation difficult[28]. However, it is important to note that the disulfide loop of conP is found near the C-terminus, where amino acid identity has less influence on NMDAR inhibitory activity. Additionally, conG analogs with engineered covalent "staples" that increase peptide helicity, are shown to be less potent than native conG[29]. So, it appears that helicity has small impacts on potency for conantokin peptides and it is likely that a non-helical conformation is formed upon receptor binding.

Although helicity has little influence on conantokin activity, the highly conserved nature of gla residues, which stabilize helical conformation, suggests that gla residues have purposeful roles. If gla residues in conantokins have purpose beyond stabilizing helical conformation, the question becomes: What functional role do gla residues have in conantokins? In order to hypothesize on this question, it is valuable to examine gla residue function in other proteins.

Gla is a modified form of glutamate that has an additional carboxyl group added posttranslationally. The result of this alteration is a nonstandard amino acid that coordinates divalent cations such as calcium. Carboxylation of glutamate to form gla is catalyzed by a vitamin-K dependent carboxylase and, in mammals, gla-containing proteins are found in blood plasma and calcified tissue[30]. In blood plasma, the gla-rich protein prothrombin is the precursor to a protease that is crucial for blood coagulation cascades[31]. Gla residues in prothrombin noncovalently tether the protein to cell membranes via a calcium ion bridge, and this interaction is important for activation of thrombin and other surface-dependent processes[31-34]. Perhaps gla residues have evolved to perform similar functions in conantokins.

Presuming that conantokin peptides evolved gla residues to perform functions similar to those observed for prothrombin, maybe it is the case that conantokins associate with the neuronal membrane prior to or during NMDAR inhibition. Tethering conotoxins to the neuronal membrane has potential evolutionary advantages for creating fast-acting and highly potent neurotoxins. For example, if conantokins became tethered to neuronal membranes, the search time for a receptor could be reduced. Confining the search to the surface of a neuron would generate a two-dimensional search from what was previously a three-dimensional search, allowing the peptides to act faster. Additionally, tethering would decrease the apparent dissociation constants for conantokins, which would help explain discrepancies observed between low concentrations of conantokins required to illicit behavioral changes and higher concentrations required for inhibition of NMDARs expressed in *Xenopus* ooctypes (Olivera lab, unpublished data). In these cases, differences in membrane composition could result in differing affinities for NMDARs. Although there is currently no experimental data to support this hypothesis, it could potentially be explored by examining

conantokin structure in the presence of lipids, or by probing for gla-mediated membrane association of conantokins.

In summary, the structure of con*R*/-B is unique among structurally characterized conantokins. It exhibits a helix-kink-helix motif that differs from other, straighter helices observed in previous structure determinations of conantokins. In the con*R*/-B structure, a straight helix is disallowed due to the steric restraints imposed by hydroxyproline at position 10. Hence, it can be assumed that con*R*/-B is not a straight helix when bound to NMDARs. This idea hints that other conantokins might not retain helicity during receptor binding, and that gla residues may have function beyond stabilizing helical structure. Consequently, alternative roles for gla residues in conantokins should be explored. Additionally, although the kinked conformation of con*R*/-B is striking, it is unlikely that the kink governs high specificity for NR2B receptors. A more reasonable hypothesis is that the amino-acid combination in the first 10 residues leads to subtype selectivity. Therefore, systematic alanine scanning and designed substitutions would be useful for understanding determinants of specificity in con*R*/-B. The results presented here and elsewhere indicate that no single residue determines subtype selectivity in conantokins. Rather, it is multiple residues, and the combinations in which they are found, that govern selective inhibition of NMDA receptor subtypes.

References

1 Haack, J. A. *et al.* Conantokin-T. A gamma-carboxyglutamate containing peptide with N-methyl-D-aspartate antagonist activity. *The Journal of Biological Chemistry* **265**, 6025-6029 (1990).

2 Mena, E. E. *et al.* Conantokin-G: a novel peptide antagonist to the N-methyl-D-aspartic acid (NMDA) receptor. *Neuroscience Letters* **118**, 241-244 (1990).

3 Hammerland, L. Conantokin-G selectively inhibits N-methyl-D-aspartate-induced currents in *Xenopus* oocytes injected with mouse brain mRNA. *European Journal of Pharmacology: Molecular Pharmacology* **226**, 239-244 (1992).

4 Prorok, M., Warder, S. E., Blandl, T. & Castellino, F. J. Calcium binding properties of synthetic gamma-carboxyglutamic acid-containing marine cone snail "sleeper" peptides, conantokin-G and conantokin-T. *Biochemistry* **35**, 16528-16534 (1996).

5 Lin, C. H., Chen, C. S., Hsu, K. S., King, D. S. & Lyu, P. C. Role of modified glutamic acid in the helical structure of conantokin-T. *Federation of European Biochemical Sciences Letters* **407**, 243-248 (1997).

6 Rigby, A. C. *et al.* Role of gamma-carboxyglutamic acid in the calcium-induced structural transition of conantokin G, a conotoxin from the marine snail *Conus geographus*. *Biochemistry* **36**, 15677-15684 (1997).

7 Warder, S. E. *et al.* The NMR solution structure of the NMDA receptor antagonist, conantokin-T, in the absence of divalent metal ions. *Federation of European Biochemical Sciences Letters* **411**, 19-26 (1997).

8 Warder, S. E. *et al.* The roles of individual gamma-carboxyglutamate residues in the solution structure and cation-dependent properties of conantokin-T. *The Journal of Biological Chemistry* **273**, 7512-7522 (1998).

9 Blandl, T., Warder, S. E., Prorok, M. & Castellino, F. J. Binding of cations to individual gamma-carboxyglutamate residues of conantokin-G and conantokin-T. *The Journal of Peptide Research* **53**, 453-464 (1999).

10 Rigby, A. C., Baleja, J. D., Furie, B. C. & Furie, B. Three-dimensional structure of a gamma-carboxyglutamic acid-containing conotoxin, conantokin G, from the marine snail *Conus geographus*: the metal-free conformer. *Biochemistry* **36**, 6906-6914 (1997).

11 Skjaerbaek, N., Nielsen, K. J., Lewis, R. J., Alewood, P. & Craik, D. J. Determination of the solution structures of conantokin-G and conantokin-T by CD and NMR spectroscopy. *The Journal of Biological Chemistry* **272**, 2291-2299 (1997).

12 Warder, S. E., Blandl, T., Klein, R. C., Castellino, F. J. & Prorok, M. Amino acid determinants for NMDA receptor inhibition by conantokin-T. *Journal of Neurochemistry* **77**, 812-822 (2001).

13 Platt, R. J. *et al.* From molecular phylogeny towards differentiating pharmacology for NMDA receptor subtypes. *Toxicon* **81**, 67-79 (2014).

14 Blandl, T., Prorok, M. & Castellino, F. J. NMDA-receptor antagonist requirements in conantokin-G. *Federation of European Biochemical Sciences Letters* **435**, 257-262 (1998).

15 Blandl, T., Zajicek, J. & Prorok, M. Sequence requirements for the N-Methyl-D-aspartate receptor antagonist activity of conantokin-R. *Journal of Biological Chemistry* **276**, 7391-7396 (2001).

16 Prorok, M. & Castellino, F. The molecular basis of conantokin antagonism of NMDA receptor function. *Current Drug Targets* **8**, 633-642 (2007).

17 Klein, R. C., Prorok, M., Galdzicki, Z. & Castellino, F. J. The amino acid residue at sequence position 5 in the conantokin peptides partially governs subunit-selective antagonism of recombinant N-methyl-D-aspartate receptors. *The Journal of Biological Chemistry* **276**, 26860-26867 (2001).

18 Twede, V. D. *et al.* Conantokin-Br from *Conus brettinghami* and selectivity determinants for the NR2D subunit of the NMDA receptor. *Biochemistry* **48**, 4063-4073 (2009).

19 Sheng, Z., Prorok, M. & Castellino, F. J. Specific determinants of conantokins that dictate their selectivity for the NR2B subunit of N-methyl-D-aspartate receptors. *Neuroscience* **170**, 703-710 (2010).

20 Gowd, K. H. *et al.* Conantokins derived from the Asprella clade impart conRl-B, an N-methyl d-aspartate receptor antagonist with a unique selectivity profile for NR2B subunits. *Biochemistry* **51**, 4685-4692 (2012).

21 Rivier, J. *et al.* Total synthesis and further characterization of the gamma-carboxyglutamate-containing "sleeper" peptide from *Conus geographus* venom. *Biochemistry* **26**, 8508-8512 (1987).

22 White, H. S. *et al.* In vitro and in vivo characterization of conantokin-R, a selective NMDA receptor antagonist isolated from the venom of the fish-hunting snail *Conus radiatus*. *The Journal of Pharmacology and Experimental Therapeutics* **292**, 425-432 (2000).

23 Jimenez, E. C. *et al.* Conantokin-L, a new NMDA receptor antagonist: determinants for anticonvulsant potency. *Epilepsy Research* **51**, 73-80 (2002).

24 Teichert, R. W. *et al.* Novel conantokins from *Conus parius* venom are specific antagonists of N-methyl-D-aspartate receptors. *The Journal of Biological Chemistry* **282**, 36905-36913 (2007).

25 Blandl, T., Warder, S. E., Prorok, M. & Castellino, F. J. Structure-function relationships of the NMDA receptor antagonist peptide, conantokin-R. *Federation of European Biochemical Sciences Letters* **470**, 139-146 (2000).

26 Klein, R. C. & Castellino, F. J. Inhibition of MK801 binding in adult rat brain sections by conantokin-G and conantokin-T. *Neuroscience Letters* **273**, 171-174 (1999).

27 Klein, R. C., Prorok, M. & Castellino, F. J. Direct binding properties of conantokins to native N-methyl-D-aspartate receptors. *The Journal of Peptide Research* **61**, 307-317 (2003).

28 Gowd, K. H. *et al.* Conantokin-P, an unusual conantokin with a long disulfide loop. *Toxicon* **52**, 203-213 (2008).

29 Platt, R. J. *et al.* Stapling mimics noncovalent interactions of gamma-carboxyglutamates in conantokins, peptidic antagonists of N-methyl-D-aspartic acid receptors. *Journal of Biological Chemistry* **287**, 20727-20736 (2012).

30 Vermeer, C. Gamma-carboxyglutamate-containing proteins and the vitamin K-dependent carboxylase. *Biochemical Journal* **266**, 625-636 (1990).

31 Bradford, H. N., Orcutt, S. J. & Krishnaswamy, S. Membrane binding by prothrombin mediates its constrained presentation to prothrombinase for cleavage. *Journal of Biological Chemistry* **288**, 27789-27800 (2013).

32 Gitel, S. N., Owen, W. G., Esmon, C. T. & Jackson, C. M. A polypeptide region of bovine prothrombin specific for binding to phospholipids. *Proceedings of the National Academy of Sciences* **70**, 1344-1348 (1973).

33 Mann, K. G., Nesheim, M. E., Church, W. R., Haley, P. & Krishnaswamy, S. Surface-dependent reactions of the vitamin K-dependent enzyme complexes. *Blood* **76**, 1-16 (1990).

34 Nelsestuen, G. L. Role of gamma-carboxyglutamic acid. An unusual protein transition required for the calcium-dependent binding of prothrombin to phospholipid. *Journal of Biological Chemistry* **251**, 5648-5656 (1976).

CHAPTER 4

HETEROLOGOUS EXPRESSION OF NMDA RECEPTOR LIGAND-BINDING DOMAINS IN *ESCHERICHIA COLI*

Preface

In order to define rules that govern subtype selective inhibition of N-methyl-D-aspartate receptors (NMDARs) by conantokin peptides, it would be useful to obtain a detailed molecular picture of the binding interface. The structure of a conantokin-NMDAR complex would elucidate mechanisms of inhibition, details of subtype selectivity, and promote development of increasingly selective conantokins. To this end, the following chapter outlines the cloning, expression, purification, and biochemical analysis of NMDAR ligand binding domains (LBDs). Unfortunately, the final experiments did not show direct interactions between LBDs and conantokins. Nonetheless, the LBD proteins produced may become useful tools for screening other NMDAR antagonists, and the negative results provided insights into mechanisms of conantokin-NMDAR binding. Furthermore, the results presented were inconclusive, and it may prove to be the case that conantokins indeed interact with the LBD albeit only weakly or only in the presence of additional protein domains and protein subunits yet to be discovered.

Introduction

To date it is unclear how and where conantokins bind NMDARs and conflicting evidence exists to support two binding mechanisms. Some studies indicate conantokins

compete with agonists at the glutamate-binding site on NR2 subunits of the NMDAR. Others suggest a noncompetitive interaction near the polyamine-binding site on the amino-terminal domain (ATD) of NR2 subunits. The details of these studies are described below.

Evidence for a noncompetitive mechanism of conantokin binding

Most evidence that conantokins bind noncompetitively to the ATD comes from studies performed on brain slices or cultured neuron preparations. For example, conG inhibition of N-methyl-D-aspartate (NMDA) stimulated responses in cultured neurons and brain slices show that conG inhibition was not overcome with saturating NMDA[1]. Also, in [^{3}H]MK-801 binding assays on rat forebrains, conG reduced spermine- and spermidine-stimulated radioligand binding but did not alter glutamate-stimulated radioligand binding[2]. Interestingly, conG analogs with tyrosine or glutamate added to the amino-terminus were observed to have polyamine-like effects that enhance [^{3}H]MK-801 binding[3]. Taken together, these studies suggest conantokins are noncompetitive NMDAR antagonists that bind to a site on the ATD that is distant and disctinct from the agonist-binding site located on the LBD.

Evidence for a competitive mechanism of conantokin binding

Contrasting evidence for a competitive mechanism of conantokins binding to the LBD comes from multiple sources. In *Xenopus* oocytes expressing NMDARs, conG inhibition of NMDA elicited current were overcome with saturating NMDA[4]. Additionally, the pre-application of conG shifts excitatory dose-response curves for glutamate, indicative of a competitive mechanism of interaction[4]. In other experimental systems, ConG inhibition of NMDA-stimulated responses in mouse cortical neurons were prevented by pre-application of NMDA[5]. Also, direct-binding studies show that NMDA and 2-amino-5-

phosphoonopentanoic acid (AP5), a known competitive antagonist of NMDARs, prevented binding of radiolabelled conG[6]. Moreover, point mutations at or near the glutamate-binding site in NMDARs were shown to alter conG potency[7,8]. As a whole, these studies suggest that conantokins are competitive NMDAR antagonists that bind to the LBD. However, when considering all of the research together, it appears that conantokins have a complex mechanism of NMDAR inhibition that may be mediated through interactions with both the LBD and the ATD.

Contents of Chapter 4

In order to examine if conantokins bind to the NMDAR LBD, I sought to create a soluble form of the LBD domain that could be studied biochemically. Full-length NMDAR clones from rat cDNA were used to generate gene constructs encoding the LBD portion of the NMDAR for NR1-2b, NR2A, NR2B, and NR2D subunits. The boundaries used to delineate NMDAR LBD domains for expression in bacteria were modeled from previous work that led to successful crystallization of LBDs from NR1 and NR2A, as well as an NR1-NR2A heterodimer[9,10]. In NMDARs two primary sequence regions, termed S1 and S2, fold together to create the ligand-binding clamshell. LBD domains described here were created by connecting S1 and S2 regions of the NMDAR with a glycine-threonine (GT) linker. The resulting proteins were expressed in bacteria, purified, and shown to bind cognate ligands. Alas, assays for conantokin-LBD binding showed no interaction. Taken in the context of previous work, the results suggest that the LBD is necessary but not sufficient for high-affinity conantokin binding.

Methods

Cloning NMDAR LBDs from rat cDNA

Clones of the NR1, NR2A, NR2B, and NR2D NMDAR subtypes from *Rattus norvegicus* cDNA libraries were used to generate LBD-encoding genes by applying polymerase incomplete primer extension (PIPE) techniques[11]. Boundaries for the LBD domain were modeled after previous work for the NR1 and NR2A subunits[10]. Sequence alignment with NR2A determined boundaries for the NR2B and NR2D subunits. DNA encoding the NMDAR LBD was placed downstream of a 8xHIS tag and inserted into a pET22b+ vector from Novagen. DNA sequences were verified through the University of Utah Health Sciences Center sequence core. Plasmid DNA was produced in DH5α bacterial cells and isolated with a plasmid purification kit (Qiagen). Plasmid DNAs were transformed using heat-shock into Origami B (Novagen) *E. coli* host strain for heterologous protein expression.

Protein expression and cell lysis

Origami B cells (Novagen) harboring NMDAR LBD encoding plasmids were grown in standard 2XYT media supplemented with 40 mM KPO_4, 5 mM glucose, 500 μg/mL amplicillin, 10μg/mL kanamycin, and 12.5 μg/mL tetracycline. Bacterial cultures were started in 2 mL media from frozen stocks and grown overnight at 37°C. Cells from overnight starter cultures were harvested with centrifugation and washed before inoculating 60 mL of fresh media. When the optical density at 600 nm (OD600) achieved a value of 0.8-1.0, bacteria from 60 mL cultures were harvested with centrifugation, washed two times with media, and used to inoculate 1 L of fresh media. One-liter cultures were grown at 37°C to an OD600 of 0.7-1.0 and then induced by cooling culture flasks in an ice bath for 5 minutes, and adding the chemical inducing agent isopropyl β-D-1-thiogalactopyanoside (IPTG).

Induced cultures were moved to a refrigerated shaking incubator maintained at 19-20°C for the protein expression phase over a period of 24-60 hours. The optimal temperature and time for protein expression was independently determined for each NMDAR subtype (see Results section). Cells were harvested with centrifugation and the resulting cell pellet was frozen at -20°C. For protein extraction, frozen cell pellets were thawed in ice-cold lysis buffer and cell lysis was performed with a combination of lysozyme treatment and sonication in lysis buffers that were optimized for each NMDAR subtype (see Results section). Insoluble portions of the bacterial lysate were removed with centrifugation and filtration. The soluble fraction was utilized for purification of NMDAR LBD proteins.

Protein purification

Clarified cell lysates containing soluble proteins were incubated with 1 mL of packed nickel-nitrilotriacetic acid (Ni-NTA) His-binding resin per 2 L of culture in batch-mode for 1-4 hours at 4°C. The resin was washed with wash buffer containing 0.1 M HEPES pH 7, 0.25 M NaCl, 50 mM glutamate, 5 mM glycine, and 25 mM imidazole and protein was eluted in elution buffer of the same composition but containing 250 mM imidazole.

Ni-NTA eluted proteins went through two stages of additional purification using fast-protein-liquid-chromatography (FPLC) on an AKTA FPLC system (GE life sciences). Size exclusion chromatography (SEC) was performed on a Superdex-75 gel filtration column and SEC buffers were optimized independently for each NMDAR LBD subtype (see Results section). Depending on the calculated iso-electric point for each protein subtype, cation or anion exchange chromatography were used as the final purification step. Ion exchange buffers were optimized independently for each protein subtype (see Results section). Protein was monitored through various stages of purification using sodium dodecyl sulfate

polyacrylamide gel electrophoresis (SDS-PAGE), following protocols adapted after Schägger and Von Jagow[12]. Protein bands were visualized by staining with coomassie blue or silver.

Results

Cloning of NMDAR LBDs

Genes encoding NMDAR LBDs were successfully integrated into pET-22b(+) vectors for the NR1-2b, NR2A, NR2B, and NR2D NMDAR subtypes. Figure 4.1 illustrates the approach for creating NMDAR LBDs from full length NMDARs. Linking two stretches of amino acid residues, termed S1 and S2 in the full-length NMDAR, created the LBD domains that were ultimately expressed in bacteria. DNAs encoding the S1 and S2 regions were cloned out of full-length NMDAR genes from rat, and S1 was connected to S2 with a two amino-acid glycine-threonine (GT). The LBD was placed downstream of a 8xHIS tag for purification and DNAs were sequenced for verification of proper gene construction.

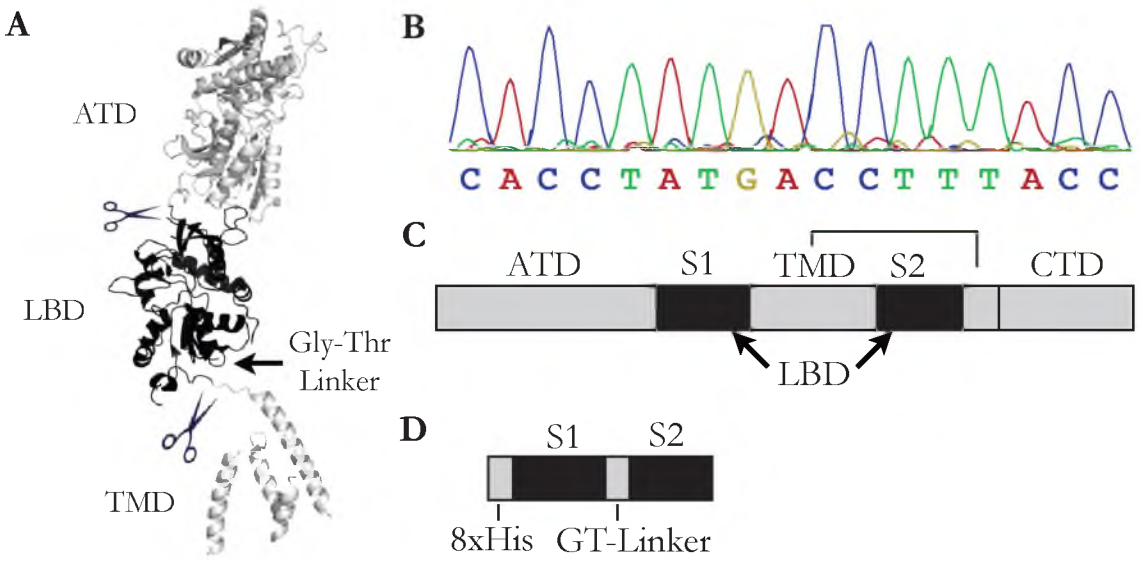

Figure 4.1: Cloning NMDAR LBDs A: LBD boundaries mapped onto the crystal structure of NR2B (pdb:4PE5). The LBD is highlighted in black. **B:** A DNA sequencing read from NR2B verifies proper cloning of LBDs. **C:** Domain organization of a NMDAR. **D:** Subdomain organization of a NMDAR LBD.

Bacterial host strains for protein expression

Two bacterial host strains were transformed with the PET-22b(+) vector containing DNA encoding NMDAR LBDs, and these were tested for protein expression. As shown by SDS-PAGE of total protein, the Rosetta (Novagen) failed to express LBD protein and the OrigamiB (Novagen) cell strain expressed LBD protein at high levels. Therefore the OrigamiB host strain was used in subsequent experiments to optimize protein expression.

NMDAR LBDs express as insoluble protein

Typical protein expression conditions, with bacterial growth temperatures from 20-37 °C and induction with 0.5-1 mM IPTG, resulted in high protein yield, but little or none of this protein was soluble. Figure 4.2 illustrates representative results obtained for these initial NR2D-LBD expression tests. Similar results were obtained for all NMDAR LBD subtypes tested.

The preponderance of insoluble protein, expressed under standard culture conditions, led to two independent approaches for generating folded and functional NMDAR LBD proteins. One approach was to denature, purify, and refold the insoluble proteins; a second approach was to optimize culture conditions to encourage expression of soluble protein.

I estimated a yield of >30mg insoluble protein per liter of culture. Denaturation and purification of denatured protein led to large yields of highly pure protein. However, refolding resulted in significant loss via protein precipitation (data not shown). Ultimately, optimization of culture conditions, selecting for those conditions that favored expression of soluble protein, was the most effective approach for obtaining soluble LBD protein

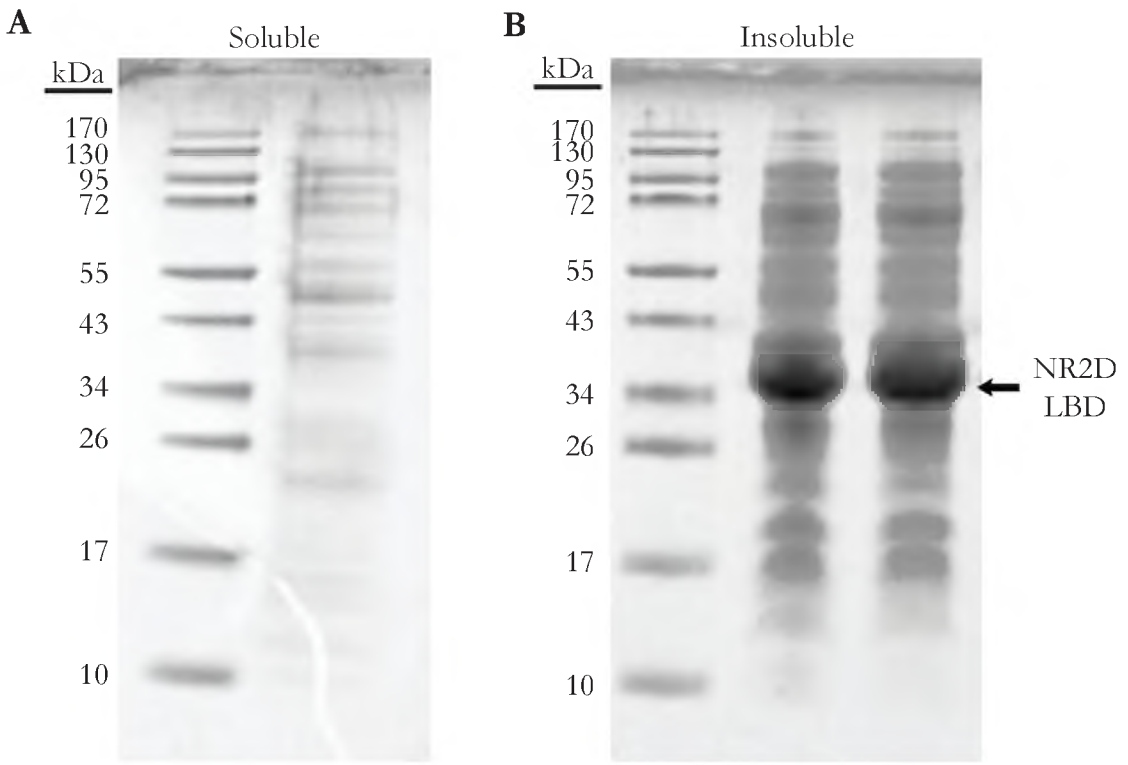

Figure 4.2: NMDAR LBDs express as insoluble proteins. A: SDS-PAGE analysis of soluble protein yield for the NR2D LBD induced with 0.5 mM IPTG for 24 hours at 20 °C. **B:** Insoluble protein yield from the same culture. NMDAR LBDs express strongly and are found in the insoluble portion of bacterial lysates.

Assay development

Soluble protein yield was not evident in SDS-PAGE analysis of crude bacterial lysates; meaning improvements in the expression of soluble protein would not be detectable with the standard assay. To overcome this, I developed a nickel-nitrilotriacetic acid (Ni-NTA) pull-down assay to analyze soluble protein yield. In the pull-down assay, crude bacterial extracts were clarified by centrifugation and the clarified extract was combined with Ni-NTA his-binding resin to capture soluble LBD proteins. To detect captured soluble protein, Ni-NTA resin was collected by centrifugation, washed in buffer, and suspended directly in SDS loading buffer for analysis by SDS-PAGE. Under these conditions, the very low levels of soluble NMDAR LBD proteins were enriched, allowing for detection and

comparison of soluble LBD protein yield as a function of different culture conditions.

Optimizing soluble protein yield

Testing the variables of temperature and IPTG concentration showed that lowering the temperature and reducing the IPTG concentration increased soluble protein yield. Reducing the IPTG concentration had the opposite effect on total protein yield, which decreased, implying that lower overall protein expression encourages the soluble form to accumulate. An IPTG concentration of 5μM with an expression temperature of 20°C provided the highest yields of soluble LBD proteins (Figure 4.3). Similar results were obtained for LBD proteins from each of the NR1, NR2A, NR2B, and NR2D subunits.

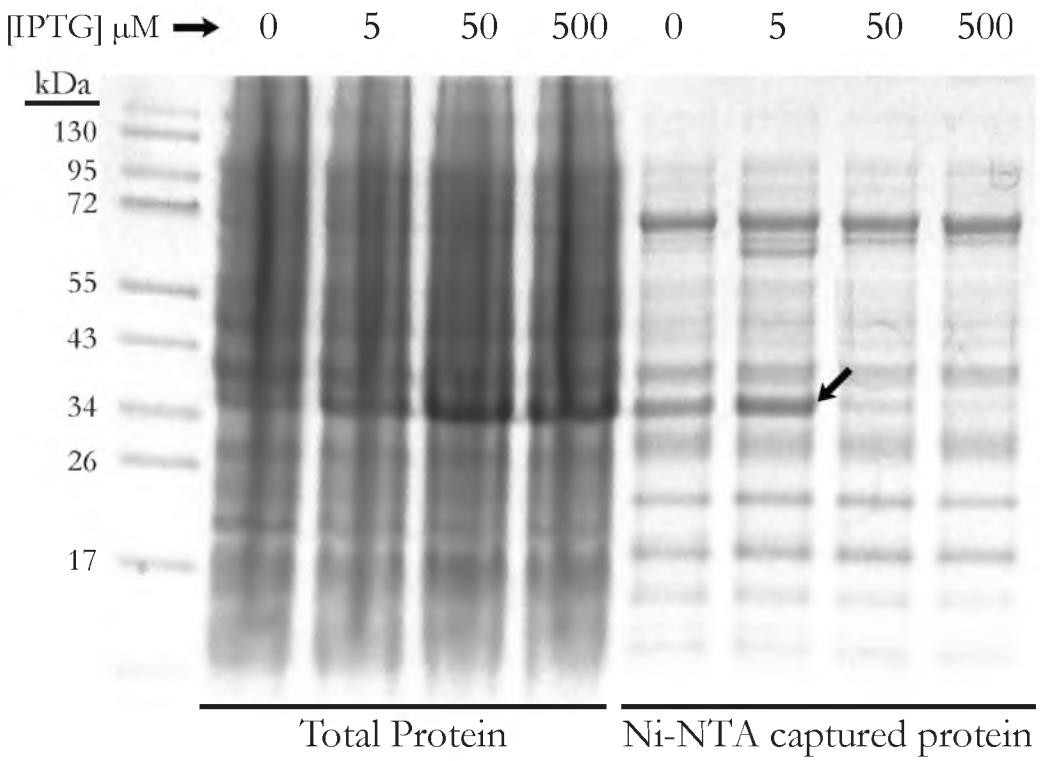

Figure 4.3 Low IPTG concentrations yield more soluble LBD protein. SDS-PAGE analysis of the NR2B LBD expressed at 20°C for 30 hours with different IPTG concentrations. Total protein yield increased with increasing IPTG concentration. However, yield of Ni-NTA captured protein (soluble) was optimal at 5μM IPTG (black arrow). IPTG concentrations above 5 μM resulted in decreased or undetectable yields of soluble protein.

In addition to induction temperature and IPTG concentration, additional variables were optimized, including the OD600 at induction, the duration of expression, and the composition of the lysis buffer (pH, ionic strength, additives). Figure 4.4 shows results obtained for the NMDAR NR2B LBD protein while optimizing OD600 at induction, duration of expression, and lysis buffer composition. For the NR2B LBD, an OD of 0.9 at induction, 30 hours expression time, and the TEB5 lysis buffer containing 0.1 M Tris pH 8.2, 50 mM glutamate, and 50 mM glycine were optimal for producing soluble protein.

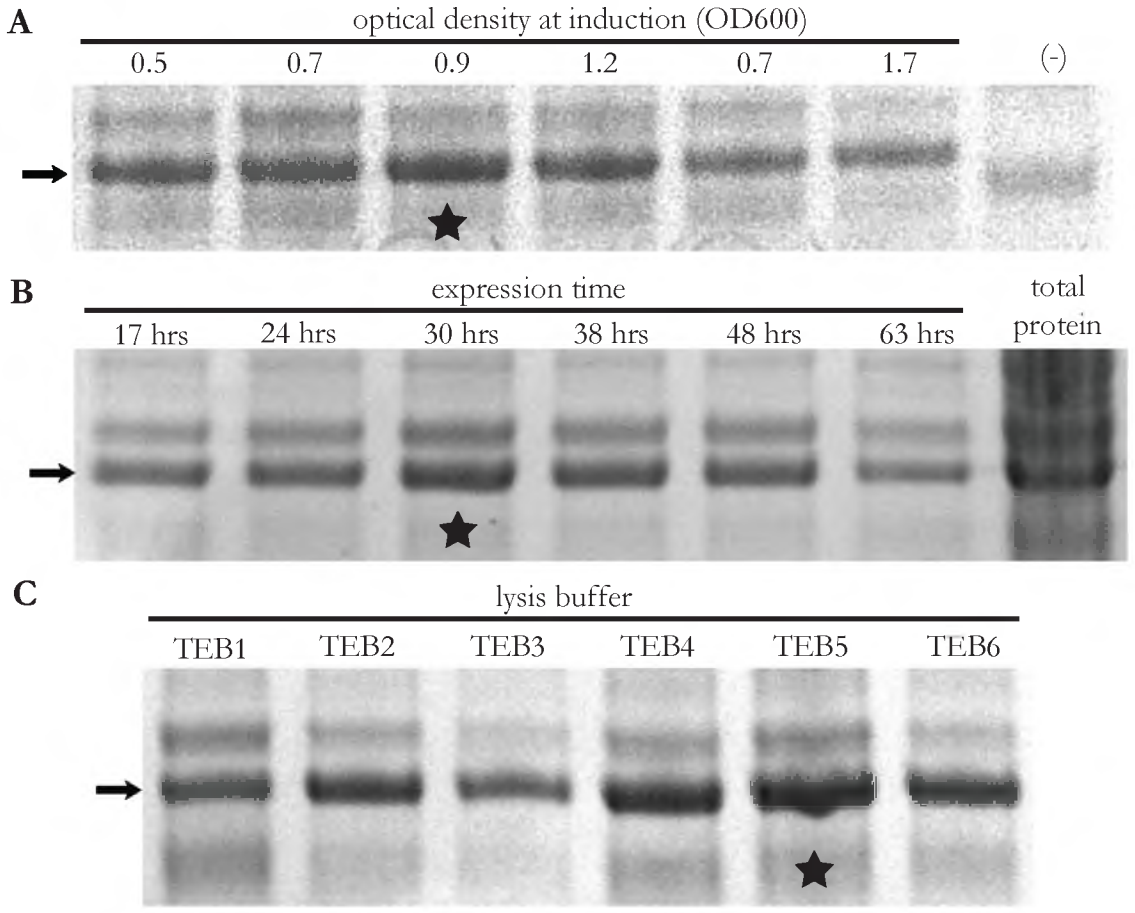

Figure 4.4: Optimization of induction timing, expression time, and lysis buffers. SDS-PAGE analyses of soluble protein yield during optimization of culture conditions for the NR2B LBD protein. The best conditions are marked with stars and arrows indicate position of the protein band corresponding to the NR2B LBD protein. **A:** Optimization of optical density at induction. **B:** Optimization of expression time. **C:** Optimization of lysis buffer.

Cell lysis, protein capture, and purification of NMDAR LBDs

Following optimization of protein expression and Ni-NTA capture, further purification of the captured proteins was necessary. NMDAR LBD proteins were eluted from Ni-NTA resin using high imidazole concentrations and purified with a combination of size exclusion and ion exchange chromatography. Optimization of buffers and purification conditions for each of the purification steps was necessary to prevent protein precipitation and product loss. Figure 4.5 shows chromatograms from SEC and ion-exchange purification of the NR2B LBD protein after optimization of protein purification conditions.

After the three-stage purification, highly purified proteins were obtained for all four NMDAR LBD protein subunits tested. The optimized conditions for protein expression and purification of each NMDAR LBD subtype are provided in Table 4.1, along with yields per liter of culture. Other parameters, not shown in Table 4.1, were found to be similar for all NMDAR LBD subtypes; these included expression temperature (19-20 °C optimal), OD at induction (0.7 - 1 optimal), and IPTG concentration (0-5 μM optimal).

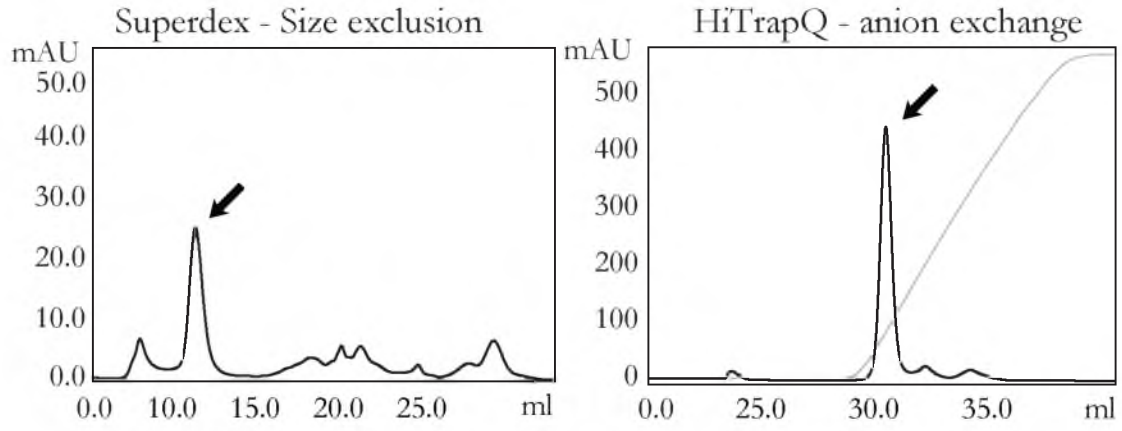

Figure 4.5: FPLC Purification of NMDAR LBD proteins. The results of size exclusion and ion exchange chromatography for the NR2B LBD protein are shown. Arrows indicate absorbance peaks corresponding to the LBD protein. The grey line on the right panel shows changes in buffer conductivity while eluting with a salt gradient from 50mM to 1M NaCl. After ion-exchange chromatography, the NMDAR LBD proteins are highly purified.

Table 4.1: Optimized expression and purification conditions for NMDAR LBD proteins

LBD subunit	[IPTG] (μM)	Induction time (hrs)	Lysis buffer	SEC buffer	IEC technique/ starting buffer	Protein yield per 3L culture
NR1	5-30	48	0.1 M Tris pH 8.2 50 mM glutamate 50 mM glycine 0.5% w/v CHAPS 1 mM PMSF 50 μg/mL lysozyme	25 mM MES pH 6.5 250 mM NaCl 10 mM glycine	Cation Exchange 25 mM MES pH 6.5 10 mM glycine 100 mM NaCl	0.8-1.2 mg
NR2A	0-5	40-63	0.1 M Tris pH 8.2 50 mM glutamate 50 mM glycine 0.5% w/v CHAPS 1 mM PMSF 50 μg/mL lysozyme	25 mM MES pH 6.5 150 mM NaCl 10 mM glutamate	Cation Exchange 25 mM MES pH 6.5 100-150 mM NaCl 10 mM glutamate	0.6-0.9 mg
NR2B	0-5	30-48	0.1 M Tris pH 8.2 50 mM glutamate 50 mM glycine 0.5% w/v CHAPS 1 mM PMSF 50 μg/mL lysozyme	25 mM Tris pH 8.5 50mM NaCl 10 mM glutamate	Anion Exchange 25 mM Tris pH 8.0 50 mM NaCl	2.2-2.8 mg
NR2D	0-5	76+	0.1 M Tris pH 8.2 50 mM glutamate 50 mM glycine 0.5% w/v CHAPS 1 mM PMSF 50 μg/mL lysozyme	25 mM Tris pH 8.5 50 mM NaCl 10 mM glutamate	*Anion Exchange* 25 mM Tris pH 8.0 100 mm NaCl *Isocratic elution at 100mM NaCl*	0.4-0.6 mg

Limited proteolysis of NMDAR LBD proteins

Limited proteolysis is a technique used to examine stability of soluble proteins and protein domains, and changes in proteolysis profiles can reflect conformational changes associated with protein-protein or protein-ligand interactions[13-15]. The technique incorporates protease enzymes, which break peptide bonds and digest proteins into smaller pieces. Proteolysis profiles reveal stable protein domains, which are seen as protease-resistant protein bands in SDS-PAGE analysis. To examine the stability of purified NMDAR LBD proteins, and to test for the possibility of ligand-LBD interactions, LBD proteins went through limited proteolysis experiments under various conditions with and without potential ligands.

At first, NMDAR LBD proteins were treated with either trypsin or chymotrypsin and the products of these reactions were analyzed by SDS-PAGE. Figure 4.6 shows the proteolysis profile obtained for the NR2B LBD following a 60-minute digest at 25 °C with varied amounts of the proteases trypsin and chymotrypsin. In the proteolysis profiles, some reaction products accumulated more than others, which can be seen as darker protein bands in the gel image. Accumulating proteolysis products suggested that the NR2B LBD had stable domains that were resistant to proteolysis. Also, the observation that the NR2B LBD resisted complete degradation, at least at lower enzyme concentrations, suggested that the protein had adopted a stable tertiary structure. Altogether, results indicated that the LBD protein had a stable fold and that limited proteolysis could be applied to test for ligand binding.

After determining that LBD proteins were adopting stable folds, limited proteolysis assays were further used to examine binding of ligands to NMDAR LBDs. First, the NR2B LBD was challenged with saturating glutamate to see if this ligand would alter results of

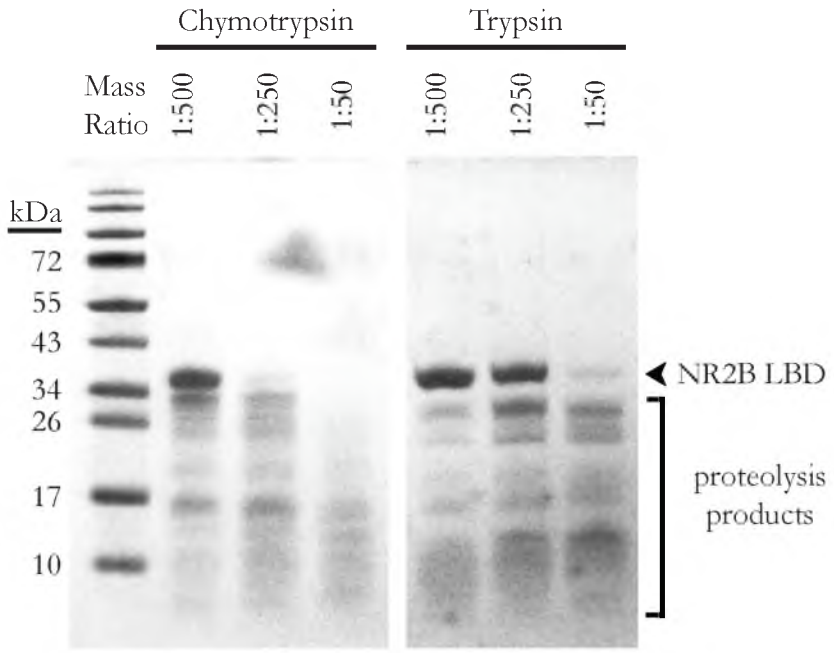

Figure 4.6: Limited proteolysis profiles for the LBD reveal stable, folded protein. SDS-PAGE analysis of proteolysis reaction products from the NR2B LBD protein after incubation with chymotrypsin or trypsin for 60 minutes at 25 °C. Mass ratio indicates the ratio of protease to LBD measured by mass. For smaller mass ratios, the NR2B LBD was resistant to proteolysis, indicating stable tertiary structure. Accumulation of particular proteolysis products indicates the presence of stable domains within the LBD. The level of the protein band corresponding to full-length NR2B LBD is specified with an arrowhead.

limited proteolysis. The binding constant for glutamate on NMDA receptor tetramers is ~1 μM; 100μM glutamate was used to achieve saturation in the assay. The results are presented in Figure 4.7, which shows that glutamate had a strong protective effect on NR2B; glutamate slowed the proteolysis of the NR2B LBD by chymotrypsin. The protective effect of glutamate was not seen for a control protein (p56α), which was not expected to interact with glutamate. Contrasting effects of glutamate on the NR2B LBD and on p56α indicates that protection from proteolysis by glutamate was mediated through interaction of glutamate with the LBD and not through inhibition of the protease by glutamate. These results suggest that the NR2B LBD protein binds to glutamate and is likely to have a structure similar to the glutamate-binding LBD domain of a complete NMDAR.

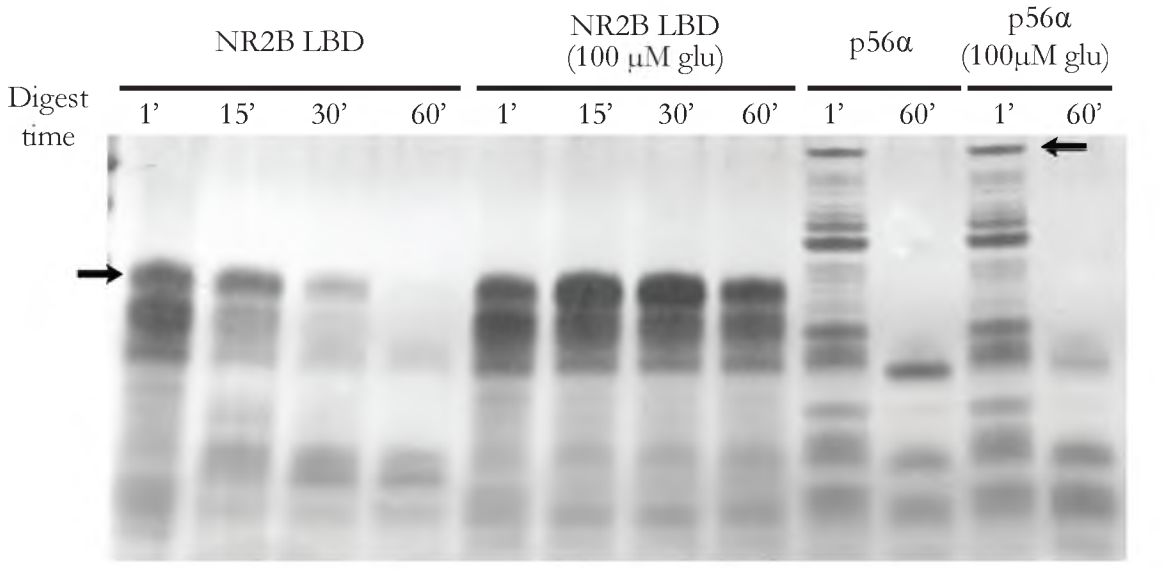

Figure 4.7: Glutamate protects the NR2B LBD from proteolysis with chymotrypsin. SDS-PAGE analysis of proteolysis reaction products over time, with experiments performed in the presence or absence of glutamate. The full length NR2B LBD (left arrow) was completely degraded after 60-minute exposure to chymotrypsin at 30 °C with a mass ratio of 1:50. In the presence of 100 μM glutamate, proteolysis of the LBD by chymotrypsin was significantly slowed and the full length LBD protein remained detectable after 60 minutes. In contrast, the control protein p56α (right arrow) was not protected by glutamate. These results show that the NR2B LBD protein interacts with glutamate.

Because glutamate exerted a protective effect on the NR2B LBD protein in proteolysis assays, additional experiments were performed utilizing the agonists NMDA and glycine, as well as the antagonists (2R)-amino-5-phsphonovaleric acid (AP-5), conantokin *R*/-B, and conantokin *R*/-E[V10O]. Interestingly, the NMDAR antagonist AP-5 had protective effects similar to those observed for glutamate and NMDA (Figure 4.8). This result would be expected, however, because any molecule that stabilizes the conformation of the LBD should limit access to protease cleavage sites and slow the rate of proteolysis. Furthermore, AP5 is known to bind to the same site as glutamate and would therefore be expected to have similar effects in proteolysis assays. In contrast to the small molecule agonists and antagonists that were tested, conantokin peptides failed to protect LBD proteins from proteolysis (data not shown). The results with conantokins could mean that conantokins do

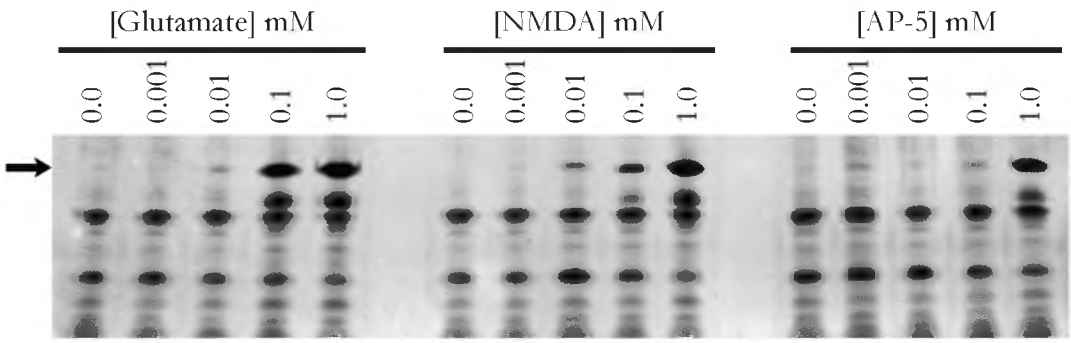

Figure 4.8: Protection from proteolysis by LBD-binding agonists and antagonists. Proteolysis reaction products analyzed by SDS-PAGE show that the NR2B LBD protein was protected against proteolysis in a concentration-dependent manner for the agonists glutamate and NMDA, and for the antagonist AP-5. These proteolysis reactions were performed with a mass ratio of 1:50 with incubation at 30 °C for 120 minutes. The arrow indicates the position of the full length LBD protein.

not bind to the NR2B LBD protein, that conantokin-LBD interactions were transient and not detected by proteolysis, or that the conantokin peptides were degraded by protease during the assay.

In NMDAR tetramers, NR1 subunits bind glycine and NR2 subunits bind glutamate. Together, the co-agonists glycine and glutamate act to open the ion channel pore. Because of this, I hypothesized that the NR1-LBD would be protected by glycine but not by glutamate or NMDA. Figure 4.9 compares proteolysis profiles obtained for NR1, NR2A, NR2B, and NR2D LBDs in the presence and absence of glycine, glutamate, and NMDA. Consistent with expectations, glycine protected the NR1 LBD protein but did not protect the NR2-LBD proteins. Also consistent with agonist-specificity, glutamate and NMDA protected all NR2-LBD proteins but not the NR1 LBD protein. Intriguingly, the degree of ligand-mediated protection for the NR2D LBD was weak by comparison with protection observed for NR2A and NR2B LBD proteins. Weaker protection may reflect weaker interaction of ligand with the NR2D LBD, or it may indicate that a portion of the NR2D LBD was improperly folded.

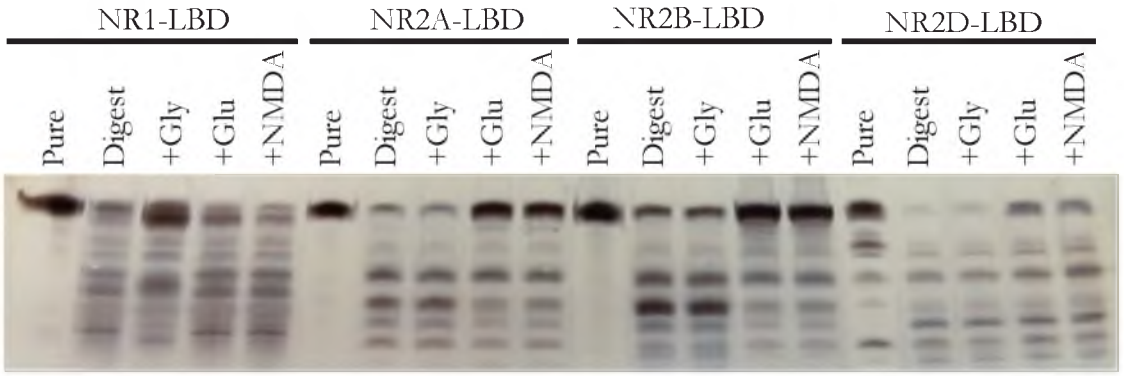

Figure 4.9: Agonist protection of NR1, NR2A, NR2B, and NR2D LBD proteins. Proteolysis products observed with SDS-PAGE after trypsin digestions in the presence and absence of various ligands. A mass ratio of 1:50 was used with a digestion time of 60 minutes at 30 °C. The assay tested protective effects of the ligands glycine, glutamate, and NMDA. Glycine protected the NR1 LBD protein, while glutamate and NMDA protected NR2 LBD proteins. These results are consistent with expectations for cognate agonists of the NR1 and NR2 subunits of the NMDAR.

Probing conantokin-NMDAR binding with SEC

Conantokin to LBD interactions were also examined by comparing elution times in SEC chromatograms. Elution times in SEC are dependent on the shape and size of protein molecules. In SEC, these features are described as the radius of gyration, which can be changed by binding to other molecules. Since the NMDAR LBD proteins range from 33.3 - 35.0 kDa and con*R*-B is 2.2 kDa, the expected size difference between the LBD and a conantokin-bound LBD (~6%) was potentially observable with SEC. However, in addition to changes in radius of gyration, the off-rate of binding must be slow to observe effects with SEC. Fortunately, con*R*-B is known to have slow off-rate kinetics in electrophysiology experiments examining NMDAR tetramers associated with the cell membrane (Olivera Lab, personal communication), and was therefore used to examine conantokin-LBD binding with SEC.

Unfortunately, elution-times were identical for the NR2B LBD protein with and without saturating con*R*-B (data not shown). These results could indicate that the LBD

protein domain is insufficient for productive toxin binding or that the uncomplexed LBD and the toxin-LBD complex have highly similar radii of gyration that have identical elution times when analyzed with SEC. To address the concern that complexed and uncomplexed LBD proteins have imperceptibly different radii of gyration, I repeated the experiment, this time examining elution times for con*Rl*-B[L5Y] in the presence and absence of LBD proteins. Con*Rl*-B[L5Y] retains similar NMDAR inhibitory activity to native con*Rl-B*[16], but is visible with absorbance at 280nm and is therefore directly detected in SEC elution profiles. Disappointingly, no difference was observed for elution time of con*Rl*-B[L5Y] in the presence and absence of the NR2B LBD protein (Figure 4.10). Therefore, the NR2B LBD is insufficient for productive toxin binding, or the complexed state is not stable enough to observe with SEC. Since the complexed state is known to be highly stable in fully assembled NMDARs

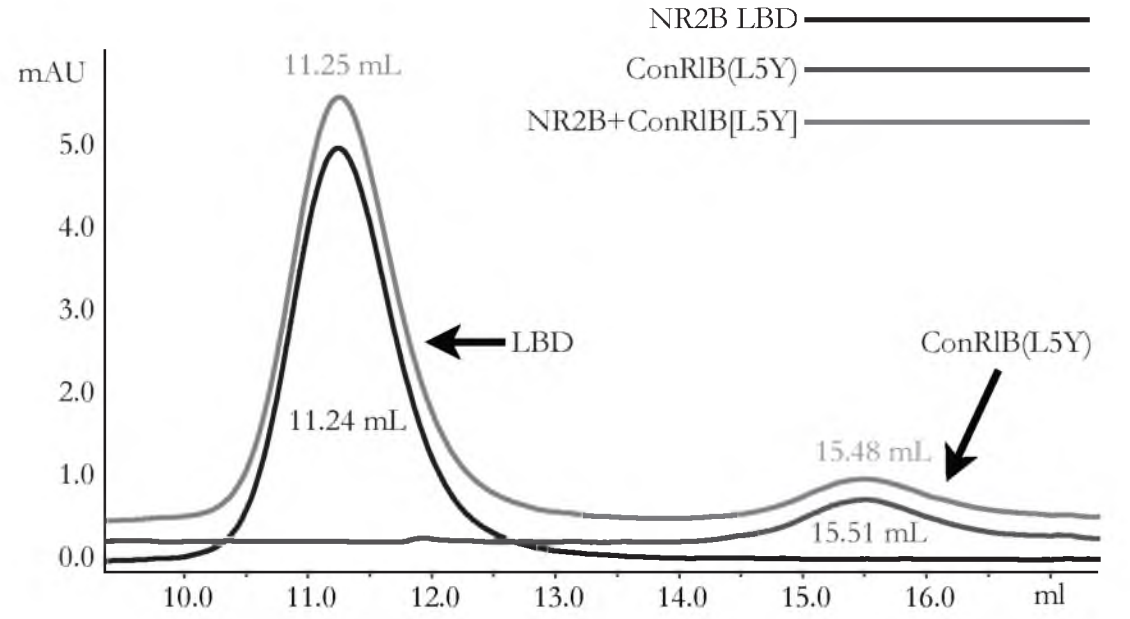

Figure 4.10: SEC chromatography shows no binding of conantokins to LBD proteins. Superdex75 SEC chromatographs for LBD, conantokin, and LBD+conantokin (1:1 molar ratio). No differences in retention time were observed for either conantokin or LBD protein, indicated with arrows, suggesting that the proteins did not interact.

Summary

Genes encoding the LBD from four different NMDAR subunits were cloned into pET-22a expression vectors, transformed into OrigamiB (Novagen) host strains, expressed as soluble proteins, purified with liquid chromatography, and tested for molecular interaction with ligands using a proteolysis assay and by SEC. Optimizations of protein expression and purification conditions for each NMDAR subtype resulted in yields of 0.6-2.8 mg per 3 L of culture. In proteolysis assays, soluble NMDAR-LBD proteins were protected by cognate ligands, which suggests that the NMDAR LBD proteins adopt a structure that is biochemically active and similar to the structure of this domain as found in the context of the assembled NMDAR tetramer. Changes in the proteolysis profile indicated a molecular response to known agonists and antagonists; however, this was not the case in tests with conantokins. The NR2B LBD tested was not protected by conantokin in the proteolysis assay, and neither LBD nor conantokin appeared to change behavior in SEC experiments. Although there are alternative explanations for these negative results, the simplest explanation is that molecular interaction between isolated LBD protein and conantokin is weak or nonexistent.

Discussion

Protein expression and purification

The NMDAR LBD constructs described here were modeled after those previously used for crystallization of NMDAR LBD monomers and heterodimers[9,10]. Those NMDA-LBD constructs were also modeled from earlier work on AMPA type glutamate receptors[17,18]. Compared to previously reported results, my yield per liter of culture for NMDAR LBD proteins was low with less than 1 mg/L culture. For well-behaved soluble proteins, a yield greater than 10 mg/L culture is often expected. With the LBD yields

obtained here, and the protein concentrations necessary for crystallization, a very large-scale expression approach would be necessary. Such approaches are both costly and time consuming. Therefore, alternative methods of heterologous protein expression may be desirable for creating complicated mammalian proteins.

Beyond bacteria, insect cells are another platform for heterologous expression of proteins that may be useful for expression of proteins from eukaryotes. Interestingly, the initial characterization of NR1 S1S2 constructs used proteins expressed from insect cell derived expression systems[19,20]. Presumably, one would desire to express a eukaryotic protein in a eukaryotic host. Eukaryotic hosts potentially express chaperone proteins and cofactors that help with expression and folding of proteins. Although insect cell expression systems have their own technical challenges, they are gaining popularity for the expression of complex eukaryotic proteins and multiprotein complexes[21-23]. Noteworthy is the observation that insect cell expression systems were used for structure determination of the tetrameric $NR1_2/NR2B_2$ NMDAR containing the ATD, LBD, and partial transmembrane helices published earlier this year[24]. Results from many current studies indicate that when recombinant proteins from eukaryotic organisms are desired, it may be of benefit to explore expression systems derived from eukaryotes as opposed to prokaryotes.

Limited proteolysis of NMDAR LBDs

Proteolysis assays performed on the NMDAR LBD proteins for NR1-2b, NR2A, NR2B, and NR2D provided evidence that soluble, purified LBD proteins were correctly folded. These proteins were not found to bind conantokin peptides, but they can now be utilized to screen novel agonists or antagonists that interact with the LBD of the NMDAR.

The negative results for conantokin binding in proteolysis assays are nonetheless revealing and should not be regarded as failures. Some research has indicated that

conantokins are competitive antagonists binding at the LBD[5,7,8] and other research has suggested conantokins are noncompetitive antagonists that bind the ATD[2,3]. The results presented here illuminate that LBD monomers are not sufficient for conantokin binding, yet previous studies illustrate the LBD is important for conantokin binding.

Taken in the context of previous studies, our results indicate that conantokins likely require the LBD and additional protein domains or subunits for tight binding. Because previous studies indicate the ATD is a site of conantokin interaction, it would be beneficial to examine conantokin interactions with ATD-LBD protein constructs. Accordingly, optimization of NMDAR ATD-LBD protein expression and purification is an ongoing project in the Horvath laboratory. Although the ATD is most likely the missing piece for conantokin-NMDAR interactions, other hypotheses should not be neglected.

Some studies have noted that NR1 splice variation can influence conantokin efficacy[5,7]. This indicates that the conantokin-binding site may be created at the interface between NR1 and NR2 subunits, as these assemble to form the complete NMDAR tetramer. Fortunately, the recent publication of a tetrameric NMDAR crystal structure[24] makes this hypothesis testable. Difference maps calculated by comparing structure factors measured for crystals of NMDAR and conantokin-NMDAR cocrystals are expected to reveal the exact location of conantokin binding. Although the current resolution limit for NMDAR crystal diffraction is 4 Å, crystals for the conantokin-receptor complex may perform better. Furthermore, even at 4 Å resolution, information regarding the location of the conantokin binding site would be invaluable in guiding design of future domain constructs to better discern molecular interactions between conantokins and the NMDAR.

Conantokins are rich in gla residues. By analogy with the role of gla residues in other proteins, I suggest that one possible explanation for failure to detect molecular interaction

between conantokins and NMDAR LBDs has something to do with removal of the LBD domains from cell membranes. Gla residues in proteins such as pro-thrombin are known to tether proteins to negatively charged groups on cell membranes via mutual interaction with bridging calcium ions[25,26]. Perhaps gla residues perform a similar function for conantokins. If such is the case, membrane-gla residue interactions may be essential for productive binding of conantokins to NMDARs. Support for this idea comes from mutagenesis studies which show that residues on the NMDAR that are critical for sensitivity to conantokin inhibition are located near the membrane when mapped onto the NMDAR crystal structure. Similarity with other gla-rich proteins and these mutagenesis studies suggest that conantokins may be tethered with the neuronal membrane during NMDAR binding.

A diagram of the membrane-tethered model for NMDAR binding is shown in Figure 4.11. In this scenario, combining energy realized by membrane association and energy realized from NMDAR interactions increases affinity of conantokins for NMDARs. In the absence of membrane association, overall binding energy is reduced, explaining why isolated LBDs showed interaction with conantokin. The membrane-tethered model could also explain why the concentration of conantokin required to observe behavioral effects in animal assays is lower than the concentration of conantokin required to inhibit NMDARs expressed on the surface of *Xenopus* oocytes. The energy component derived from membrane association would depend on membrane composition. Since oocytes and neurons have different membrane compositions, it is likely that binding affinity is also different. The binding affinity reduction incurred by nonnative membrane composition is probably less than that incurred by removal of the membrane altogether, explaining why conantokins inhibit NMDARs expressed on the surface of *Xenopus* oocytes but showed no molecular interaction with isolated LBDs in experiments described in this chapter.

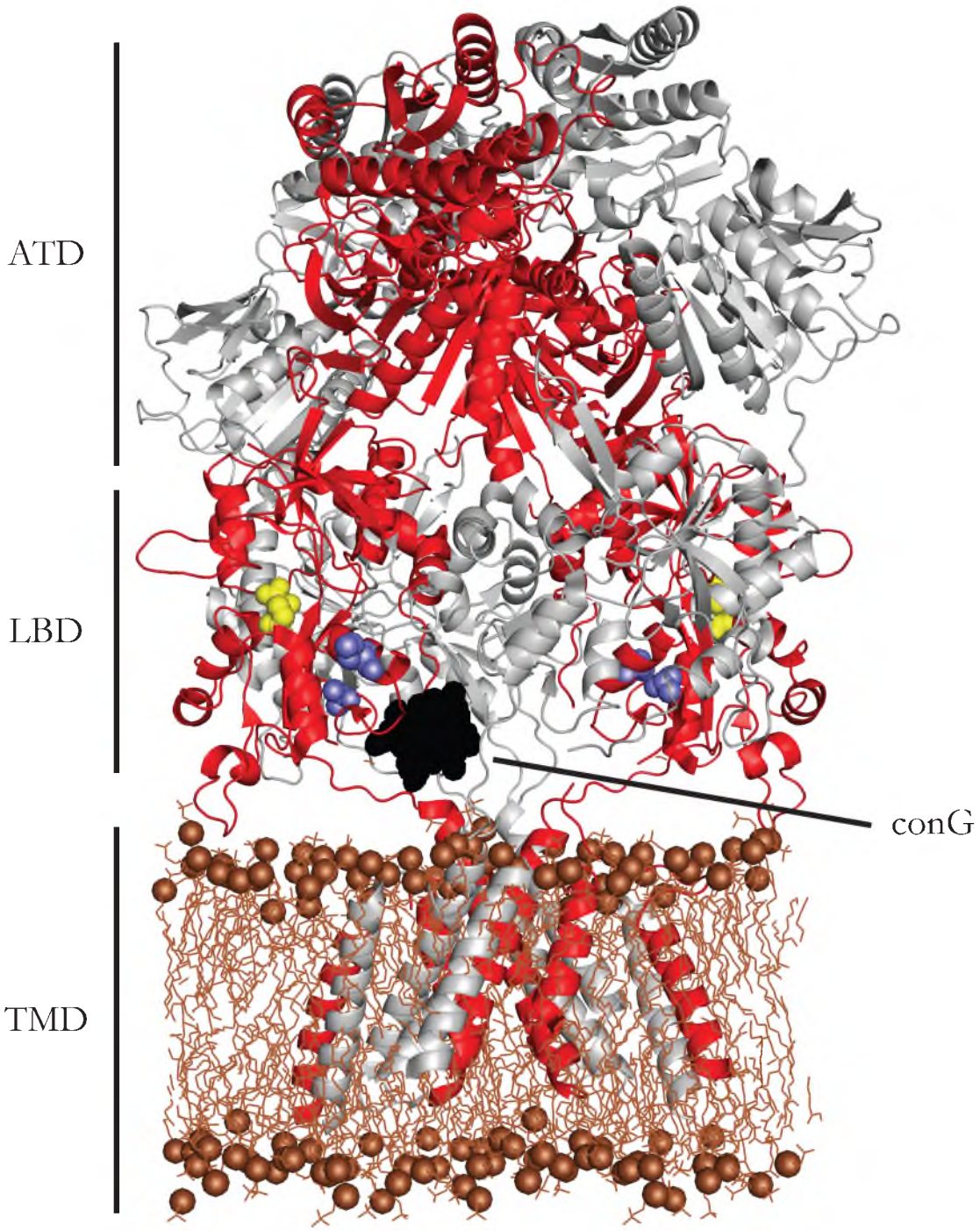

Figure 4.11: A hypothetical model of conantokin binding. The model illustrates conG (black spheres) bound to an NMDAR tetramer (cartoon, NR1 subunits grey, NR2 subunits red) embedded in a phospholipid bilayer (brown lines with phosphates as spheres). Residues on the NMDAR that influence conantokin sensitivity (blue spheres) are near the modeled conantokin-binding site. Glutamate (yellow spheres) is shown bound to the LBD. In this model, calcium ions could bridge conantokin to the membrane for increased binding energy.

Conclusion

At present, the mechanism of conantokin-NMDAR binding is still unclear. Still, it is likely that multiple protein domains of the NMDAR, and the membrane context of the NMDAR, each contribute to conantokin binding in some manner. Future studies on conantokin-NMDAR interactions will have to examine more complex possibilities for a conantokin-binding interface on NMDARs. Researchers should probe binding in more complete combinations of extracellular domains (e.g., ATD-LBD constructs), and assess the potential for conantokin interactions that require multimeric NMDAR structure. Fortunately, the exact molecular picture of binding will likely be revealed when a conantokin-NMDAR cocrystal structure is finally determined.

References

1 Mena, E. E. *et al.* Conantokin-G: a novel peptide antagonist to the N-methyl-D aspartic acid (NMDA) receptor. *Neuroscience Letters* **118**, 241-244 (1990).

2 Skolnick, P., Boje, K., Miller, R., Pennington, M. & Maccecchini, M. L. Noncompetitive inhibition of N-methyl-D-aspartate by conantokin-G: evidence for an allosteric interaction at polyamine sites. *Journal of Neurochemistry* **59**, 1516-1521 (1992).

3 Chandler, P., Pennington, M. & Maccecchini, M. Polyamine-like actions of peptides derived from conantokin-G, an N-methyl-D-aspartate (NMDA) antagonist. *Journal of Biological Chemistry* **268**, 17173-17178 (1993).

4 Hammerland, L. Conantokin-G selectively inhibits N-methyl-D-aspartate-induced currents in *Xenopus* oocytes injected with mouse brain mRNA. *European Journal of Pharmacology: Molecular Pharmacology* **226**, 239-244 (1992).

5 Donevan, S. D. & McCabe, R. T. Conantokin G is an NR2B-selective competitive antagonist of N-methyl-D-aspartate receptors. *Molecular Pharmacology* **58**, 614-623 (2000).

6 Klein, R. C., Prorok, M. & Castellino, F. J. Direct binding properties of conantokins to native N-methyl-D-aspartate receptors. *The Journal of Peptide Research* **61**, 307-317 (2003).

7 Wittekindt, B. *et al.* Point mutations identify the glutamate binding pocket of the N-methyl-D-aspartate receptor as major site of Conantokin-G inhibition. *Neuropharmacology* **41**, 753-761 (2001).

8 Sheng, Z., Liang, Z., Geiger, J. H., Prorok, M. & Castellino, F. J. The selectivity of conantokin-G for ion channel inhibition of NR2B subunit-containing NMDA receptors is regulated by amino acid residues in the S2 region of NR2B. *Neuropharmacology* **57**, 127-136 (2009).

9 Furukawa, H. Mechanisms of activation, inhibition and specificity: crystal structures of the NMDA receptor NR1 ligand-binding core. *The European Molecular Biology Organization Journal* **22**, 2873-2885 (2003).

10 Furukawa, H., Singh, S. K., Mancusso, R. & Gouaux, E. Subunit arrangement and function in NMDA receptors. *Nature* **438**, 185-192 (2005).

11 Klock, H. E. & Lesley, S. A. The Polymerase Incomplete Primer Extension (PIPE) method applied to high-throughput cloning and site-directed mutagenesis. *Methods in Molecular Biology* **498**, 91-103 (2009).

12 Schägger, H. & von Jagow, G. Tricine-sodium dodecyl sulfate-polyacrylamide gel electrophoresis for the separation of proteins in the range from 1 to 100 kDa. *Analytical Biochemistry* **166**, 368-379 (1987).

13 Fontana, A., de Laureto, P. P., Spolaore, B. & Frare, E. Probing protein structure by limited proteolysis. *Acta Biochimica Polonica* **51**, 229-321 (2004).

14 Fontana, A., Zambonin, M. & de Laureto, P. P. Probing the conformational state of apomyoglobin by limited proteolysis. *Journal of Molecular Biology* **266**, 223-230 (1997).

15 Reed, R. G., Feldhoff, R. C., Clute, O. L. & Peters, J., T. Fragments of bovine serum albumin produced by limited proteolysis. Conformation and ligand binding. *Biochemistry* **14**, 4578-4583 (1975).

16 Gowd, K. H. *et al.* Conantokins derived from the Asprella clade impart conRl-B, an N-methyl d-aspartate receptor antagonist with a unique selectivity profile for NR2B subunits. *Biochemistry* **51**, 4685-4692 (2012).

17 Chen, G.-Q., Sun, Y., Jin, R. & Gouaux, E. Probing the ligand binding domain of the GluR2 receptor by proteolysis and deletion mutagenesis defines domain boundaries and yields a crystallizable construct. *Protein Science* **7**, 2623-2630 (1998).

18 Armstrong, N., Sun, Y., Chen, G. Q. & Gouaux, E. Structure of a glutamate-receptor ligand-binding core in complex with kainate. *Nature* **395**, 913-917 (1998).

19 Ivanovic, A., Reiländer, H., Laube, B. & Kuhse, J. Expression and initial characterization of a soluble glycine binding domain of the N-methyl-D-aspartate receptor NR1 subunit. *The Journal of Biological Chemistry* **273**, 19933-19937 (1998).

20 Jun-ichi, M., Shigetada, N. & Hisato, J. Expression and characterization of a glycine-binding fragment of the N-methyl-D-aspartate receptor subunit NR1. *Biochemical Journal* **340**, 687-692 (1999).

21 Berger, I., Fitzgerald, D. J. & Richmond, T. J. Baculovirus expression system for heterologous multiprotein complexes. *Nature Biotechnology* **22**, 1583-1587 (2004).

22 Jarvis, D. L. Developing baculovirus-insect cell expression systems for humanized recombinant glycoprotein production. *Virology* **310**, 1-7 (2003).

23 Possee, R. D., Hitchman, R. B. & King, L. A. Baculovirus expression systems for recombinant protein production in insect cells. *Recent Patents on Biotechnology* **3**, 46-54 (2009).

24 Karakas, E. & Furukawa, H. Crystal structure of a heterotetrameric NMDA receptor ion channel. *Science* **344**, 992-997 (2014).

25 Bradford, H. N., Orcutt, S. J. & Krishnaswamy, S. Membrane binding by prothrombin mediates its constrained presentation to prothrombinase for cleavage. *Journal of Biological Chemistry* **288**, 27789-27800 (2013).

26 Vermeer, C. Gamma-carboxyglutamate-containing proteins and the vitamin K-dependent carboxylase. *Biochemical Journal* **266**, 625-636 (1990).

CHAPTER 5

USE OF CONANTOKINS TO IDENTIFY NMDA RECEPTOR SUBTYPES IN LIVE NEURONS FROM MOUSE CEREBELLUM

Introduction

Understanding the molecular mechanisms that govern N-methyl-D-aspartate receptor (NMDAR) inhibition by conantokins has important implications for developing a toolset of subtype selective NMDAR inhibitors. A toolset of selective NMDAR inhibitors, in turn, has important implications for understanding the physiological role of NMDA receptors in the mammalian nervous system. As novel conantokins are discovered or developed, those with unique selectivity for NMDAR subtypes become new tools for studying NMDARs of the nervous system. Ultimately, a toolset of conantokins with specificity for all NMDAR subtypes would be expected to reveal which NMDAR subtypes are present in particular regions of the nervous system and offer insights into the physiological role of those receptors. To this end, this chapter describes the first use of selective conantokin peptides to reveal NMDAR composition in a large population of neurons from mouse cerebellum.

NMDARs of the cerebellum

NMDARs are expressed throughout the central nervous system of mammals. Different NMDAR subtypes show unique spatial expression patterns and NMDAR subtype expression can change dramatically during development. Since the NR1 subunit is an

obligatory component of all NMDAR tetramers, NR1 is expressed ubiquitously throughout the brain during all stages of development[1]. In contrast, NR2 subunits have unique spatial expression patterns that change throughout development[1-4]. The restricted expression patterns, and the developmental changes that occur for NR2 expression, suggest that different NMDAR subtypes have specific developmental and physiological roles.

One region of the brain where developmental changes of NR2 subtype expression are particularly dramatic is the cerebellum. In murine cerebellum, NR2B is highly expressed at birth but drops to undetectable levels by adulthood[5,6]. Concomitant with the decrease in NR2B expression, expression of NR2C increases and persists into adulthood[5,6]. These developmental changes implicate NR2B NMDAR subtypes in formation of neuronal connections, and NR2C NMDAR subtypes in maintaining NMDAR-mediated excitatory neurotransmission in the cerebellum. Additionally, functional molecular properties of cerebellar NMDARs change developmentally in a manner that is consistent with a shift to NR2C NMDAR subtypes; mature neurons express NMDA receptors with low conductance and slow kinetics[7,8].

Although NR2 subtype expression in the cerebellum changes dramatically through development, it is unclear how the transition from NR2B to NR2C occurs in individual neurons. Potential pathways for this transition include: NR2B expressing neurons start expressing NR2C and the cells transition through $NR1_2$-$NR2B_1$-$NR2C_1$ triheteromeric NMDARs; NR2B expressing neurons start expressing NR2C and cells contain a mixed population of $NR1_2$-$NR2B_2$ and $NR1_2$-$NR2C_2$ diheteromeric NMDARs; or a nascent population of neurons arises that express NR2C (but not NR2B) and contain $NR1_2$-$NR2C_2$ diheteromeric NMDARs, which ultimately replace NR2B expressing neurons. Determining which of these models is correct is, in part, a technical problem that arises from limitations

of electrophysiology and lack of selective NMDAR pharmacology. Electrophysiological recordings provide information on single cells, and therefore mask potential diversity among cells. Therefore, alternative methods that facilitate observation of a mixed population of many neurons simultaneously would be beneficial. Fortunately, recent technical advances with calcium imaging provide the opportunity to observe large and diverse populations of neurons from the central nervous system. Also, the recent emergence of truly of subtype-selective conantokins provides tools that can identify the presence of certain NMDAR subtypes using calcium imaging.

Constellation pharmacology

Constellation pharmacology is a recently developed technique that allows the simultaneous functional characterization of hundreds neurons within a single experiment[9]. It uses calcium imaging, where a calcium-sensitive dye is trapped inside neurons and provides an indicator of intracellular calcium levels. Since many ion channels expressed in neurons are permeable to calcium, constellation pharmacology can be used to probe the ion channel composition of those neurons. Also, depolarization of the cell triggered by receptors that are not permeable to calcium generally results in activation of voltage-gated calcium channels, which allows for calcium impermeable channels to be studied as well. In all, thousands of neurons can be analyzed to provide characterization of the different neuronal subtypes and the frequency of those subtypes in particular areas of the brain.

The ability to define ion channel compositions of neurons with constellation pharmacology is made possible with pharmacological tools that selectively activate or inhibit specific ion-channel subtypes. Previous experiments applying constellation pharmacology have successfully defined neurons by their ion channel composition in both the dorsal root ganglion (DRG)[9,10] and the central nervous system (CNS)[11]. These examples illustrate that

constellation pharmacology is an effective method for understanding neuronal diversity, and cell-specific ion channel expression. However, these experiments have not thoroughly examined NMDA receptors and have been performed on select regions of the brain and spinal cord. Thus, combining constellation pharmacology with selective conantokin peptides is a natural progression in efforts to understand NMDARs of the mammalian nervous system. Additionally, extending constellation pharmacology to new regions of the brain deepens our scientific knowledge of neuronal organization in the CNS.

Methods

Cerebellar cell preparations and culture

The methods described for preparing cerebellar neurons were adapted from those previously described for CNS neurons of the ventral respiratory column[11]. Mice (WT C57BL/6) at postnatal day 7-14 were anesthetized on ice and sacrificed with decapitation per Institutional Animal Care and Use Committee (IACUC) approved protocols. The mouse head was pinned to a silicone-covered culture dish for dissection and removal of the cerebellum. Skin and connective tissue were removed to reveal the skull and the skull was pierced at the seam connecting hind and fore skull plates. After opening the skull, ice-cold artificial cerebro-spinal fluid (ACSF) pH 7.6 bubbling with carbogen was applied to the brain tissue every 2-3 minutes to keep tissue cold, moist, and oxygenated.

The hind skull was removed by clipping along the boundary between parietal and intraparietal skull bones to expose the midbrain and cerebellum. A single cut was made with a fresh razor blade above the cerebellum at a 20° below-vertical angle to remove the cerebellum, brainstem, and underlying tissue. The cerebellum was isolated from other tissue with a razor blade and transferred to a bath of ice-cold ACSF. The isolated cerebellum was

dissected into 2 mm x 2 mm pieces. Cerebellar pieces were transferred to 900μL ice-cold Hank's balanced salt solution (HBSS), 100 μL of 2.5 % wt./vol. trypsin was added, and the resulting mixture was incubated for 5 minutes at 37° C. Protease was removed through dilution by rinsing the cerebellar tissue 3x with 10 mL ice-cold ACSF and 1x with 4mL Eagle's minimal essential medium (MEM) supplemented with 10% vol./vol. FBS (HyClone), 100 U/mL penicillin, 100 μg/mL streptomycin, 1X Glutamax (Invitrogen), 10 mM HEPES pH 7, and 0.4% wt./vol. glucose.

Cerebellar tissue in MEM media was triturated with a series of four fire-polished pasture pipettes of decreasing diameters until the solution was cloudy with few visble chunks. The cell suspension was then diluted 1:5 for plating. Twenty μL of the diluted cell suspension was pipetted into the center of a silicone donut affixed to a poly-lysine coated 24-well tissue culture plate. Cells were allowed to adhere to the plate for 1 hour in a 37 °C incubator prior to flooding the well with 1 mL MEM containing supplements. Wells not containing cells were filled with sterile distilled water to increase humidity during culture. Adhered cells in MEM media were cultured overnight for 16-20 hours in a 37 °C incubator with 5% CO_2.

Calcium imaging

Calcium imaging was performed as previously described[9-11]. Briefly, cerebellar neurons were incubated with Fura-2-acetoxymethyl ester in MEM culture media for 1 hour following overnight culture. At initiation of experimental imaging, the Fura-2/MEM media was replaced with ACSF pH 7.4 at room temperature. Fluorescence emission intensity was measured at wavelength 510 nm with alternating excitation wavelengths of 340 and 380 nm. Data were recorded as the ratio of emission intensity measured for each excitation

wavelength (340:380 ratio) per standard calcium imaging techniques. Deflections of the 340:380 ratio are indicative of changes in cytosolic calcium levels with an increasing ratio representing an increase of calcium.

Data analysis

Calcium imaging data were analyzed using the imaging software NIS-elements (Nikon) and using an R-based program, ProcConstPharm, written by Dr. Kevin Chase (University of Utah, departments of biology and mathematics). In ProcConstPharm, cell phenotypes were defined using a binary scoring system of response (1) or no response (0) to various chemical inputs. Cluster analysis was used to group cells by response phenotype and calculate cell-class percentages. Quantitative analysis of peak heights was performed using ProcConstPharm. Peak heights were calculated by subtracting baseline from the maximum response within a user defined response window. ProcConstPharm facilitated an unbiased scoring of cell phenotypes using baseline-corrected data and user-defined peak recognition criteria (e.g., peak height and peak signal to noise). Cell culture images were produced with NIS-Elements (Nikon), individual cell traces were generated with ProcConstPharm, and dose-response curves were plotted with Prism6 (GraphPad Software, La Jolla, California USA).

Results

Culture of dissociated cerebellar neurons

Slight modification of protocols developed for culturing neurons of the ventral respiratory column (VRC)[11] led to viable cerebellar neuron cultures. Figure 5.1 shows the typical appearance of cerebellar neurons following tissue dissociation and overnight cell culture from a postnatal day 7 (P7) mouse. The neurons of the cerebellum showed similar

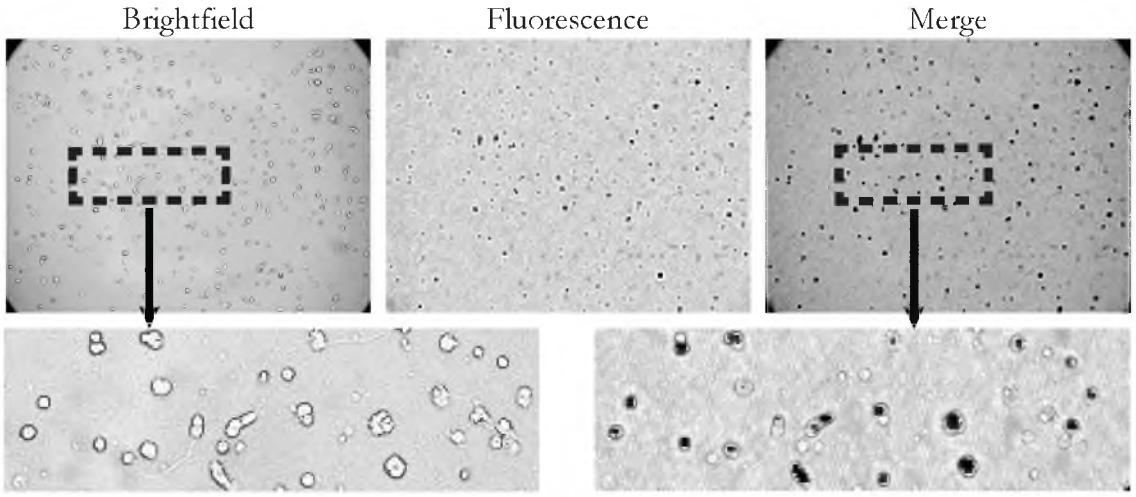

Figure 5.1: Culture of cerebellar neurons from P7 mouse. The brightfield, fluorescence, and merge images of cultured cerebellar neurons show a high proportion of small cells. These results were typical when culturing cerebellar neurons.

morphology to those of the VRC, but exhibited a higher frequency of small neurons that were less than 100 μm^2 in cross-sectional area. In contrast to dorsal-root ganglion cultures, the cerebellar cultures did not contain very large neurons >400 μm^2 and generally neurons had cross-sectional areas that were less than 350 μm^2.

Neuronal phenotypes are defined with agonist challenge experiments

To define different neuronal phenotypes of the cerebellum, an agonist challenge protocol identified glutamatergic and cholinergic neurons. Cluster analysis defined cell classes according to how each neuron responded to various glutamatergic and cholinergic agonists including NMDA, glutamate, glycine, acetylcholine, carabamylcholine (carbachol), and nicotine. Figure 5.2 shows representative traces from single cells that illustrate the pattern of response for the 12 most frequently encountered neuronal phenotypes of the cerebellum. In most cases, neurons responded only to glutamatergic inputs (34.1% of cells) or responded only to cholinergic inputs (15.5% of cells). However, some neurons responded to both glutamatergic and cholinergic agonists (3.7% of cells)

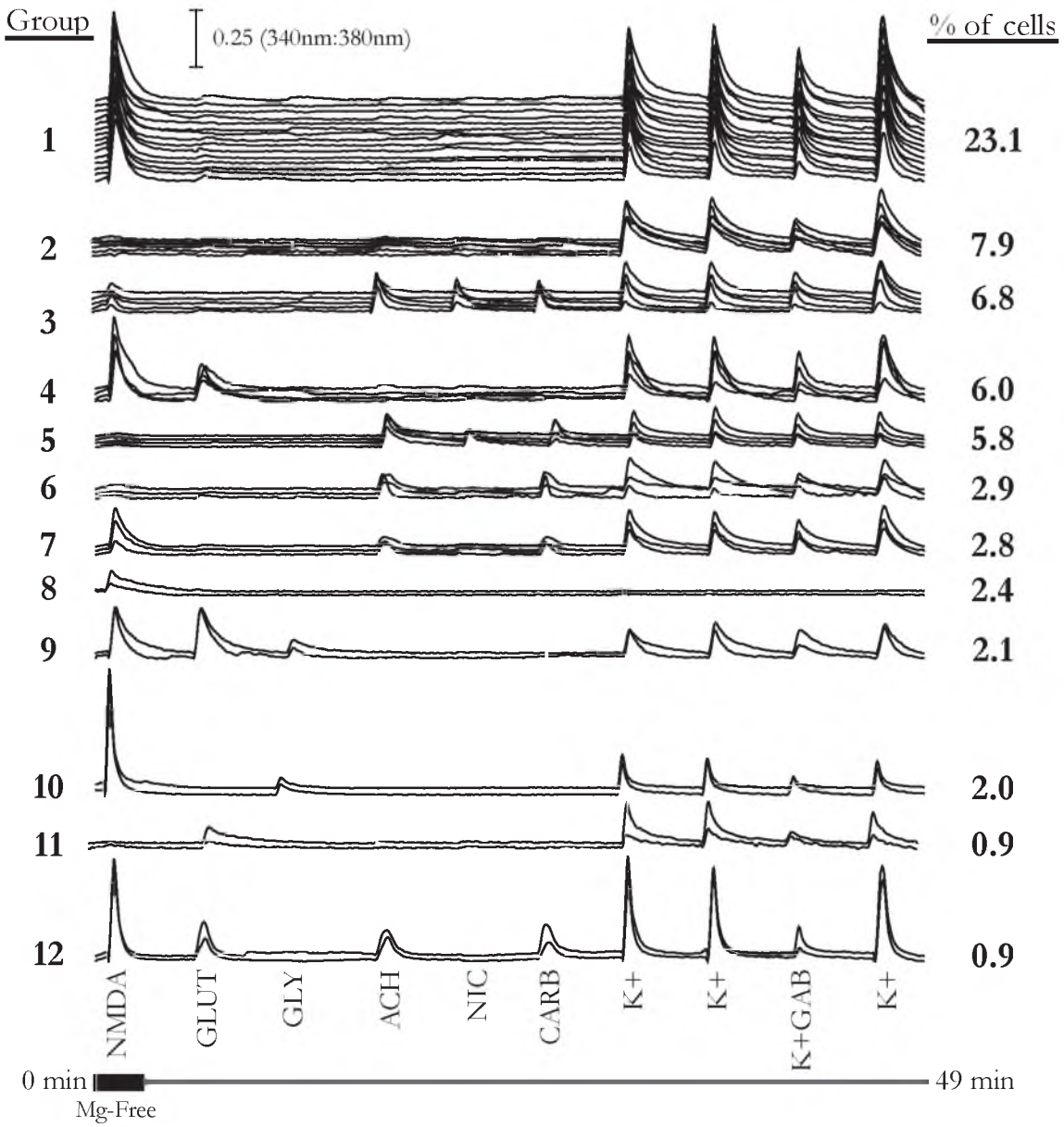

Figure 5.2: Diversity of glutamatergic and cholinergic neurons in mouse cerebellum. Representative traces for the 12 most-common response phenotypes and frequencies of those phenotypes are shown. Agonist application protocol is shown at the bottom with the following abbreviations: NMDA=200μM NMDA/20μM D-serine, GLUT=300μM glutamate, GLY=200μM glycine, ACH=1mM acetylcholine, NIC=200μM nicotine, CARB=1mM carbamylcholine, K+=30mM potassium, K+GAB=30mM potassium/1mM GABA. Each agonist was applied for 10 seconds. Group frequencies were calculated from 8 experiments, 5 mice, and 2,866 neurons.

The most frequently encountered neuronal phenotypes were glutamatergic and responded to strongly to NMDA / D-serine, and responded to depolarization (Figure 5.2, group 1). The second most-frequent neuronal phenotype only responded to depolarization (Figure 5.2, group 2). Presumably group-2 neurons would respond to other excitatory neurotransmitters that are not glutamatergic or cholinergic (e.g., serotonin). The third most frequent phenotype generally responded weakly to NMDA and responded more strongly to cholinergic agonists and to depolarization (Figure 5.2, group 3). Less frequent glutamatergic-only phenotypes were also observed and can be seen in Figure 5.2, groups 4, 8, 9, 10, and 11. Also, less frequent cholinergic-only phenotypes were observed and are shown in Figure 5.2, groups 5 and 6. There were two neuronal phenotypes that responded to both glutamatergic and cholinergic agonists (Figure 5.2, groups 7 and 12).

In addition to the neuronal phenotypes shown in Figure 5.2, 4.6% of cells did not respond to any agonists tested in this protocol. These are likely to be glial cells, which support cells of the nervous system but generally do not express ion-channels or otherwise participate in neurotransmission. The remaining 31.8% of cells that did not fit into already described phenotypes were placed into a miscellaneous group. The miscellaneous group included cells that died during the experiment, cells with large shifts in baseline, and cells with infrequently observed response patterns. Infrequent response patterns were generally seen in less than 1% of all cells and were found in less than four of the six experiments performed. The high frequency at which neurons were placed in the miscellaneous category by automated response detection in *ProcConstPharm* merits some comments. In order to confidently assign cells to a particular phenotype and avoid misdiagnosis, there had to be clear evidence of a response-pattern match. Many of the neurons assigned to the miscellaneous cell category probably could be assigned to a particular phenotype if criteria

for a response-pattern match were more relaxed. However, this would create the situation of a particular cell being matched to more than one phenotype or even being matched to the wrong phenotype. To avoid such ambiguity, and to avoid a source of bias, I decided to keep the pattern-matching criteria stringent and not further consider cells that had been assigned to the miscellaneous category.

To further investigate neuronal phenotypes found with constellation pharmacology, I undertook experiments using agonists and antagonists with selectivity for individual ion channel subtypes. The glutamate responses seen in Figure 5.2 could have come from activation of AMPA or kainate type glutamate receptors. Thus, I utilized AMPA as a selective agonist to determine which receptor was responsible for glutamate responses. In these experiments, all cells that responded to glutamate also responded to AMPA, and the responses for glutamate and AMPA were of similar magnitude (data not shown). Thus, it appears AMPA-type glutamate receptors are the predominant non-NMDA receptor in cerebellar neurons.

I was surprised to observe cells that responded to acetylcholine (ACh) and carbamylcholine (carbachol) but not to nicotine (groups 6, 7, 12). Carbachol is often used as a more stable substitute for ACh and is known to activate nicotinic acetylcholine receptors. I hypothesized that the ACh/carbachol-responding cells might contain muscarinic ACh receptors. To test this hypothesis, I utilized the muscarinic acetylcholine receptor antagonist atropine. Atropine completely blocked ACh response in the ACh/carbachol-responsive cells, but did not completely block ACh response in ACh/nicotine/carbachol-responsive cells (data not shown). Therefore, cells in groups 6, 7, and 12 contain muscarinic acetylcholine receptors but not nicotinic acetylcholine receptors. Altogether, the results show that 12 or more neuronal cell types exist in the cerebellum, and these cell types exist in different

frequencies and can be differentiated by neuronal phenotypes displayed during constellation pharmacology experiments that reflect the combinations of ion channels each cell expresses.

I was curious to compare the cell types identified by constellation pharmacology with cell types defined by other classification systems. Cell types of the cerebellum have been previously defined based on network connectivity, cell morphology, and cell-body size[12,13]. For example, Purkinje neurons are large and highly branched, while granule neurons are small with limited branching[13]. Although dendritic branching is lost upon dissociation, I believe cell body size in culture is an accurate reflection of cell body size found in the brain. Consequently, I examined cell cross sectional area from cerebellar cultures to see if correlations with phenotype could be drawn.

The distribution of cell areas for each of the major neuronal phenotypes identified for P7 mouse cerebellar neurons is presented in Figure 5.3. The observed range of cell areas for each phenotype was broad. The majority of cells in all groups were found to have cell areas between 50μm^2 and 200μm^2, but some larger cells (cell area >200 μm^2) were also present. Interestingly, groups that responded to cholinergic inputs consistently had larger mean cell areas than neurons that responded only to glutamatergic inputs. However, the broad range of cell sizes characterizing each of the neuronal phenotypes defined by constellation pharmacology indicates cell area should not be used as an indicator of neuron type, at least not for small cells derived from mouse cerebellum. In contrast to the results presented here, dorsal root ganglion neurons from the peripheral nervous system fall into distinct size categories that strongly correlate with phenotype (Olivera Lab, unpublished data). Examining cerebellar neurons from older mice that are more developed would possibly reveal stronger correlations between phenotype and cell size.

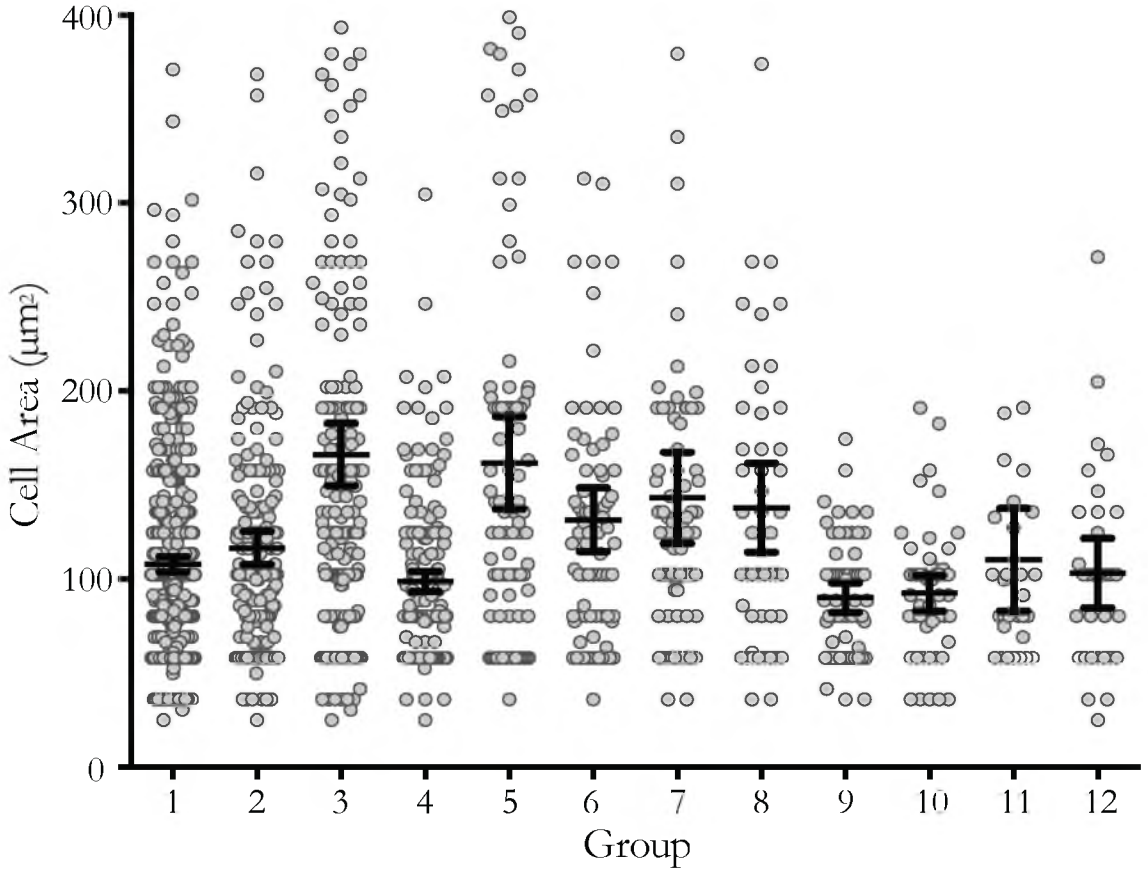

Figure 5.3: Cell areas of neuronal groups defined with constellation pharmacology. Individual cell area data points for neurons within each group are shown as grey dots. Mean cell areas for each group are shown (center horizontal black bar) along with 95% confidence intervals (upper and lower horizontal bars).

Conantokin inhibition of NMDA response in cerebellar neurons

In agonist challenge experiments, a majority of neurons from the cerebellum responded to the agonists NMDA/D-serine, indicating the presence of NMDARs. I sought to characterize the NMDAR composition in these neurons using the conantokin peptide con*R*-B. Con*R*-B is highly potent and selective for NR2B containing NMDARs with an IC_{50} value of 0.1 μM on NR2B, and IC_{50} values greater than 10 μM on all other NMDAR subtypes[14]. The protocol for these experiments incorporated multiple NMDA/D-serine pulses and pre-incubation with con*R*-B at various concentrations. Representative traces from experiments performed on cerebellar neurons of a P7 mouse are shown in Figure 5.4.

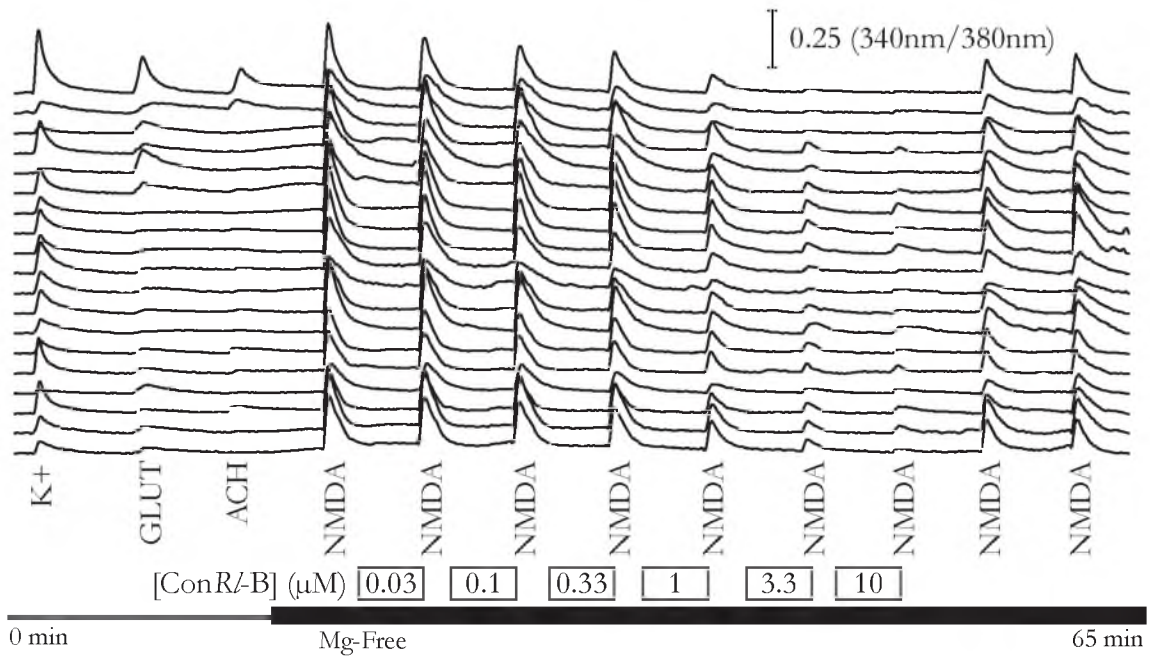

Figure 5.4: Con*Rl*-B inhibits NMDA response in cerebellar neurons. Calcium imaging traces depicting the effects of con*Rl*-B on neurons from the cerebellum. All NMDA responsive neurons were inhibited to some degree by con*Rl*-B. K+=30mM potassium, GLUT=300μM glutamate, ACH=1mM acetylcholine, NMDA=200μM NMDA/20μM D-serine. Magnesium free conditions were used starting just after the ACH pulse (indicated by black bar).

The results of this experiment showed that all NMDA-responsive neurons were blocked by con*Rl*-B in a dose-dependent manner. This suggests that all NMDA responsive P7 cerebellar neurons express NMDA receptors containing the NR2B subunit. Interestingly, at 10 μM con*Rl*-B some cells were completely blocked while others had residual calcium influx. The cells with residual calcium influx even in the presence of saturating con*Rl*-B may be expressing additional NMDAR subtypes. These might have a non-NR2B population of diheteromeric NMDARs that mix with NR2B diheteromeric NMDARs, or these may express triheteromeric NMDARs that contain NR2B and another NMDAR subunit. Of note, no NMDA responsive neurons from P7 mouse cerebellum were con*Rl*-B insensitive, which indicates a strong NR2B-mediated component to NMDAR signaling in cerebellar neurons of the developing mouse.

Following observations that conantokins could be used to examine NMDARs of live neurons, I wondered how the effect of conantokins on those neurons would compare to the effect of conantokins observed *in vitro* by means of electrophysiology using *Xenopus* oocytes expressing NMDARs. To compare results from these two experimental techniques I created dose-response curves for conantokins acting on living neurons, which could be compared to dose-response curves for conantokins acting on oocytes.

Using *ProcConstPharm*, peak heights were extracted for NMDA-responsive neurons in the conantokin assay. The data were normalized to the first NMDA pulse, plotted, and fit to the Hill equation (Figure 5.5). NMDA responsive neurons from the cerebellum exhibited a spectrum of sensitivities to con*R*/-B with IC_{50} values ranging from 0.2-2.8 μM. The mean IC_{50} for con*R*/-B inhibition of NMDAR response was 0.64±0.31 μM. Hill coefficients ranged from -1.60 to -0.43 with a mean value of -0.92±0.19 (Figure 5.6), indicating that conantokin inhibition of NMDARs is not a cooperative process.

To determine if sensitivity to con*R*/-B, as assessed by IC_{50}, correlated with neuronal phenotype, the NMDA responsive phenotype was further segregated on the basis of response patterns involving glutamate and acetylcholine. This subdivision of NMDA responsive cells resulted in four types: those that responded to NMDA only, those that responded to NMDA and glutamate, those that responded to NMDA and acetylcholine, and those that responded to all three agonists, NMDA, glutamate, and acetylcholine. The mean IC_{50} value for con*R*/-B inhibition of NMDA response in each of these groups was not statistically different (data not shown). Therefore, various neurons that contain NMDARs appear to express the same NMDA receptor subtypes regardless of co-expression of other glutamate and acetylcholine receptors.

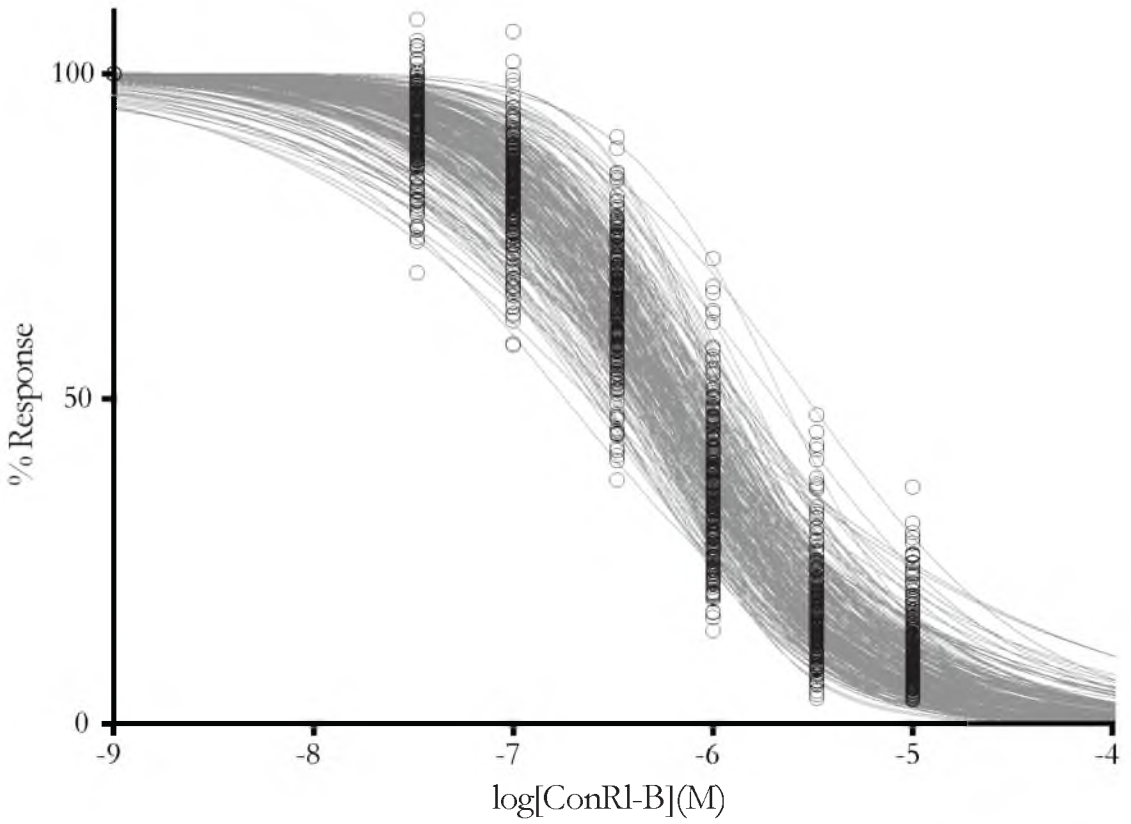

Figure 5.5: Curve fits for con*RI*-B inhibition of NMDA response in cerebellar neurons. Peak heights were normalized to the first NMDA pulse and plotted as a function of log[con*RI*-B](M). Curve fits were produced using the Hill equation for normalized data with the Hill coefficient left as an adjustable parameter. (n= 238 cells)

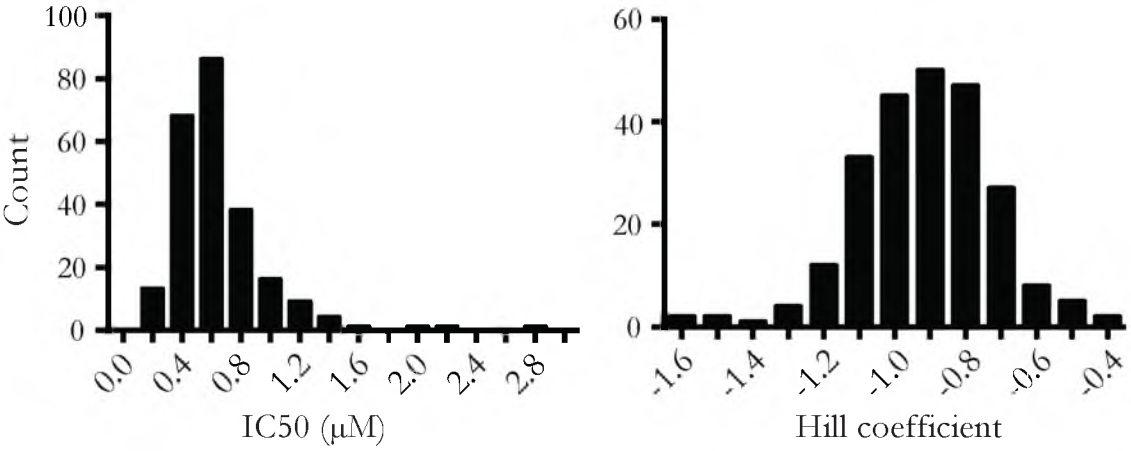

Figure 5.6: Distribution of IC_{50} values and Hill coefficients for con*RI*-B inhibition of NMDA response in cerebellar neurons. The IC_{50} values and Hill coefficients for con*RI*-B inhibition of NMDARs in live cerebellar neurons are close to the values observed for NR2B NMDARs expressed *in vitro*.

Developmental changes in NMDAR subtype expression

Because NMDAR subtype expression in the cerebellum is known to change during brain development[1,5,6,15,16], I wondered how the effects of con*Rl*-B would compare for neurons harvested from young and from older mice. Unfortunately, there are significant technical challenges associated with the culture of neurons from adult mice. Generally, only dead or nonresponsive cells were observed when dissociated cerebellar neurons were prepared from a P21 mouse. However, slight modifications of protocols and the use of intermediate-aged P14 mice resulted in improved cultures with NMDA responsive, living cells. The modified protocol incorporated an altered culture media that contained a 50 % MEM media and 50% Neurobasal media augmented with glial cell line-derived neurotrophic factor (GDNF). GDNF is a hormone known to promote neuronal growth and axon sprouting[17,18].

Calcium imaging traces from an experiment using the modified culture protocol on a P14 mouse are presented in Figure 5.7. Similar to what was observed for P7 neurons, most NMDA-responsive cerebellar neurons from the P14 mouse showed sensitivity to con*Rl*-B. Furthermore, the sensitivity was similar to that observed for P7 neurons with IC_{50} values centered around 1 μM. However, in addition to con*Rl*-B sensitive neuorns, a distinct population of NMDA-responsive and con*Rl*-B insensitive neurons were also observed (4 of 100 cells). This NMDA-responsive and con*Rl*-B insensitive phenotype was not observed in P7 cerebellar neurons, suggesting that between developmental stages of P7 and P14 a new NMDAR subtype is expressed in cerebellar neurons. Taken together with previous results from *in situ* hybridizations, which showed increased levels of NR2C MRNA in the cerebellum of older mice, the con*Rl*-B insensitive neurons are likely expressing NR2C c NMDAR subtypes.

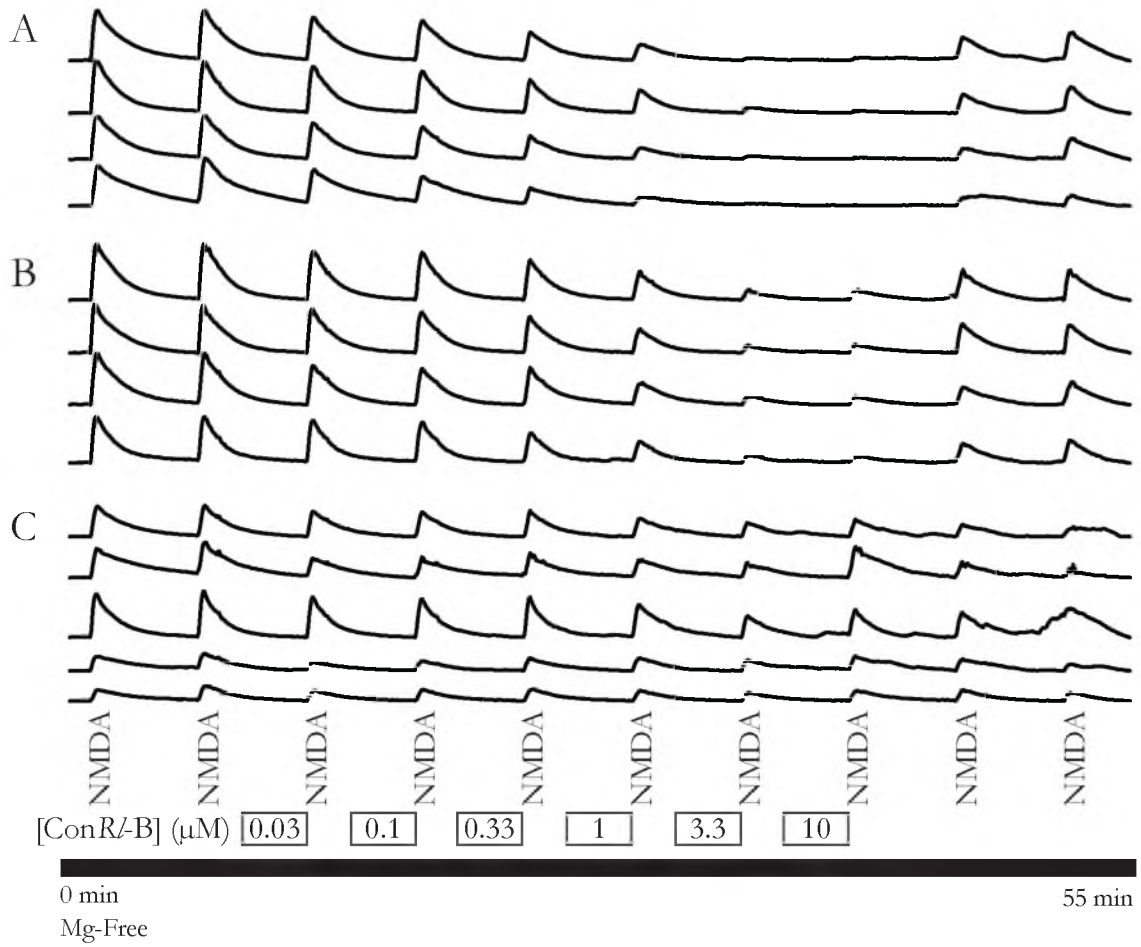

Figure 5.7: Phenotypes observed for P14 cerebellar neurons. Three cell phenotypes defined by NMDA response and sensitivity to con*RI*-B. **A:** NMDA responsive neurons that were completely blocked by 10μM con*RI*-B. **B:** NMDA responsive neurons that were incompletely blocked by 10μM con*RI*-B. **C:** NMDA responsive neurons that were insensitive to block by con*RI*-B. Traces in panel C report the behavior of neurons that no longer express NR2B NMDAR subtypes and that likely express NR2C NMDAR subtypes.

Discussion

Results summary

In this chapter, constellation pharmacology was used to define the glutamatergic and cholinergic populations of neurons found in mouse cerebellum. Using an agonist challenge assay, the majority of neurons in mouse cerebellum were found to be small, glutamatergic neurons. These neurons were further subdivided based on responses to glutamate, NMDA, glycine, and depolarization. The cholinergic neurons of mouse cerebellum were generally

larger in size and could be subdivided based on responses to acetylcholine, nicotine, carbachol, and depolarization. For NMDA-responsive glutamatergic neurons, NMDAR composition was examined using conantokin peptides. These experiments revealed that in young mice all NMDA responsive neurons were sensitive to inhibition by con*R*-B. Therefore, young mice express NR2B NMDAR subtypes. In older mice, a population of con*R*-B insensitive neurons was discovered that presumably express the NR2C NMDAR subtype. Thus, neurons in older developing mice express a mixture of NR2B and other NMDA receptor subtypes.

Constellation pharmacology

Calcium imaging is a technique that has been used for decades to measure changes in cytosolic calcium levels[19]. Since many different ion channels are permeable to calcium[20], calcium imaging is useful for studying ion channel composition in live cells[21]. Recently, constellation pharmacology has shown its utility in understanding ion channel compositions in large populations of dissociated neurons[9-11,22]. These studies illustrate that the fusion of calcium imaging with pharmacological agents can define ion channel composition in single neurons.

This dissertation has advanced constellation pharmacology in two distinct ways. First, I have presented the initial characterization of cerebellar neurons using constellation pharmacology, thereby extending the technique to a new area of the brain. Second, I have demonstrated the first use of conantokin peptides to define NMDAR subtypes of living neurons at different stages of development. These experiments provide the first examination of NMDAR subtypes in a large and diverse set of neurons and set forth a new path for understanding the distribution and physiological role of different NMDAR subtypes.

Diversity of cerebellar neurons

Agonist challenge experiments revealed that the most frequently encountered neurons of the cerebellum responded to NMDA/D-serine and membrane depolarization, and had small cell areas. Anatomical studies of the cerebellum have identified granule cells as the most common and smallest cells of the cerebellum[12]. Also, granule cells receive glutamatergic inputs that are in part transmitted by NMDA receptors[23-25]. I hypothesize that group 1 neurons classified by constellation pharmacology correspond with granule cells of the cerebellum. Also, it has been shown that glutamate receptors expressed in cerebellar granule cells can include AMPA, kainate, and metabotropic receptors[24,26-29]. Consequently, I further hypothesize that the subset of small neurons belonging to groups 4, 9, and 10 defined by constellation pharmacology represent additional populations of granule cells. To test these hypotheses, further experiments will need to definine the exact mixture of glutamate receptors in the phenotypic groups and correlate those groups to cells of known anatomical loci. Hopefully, future experiments will elucidate how each phenotype defined by constellation pharmacology presented here is related to known cerebellar cells that include granule, stellate, basket, Golgi, and Purkinje neurons.

Analysis of cell areas

Since specific neurons of the cerebellum are known to have well defined sizes (e.g., granule cells are small, Purkinje cells are large), I expected that phenotypic groups from calcium imaging would fall into tightly grouped size classes. However, I observed a broad range of cell sizes within each phenotypic group, which presents a challenge for connecting cell phenotype defined by constellation pharmacology to known cerebellar neurons.

It may be the case that dissociation protocols alter the size of neurons. However, I believe significant changes to cell body size are unlikely with the current protocols. It is also

possible that many cells have not matured to their final sizes in P7 mice, which could cause variability of cell sizes within groups. Nonetheless, it would be helpful to explore less intrusive methods of cell dissociation, and to examine cell size distribution in older mice. Maybe stronger phenotype-cell size correlations will be found in fully developed animals.

Another hypothesis that can explain diversity of cell sizes within a group is that there may be phenotypic variation for any given cell type (e.g., granule or Purkinje cell). For instance, Purkinje cells as a class could exhibit multiple phenotypes as defined by agonist challenge protocols. If this hypothesis is true and diverse neuronal phenotypes exist within the population of Purkinje neurons, which are highly homogeneous in morphology, it would be an exciting and unexpected result that could change current views of what defines neuron cell identity. In order to test this hypothesis, experiments that allow correlation of constellation pharmacology phenotypes to cell types in the intact cerebellar milieu will be necessary.

From dissociated cells to intact networks

In order to draw stronger conclusions with constellation pharmacology there is need to associate specific neurons from specific brain loci to functional phenotypes defined by calcium imaging in dissociated culture. Consequently, cell-specific markers that allow positive identification of the same neurons in slice and in dissociated culture preparations are desired. Such markers would allow correlation of cell phenotype observed in constellation pharmacology to cell type based on anatomical location and connectivity. Accordingly, experiments are being pursued to identify specific populations of neurons using fluorescent markers. Scientists in the Olivera lab are currently exploring the use of green-fluorescent protein expression controlled by cell-specific promoters. In a second approach, researchers are using fluorescent antibodies to identify cell-specific proteins. Successful implementation

of these techniques will lead to pivotal discoveries regarding ion channel composition in specific neuron populations and allow for the correlation of cell phenotype observed in constellation pharmacology to cell type based on anatomical location and connectivity.

Possible sources of NMDAR heterogeneity in cerebellar neurons

Experiments exploring conantokin inhibition of NMDA response in cerebellar neurons showed that con*R*-B inhibited responses in *all* neurons of P7 mice with a mean IC_{50} of 0.6 μM. Under the assumption that conantokin affinity is similar for NMDARs in oocytes and NMDARs in neurons, this indicates that during the P7 developmental stage all neurons express NR2B NMDAR subtypes. Interestingly, there was a broad distribution of IC_{50} values, which may indicate that not all cerebellar neurons contained identical NMDAR compositions.

One explanation for the broad IC_{50} distribution is that different NR1 splice variants are found in these neurons. It has been documented that differences in the NR1 splice variants can have effects on conantokin inhibition[30,31]. Another explanation is that other NR2 and/or NR3 subunits coassemble with NR2B to create triheteromeric receptors that are differentially sensitive to con*R*-B. Previous work has shown that triheteromeric NMDARs exist in the cerebellum[32,33]. However, the effects of subtype selective conantokin peptides on triheteromeric NMDARs are yet to be examined. This should be explored by exploiting systems that can enrich for triheteromeric NMDARs.

In order to decode the underlying meaning of the results from con*R*-B inhibition of cerebellar neurons and to further define NMDAR subtypes, there is need to employ additional NMDAR inhibitors with selectivity profiles that differ from con*R*-B. Some possibilities include con*R*, which inhibits both NR2A and NR2B containing NMDARs[34] and

Quinazolin-4-one derivatives, which inhibit NR2C and NR2D containing NMDARs[35]. Additionally, magnesium sensitivity could be used to identify NR2A and NR2B containing receptors, and other subtype-dependent properties of NMDARs could be exploited to decipher exact subunit combinations. These include channel kinetics and sensitivity to various effectors including zinc and pH.

Examining developmental transitions in NMDAR subtype expression

The conantokin inhibition experiments on P14 mice revealed a population of con*R*-B insensitive neurons that were not found in younger mice. Taken in the context of previous works, these cells are likely expressing NMDARs that contain the NR2C subunit. However, it is still unclear how the switch from NR2B to NR2C occurs. Do cells transition through expression of triheteromeric $NR1_2$/NR2B/NR2C receptors, do transitional cells express a mixture of $NR1_2/NR2B_2$ and $NR1_2/NR2C_2$ diheteromers, or are there newly integrated cells that express $NR1_2/NR2C_2$ diheteromeric receptors? To answer these questions additional work needs to be done, and identifying exact receptor combinations may require a more sensitive technique than calcium imaging. Perhaps calcium imaging combined with electrophysiology of the same cell populations can provide answers on subunit composition; electrophysiology allows sensitive measurement of channel properties that can lead to determination of exact subunit compositions.

Summary

The work described here was the first to demonstrate conantokin inhibition of NMDAR responses in a large and diverse population of live neurons. The findings revealed that all cerebellar neurons in P7 mouse were sensitive to inhibition by con*R*-B, suggesting that those cells expressed NMDARs containing the NR2B subunit. In P14 mice, however, a

population of con*RI*-B insensitive neurons was observed. These most likely expressed NMDARs lacking the NR2B subunit, but containing the NR2C subunit. Ultimately, the results show that cerebellar neurons of young mice have a dominant population of NR2B NMDAR subtypes, and that as the mouse develops a population of neurons expressing a different NMDAR subtypes arises. The results are consistent with expectations drawn from previous work examining mRNA levels in cerebellar tissue. This consistency suggests that the techniques described herein will be useful for studying unknown properties of NMDARs in single neurons of the mammalian brain. Clearly, the combination of conantokin peptides and constellation pharmacology presents a new frontier for studying the physical architecture and physiological function of NMDARs.

References

1 Watanabe, M., Inoue, Y., Sakimura, K. & Mishina, M. Developmental changes in distribution of NMDA receptor channel subunit mRNAs. *Neuroreport* **3**, 1138-1140 (1992).

2 Monyer, H., Burnashev, N., Laurie, D. J., Sakmann, B. & Seeburg, P. H. Developmental and regional expression in the rat brain and functional properties of four NMDA receptors. *Neuron* **12**, 529-540 (1994).

3 Stocca, G. & Vicini, S. Increased contribution of NR2A subunit to synaptic NMDA receptors in developing rat cortical neurons. *The Journal of Physiology* **507**, 13-24 (1998).

4 Sheng, M., Cummings, J., Roldan, L. A., Jan, Y. N. & Jan, L. Y. Changing subunit composition of heteromeric NMDA receptors during development of rat cortex. *Nature* **368**, 144-147 (1994).

5 Watanabe, M., Mishina, M. & Inoue, Y. Distinct spatiotemporal expressions of five NMDA receptor channel subunit mRNAs in the cerebellum. *Journal of Comparative Neurology* **343**, 513-519 (1994).

6 Akazawa, C., Shigemoto, R., Bessho, Y., Nakanishi, S. & Mizuno, N. Differential expression of five N-methyl-D-aspartate receptor subunit mRNAs in the cerebellum of developing and adult rats. *The Journal of Comparative Neurology* **347**, 150-160 (1994).

7 Farrant, M., Feldmeyer, D., Takahashi, T. & Cull-Candy, S. G. NMDA-receptor channel diversity in the developing cerebellum. *Nature* **368**, 335-339 (1994).

8 Takahashi, T. *et al.* Functional correlation of NMDA receptor epsilon subunits expression with the properties of single-channel and synaptic currents in the developing cerebellum. *The Journal of Neuroscience* **16**, 4376-4382 (1996).

9 Teichert, R. W. *et al.* Functional profiling of neurons through cellular neuropharmacology. *Proceedings of the National Academy of Sciences* **109**, 1388-1395 (2012).

10 Teichert, R. W. *et al.* Characterization of two neuronal subclasses through constellation pharmacology. *Proceedings of the National Academy of Sciences* **109**, 12758-12763 (2012).

11 Raghuraman, S. *et al.* Defining modulatory inputs into CNS neuronal subclasses by functional pharmacological profiling. *Proceedings of the National Academy of Sciences* **111**, 6449-6454 (2014).

12 Gray, E. G. The granule cells, mossy synapses and Purkinje spine synapses of the cerebellum: light and electron microscope observations. *Journal of Anatomy* **95**, 345 (1961).

13 Sotelo, C. Viewing the brain through the master hand of Ramon y Cajal. *Nature reviews. Neuroscience* **4**, 71-77 (2003).

14 Gowd, K. H. *et al.* Conantokins derived from the Asprella clade impart conRl-B, an N-methyl d-aspartate receptor antagonist with a unique selectivity profile for NR2B subunits. *Biochemistry* **51**, 4685-4692 (2012).

15 Cathala, L., Misra, C. & Cull-Candy, S. Developmental profile of the changing properties of NMDA receptors at cerebellar mossy fiber–granule cell synapses. *The Journal of Neuroscience* **20**, 5899-5905 (2000).

16 Lim, C. R., Fukakusa, A. & Matsubara, K. Gene expression profiling of mouse postnatal cerebellar development using cDNA microarrays. *Gene* **333**, 3-13 (2004).

17 Blesch, A. & Tuszynski, M. H. Cellular GDNF delivery promotes growth of motor and dorsal column sensory axons after partial and complete spinal cord transections and induces remyelination. *Journal of Comparative Neurology* **467**, 403-417 (2003).

18 Paveliev, M., Airaksinen, M. S. & Saarma, M. GDNF family ligands activate multiple events during axonal growth in mature sensory neurons. *Molecular and Cellular Neurosciences* **25**, 453-459 (2004).

19 Williams, D. A., Fogarty, K. E., Tsien, R. Y. & Fay, F. S. Calcium gradients in single smooth muscle cells revealed by the digital imaging microscope using Fura-2. *Nature* **318**, 558-561 (1985).

20 Hille, B. *Ion channels of excitable membranes.* (Sinauer Associates, 2001).

21 Grienberger, C. & Konnerth, A. Imaging calcium in neurons. *Neuron* **73**, 862-885 (2012).

22 Teichert, R. W., Memon, T., Aman, J. W. & Olivera, B. M. Using constellation pharmacology to define comprehensively a somatosensory neuronal subclass. *Proceedings of the National Academy of Sciences* **111**, 2319-2324 (2014).

23 Cull-Candy, S. G. & Usowicz, M. M. Multiple-conductance channels activated by excitatory amino acids in cerebellar neurons. *Nature* **325**, 525-528 (1987).

24 Howe, J. R., Cull-Candy, S. G. & Colquhoun, D. Currents through single glutamate receptor channels in outside-out patches from rat cerebellar granule cells. *The Journal of Physiology* **432**, 143-202 (1991).

25 Traynelis, S. F. & Cull-Candy, S. G. Pharmacological properties and H+ sensitivity of excitatory amino acid receptor channels in rat cerebellar granule neurones. *The Journal of Physiology* **433**, 727-763 (1991).

26 Pearce, I. A., Cambray-Deakin, M. A. & Burgoyne, R. D. Glutamate acting on NMDA receptors stimulates neurite outgrowth from cerebellar granule cells. *Federation of European Biochemical Sciences Letters* **223**, 143-147 (1987).

27 Wisden, W. & Seeburg, P. H. A complex mosaic of high-affinity kainate receptors in rat brain. *The Journal of Neuroscience* **13**, 3582-3598 (1993).

28 Rumbaugh, G. & Vicini, S. Distinct synaptic and extrasynaptic NMDA receptors in developing cerebellar granule neurons. *The Journal of Neuroscience* **19**, 10603-10610 (1999).

29 Savidge, J. R., Bleakman, D. & Bristow, D. R. Identification of kainate receptor-mediated intracellular calcium increases in cultured rat cerebellar granule cells. *Journal of Neurochemistry* **69**, 1763-1766 (2002).

30 Donevan, S. D. & McCabe, R. T. Conantokin G is an NR2B-selective competitive antagonist of N-methyl-D-aspartate receptors. *Molecular Pharmacology* **58**, 614-623 (2000).

31 Wittekindt, B. *et al.* Point mutations identify the glutamate binding pocket of the N-methyl-D-aspartate receptor as major site of Conantokin-G inhibition. *Neuropharmacology* **41**, 753-761 (2001).

32 Brickley, S. G., Misra, C., Mok, M. H. S., Mishina, M. & Cull-Candy, S. G. NR2B and NR2D subunits coassemble in cerebellar Golgi cells to form a distinct NMDA receptor subtype restricted to extrasynaptic sites. *Journal of Neuroscience* **23**, 4958-4966 (2003).

33 Misra, C., Brickley, S. G., Farrant, M. & Cull-Candy, S. G. Identification of subunits contributing to synaptic and extrasynaptic NMDA receptors in Golgi cells of the rat cerebellum. *The Journal of Physiology* **524**, 147-162 (2000).

34 Blandl, T., Zajicek, J. & Prorok, M. Sequence requirements for the N-Methyl-D-aspartate receptor antagonist activity of conantokin-R. *Journal of Biological Chemistry* **276**, 7391-7396 (2001).

35 Mosley, C. A. *et al.* Quinazolin-4-one derivatives: a novel class of noncompetitive NR2C/D subunit-selective N-methyl-D-aspartate receptor antagonists. *Journal of Medicinal Chemistry* **53**, 5476-5490 (2010).

CHAPTER 6

CONANTOKINS, CONSTELLATION PHARMACOLOGY, AND THE FUTURE

Perspectives on this dissertation

Structural studies on conantokins

Chapter 2 described the discovery and characterization of conantokins from *Conus bocki*. The conantokins discovered were found to have highest affinities for NR2D NMDAR subtypes and the nuclear magnetic resonance (NMR) structure of con*Bk*-B was determined. The most important results were the discovery of an ultra-short 9-residue conantokin, the finding that conantokins can have preference for NR2D NMDAR subtypes, and the identification of residues 5, 6, and 8 as determinants of selectivity.

Chapter 3 described NMR structure determination for con*Rl*-B from *Conus rolani*. Con*RL*-B is the most NR2B-selective conantokin yet discovered and structure determination revealed a helix-kink-helix motif that is distinctive among known conantokin structures. In con*RL*-B, a hydroxyproline residue at position 10 caused the kinked conformation. Interestingly, this conformation does not have strong influence on NR2B selectivity; it has been shown that mutating this residue does have small effects on toxin potency and selectivity[1]. Nonetheless, the structure of con*RL*-B was striking, and with structural comparisons provided insights into mechanisms of conantokin selectivity.

Comparison of the con*Bk*-B and con*Rl*-B structures, together with mutational analysis presented here and elsewhere, indicate that NMDAR selectivity in conantokin peptides is determined by the combination of amino-acid residues near the amino-terminus. For conantokin peptides, the assemblage of residues at positions 5, 6, 8, and 10 govern selectivity. Of these residues, no single residue can confer selectivity by itself. Rather, the combination of residues, and the context in which these are found, determines subtype selectivity in conantokin peptides.

The conclusions from Chapters 2 and 3 have important implications for the future of conantokin and NMDAR research. Firstly, the discovery of the NR2D-preferring conantokins from *Conus bocki* suggests that other conantokins with selectivity for NMDAR subtypes beyond NR2B exist and are likely to be found with continued searching. Future investigations into different species of *Conus* will likely result in discovery of novel conantokins with selectivity for additional NMDAR subtypes Secondly, the structure-activity relationships seen for con*Bk*-B and con*Rl-B* indicate that the first 10 residues of conantokins should be a focus for development of increasingly selective conantokins. I anticipate that systematic mutational scanning near the amino terminus in conantokins will provide new insights into the combinations of amino acids that lead to subtype selectivity. Thirdly, the discovery of a 9-residue conantokin and the importance of residues near the amino terminus imply that short conantokin analogs should be more thoroughly investigated. Shorter conantokins may be easier to work with and may be more translatable into medicine. Ideally, the findings in Chapters 2 and 3 will guide discovery and development of novel conantokins with selectivity for all NMDAR subtypes. Subsequently, a panel of conantokin peptides with selectivity for all NMDAR subtypes can become tools that will be utilized to examine NMDAR subtypes and their physiological roles in the mammalian nervous system.

Biochemical analysis of NMDAR LBDs

Chapter 4 described the cloning, expression, purification, and biochemical analysis of NMDAR ligand binding domains (LBDs). The primary findings were that soluble NMDAR LBD proteins could be heterologously expressed in bacteria and purified for NR1, NR2A, NR2B, and NR2D subtypes, that the LBD proteins were active in binding known ligands, and that conantokin peptides did not show strong interactions with the LBD domains.

Although results from conantokin binding assays were negative, insights into the mechanism of conantokin-NMDAR interaction can still be drawn. One explanation for lack of interaction between con*R*-B and the LBD derived from NR2 subunits is that an additional NMDAR domain is required for conantokin interaction (e.g., the ATD or the NR1 subunit). This hypothesis has led the Horvath lab to create NMDAR ATD-LBD constructs and systems that co-express the NR1 subunit-derived protein together with the NR2 subunit proteins. However, it is also possible that conantokin binding requires a complete NMDAR tetramer, or that conantokins have more complex associations with both NMDARs and neuronal membranes. Additionally, proteolysis and chromatography experiments described in this dissertation would have only revealed a tightly bound conantokin-NMDAR complex. Therefore, the negative results described in Chapter 4 do no rule out the possibility that a weak conantokin-LBD interaction indeed exists. If this is the case, crosslinking studies could be used to examine such weak conantokin-LBD association and map the binding interface.

Although there are many techniques that can be used to investigate conantokin-NMDAR interactions, the most direct approach would be through collaboration with the Furukawa group, who recently published the crystal structure of the NMDAR $NR1_2$-$NR2B_2$ tetramer[2]. In theory, going from the tetrameric NMDAR crystal structure to cocrystal

structure bound to conantokin should not be exceedingly difficult. Potentially, conantokin peptides could be soaked into crystals obtained from a repeat of published protocols. If a soaking approach is unsuccessful, additional crystal trials could be pursued. A cocrystal structure of the NMDAR tetramer in complex with conantokin would be extremely rich in information. Assuming the structure was high resolution, it would reveal mechanisms of NMDAR inhibition, elucidate the conantokin-binding site, show which NMDAR domains and subunits are influenced, and divulge specific contacts that govern subtype selectivity in conantokins. Such discoveries would rapidly advance development of conantokin peptides with selectivity for each of the NMDAR subtypes.

Defining NMDAR composition in live neurons with conantokins

Chapter 5 employed the NR2B selective con*R*-B to examine NMDAR receptor subtypes in individual neurons of developing mouse cerebellum. These investigations revealed that all NMDA responsive cerebellar neurons expressed the NR2B NMDAR subtype at postnatal day 7 (P7) and that a population of cells expressing a different NMDAR subtype had developed by postnatal day 14 (P14). The discovery of functional NR2B NMDAR subtypes at postnatal day 7 (P7) is consistent with previous work that has shown NR2B mRNA at this developmental stage using *in situ* hybridization[3,4]. Therefore, the results indicate that dissociated neurons functionally express the same ion-channels as those inferred from detection of mRNA *in vivo*. Previous studies have also shown that expression of NR2C in the cerebellum is very low at birth, but increases into adulthood to become the predominant NMDAR subtype[3-6]. When taken in the context provided by these studies, the observation that con*R*-B insensitive neurons were found at P14 suggests that a population of NR2C-expressing neurons begins to form in the developing mouse cerebellum. To further explore this hypothesis, additional NMDAR pharmacology should be applied with

calcium imaging to confirm or rule out the presence of the NR2C NMDAR subtypes in cerebellar neurons of older mice. To extend the findings, the mechanism by which NR2C becomes dominant could be explored. It is unknown whether NR2C is expressed in the same, or different, cells than those expressing NR2B, and this is a question that could be answered with the techniques described in this dissertation.

One of my questions was whether inhibition of NMDAR response in cerebellar neurons by conantokins was similar to conantokin inhibition of heterologously expressed NMDARs in *Xenopus* oocytes. Consequently, dose-inhibition curves for con*R*/-B on cerebellar neurons were examined and compared to previously published results that used oocytes. The IC_{50} values for con*R*/-B inhibition of NMDA response at P7 was found to range from 0.2 to 2.8 μM. Con*R*/-B has an IC_{50} of 0.1 μM on $NR1_2$-$NR2B_2$ diheteromers and an IC_{50} > 100 μM for other diheteromeric combinations expressed in *Xenopus* oocytes[1]. Therefore, it appears that in cerebellar neurons, all cells express some type of NR2B containing NMDAR. However, the range of sensitivities may suggest that different combinations of NMDAR subtypes may be present in these neurons. Under the assumption that con*R*/-B can inhibit triheteromeric receptors that contain the NR2B subunit, the spectrum of observed IC_{50} values hint that P7 cerebellar neurons may contain triheteromeric receptors with just one NR2B subunit.

Because previous studies have revealed the presence of triheteromeric $NR1_2$-NR2A-NR2B and $NR1_2$-NR2B-NR2D receptors[7-9], it could be the case that the developing cerebellum may contain $NR1_2$-NR2B-NR2C triheteromers. For young mice in my experiments, some cells were observed that had residual NMDA response at the highest con*R*/-B concentrations tested. The residual calcium signal could be mediated by triheteromeric NMDAR subtypes, or it could be that cells express additional NMDAR

subtypes that do not contain the NR2B. Overall, it appears that within an individual cell there is probably functional expression of multiple NMDAR complexes that differ in subunit composition. Whether these differences are manifested through triheteromeric receptors or through co-expression of multiple diheteromeric receptors will need to be more thoroughly investigated.

In cerebellar neurons observed with calcium imaging, multiple NMDAR variants probably coexist. Based on *in situ* hybridizations, these could include $NR1_2$-$NR2B_2$, $NR1_2$-$NR2C_2$, $NR1_2$-$NR2B_1$-$NR2C_1$, and possibly receptors containing NR2A subunits. Opportunely, the emerging availability of selective conantokin peptides paired with constellation pharmacology, electrophysiology, and other techniques, is creating a situation where researchers will be poised to decipher NMDAR subunit combinations in living neurons. These findings will extend the ability of future neurobiologists to examine the physiological role of NMDARs.

Developing conantokins as tools for science and medicine

The importance of developing a toolkit of highly selective NMDAR inhibitors cannot be overstated. This dissertation has delineated structural themes for conantokins, provided mechanistic insights explaining conantokin selectivity, revealed that conantokins require more than the LBD of NMDARs for high affinity binding, and illustrated the utility of conantokins for examining NMDAR subtypes in live neurons. Cumulatively, these results will contribute to developing a needed toolkit for investigating NMDAR subtypes in the nervous system. Furthermore, the selectivity of conantokins as NMDAR inhibitors makes them potential drug leads. Various NMDAR inhibitors with lower selectivity have gone through clinical trials for the treatment of stroke, brain injury, Huntington's disease, epilepsy, seizure, and Alzheimer's disease, and many have failed due to disruption of normal NMDAR

activity[10-13]. Consequently, the key to medical applications may rest on the availability of truly selective conantokins or conantokins derivatives. Highly selective conantokins, such as con*R*-B, may prove to be practical and therapeutic for treatment of neuropathologies because high selectivity means unintended targets will be avoided, thus reducing the risk of unwanted side effects.

Perspectives on exploring *Conus* venoms

Conantokins are one of many conotoxins found in *Conus* venom, and the techniques used to discover interesting conantokins can be applied to all conotoxin families. For instance, Chapter 2 illustrated the use of molecular phylogeny to identify conantokin peptides from *Conus bocki* with desired properties (e.g., NR2D potency). Molecular phylogeny as a guide for exploration of *Conus* venoms expedited the discovery of useful compounds and has proven its worth by providing conotoxins of particular interest[14-16]. With more than 500 species of cone snails, more than 10,000 venomous snails, and numerous toxins within each species, there are too many toxins for a comprehensive examination. However, with the current state of conotoxin research, the use of molecular phylogeny to predict which *Conus* species will have peptides of specific function should lead to many scientific breakthroughs. Furthermore, the rates of discovering conotoxins with usefulness in science and medicine are anticipated to increase in the forthcoming decades as the ability to predict where useful conotoxins will be discovered improves.

Perspectives on constellation pharmacology

Neuronal profiling with calcium imaging

Although calcium-imaging techniques have been used for decades to observe increases in intracellular calcium concentrations of neurons[17-20], improvements in calcium

sensitive dyes and optical techniques are leading to new frontiers in neuroscience. Recently, constellation pharmacology provided the first demonstration that large and diverse populations of neurons could be analyzed simultaneously and the results could be used to define ion-channel composition in individual neurons[21-23]. Chapter 5 offered an extension of these techniques by examining a new brain region, by using *ProcConstPharm* (Kevin Chase, University of Utah) for rapid and unbiased analysis of large data sets, and by exhibiting the first use of conantokins for examining NMDAR subtypes in live neurons.

In the future, neuronal profiling experiments similar to those presented in Chapter 5 should be performed on other regions of the brain (e.g., cortex, thalamus, brainstem, frontal lobes, etc). Potentially, a map of the neuronal composition for the whole brain could be developed, which would have far-reaching influences in neuroscience and medicine. For example, mRNA expression patterns for NMDA receptor subtypes are well defined in various regions of the mammalian brain, but far less is known about function expression of the assembled receptors or about the subunit composition of functional NMDARs in different brain regions throughout development[3-5,24-27]. Constellation pharmacology paired with conantokin peptides presents the best opportunity to define NMDAR subunit composition in neurons from many brain regions during the course of development, which will ultimately provide insight into the physiological role played by NMDARs in brain development, normal brain function, and neurological disorders.

Potential for technical improvements

The scientific impact of constellation pharmacology could be broadened with technical improvements. For example, it would be ideal to connect phenotypes observed for dissociated cells to neurons found in intact brains. In parallel with this goal, two techniques are currently being pursued that exploit cell-specific gene expression: 1) The use of

immunohistochemistry to label neurons expressing a specific protein and 2) the use of genetic mouse models with cell-specific expression of fluorescent proteins. Successful integration of these methods will strengthen conclusions drawn from constellation pharmacology and allow hypothesis to be tested using less intrusive methods.

In addition to imaging individual dissociated neurons, imaging connected networks of neurons slice (while retaining single cell resolution) would be beneficial. Examination of neural networks with constellation pharmacology would allow additional questions to be answered. For example, NMDA receptors have significant influence on synaptic plasticity and activation of NMDARs generally strengthens synaptic connections[28-30]. Yet, it is unclear whether these changes are dependent on NMDAR subtypes and it is unclear what mechanisms drive synaptic gain. Imaging connected networks, combined with the use of selective conantokin peptides, would allow examination of synaptic plasticity in real time and facilitate determination of NMDAR subtype dependency, if present.

There are, however, challenges associated with calcium imaging of neurons within a slice. Of note, high background levels present for slices loaded with fluorescent dye would need to be overcome. Maybe this challenge could be circumnavigated by injecting dye directly into cells through glass microelectrodes. Under these conditions, background fluorescence can be removed from closely spaced neuronal milieus and individual neurons can be observed in a more natural setting. Ultimately, imaging neural networks would extend the reach of constellation pharmacology by facilitating experiments that observe the emergent properties of natural neural networks.

Screening Conus venoms with calcium imaging

Constellation pharmacology also provides a new platform for high-content screening of animal venoms for neuro-active compounds. As ion-channel compositions of individual

neurons are defined, those neuronal phenotypes become readout for screening assays. Specifically, neurons expressing a precise ion channel subtype can be used to screen for compounds that influence that exact channel. Also, as more neuronal phenotypes are defined, screening methods will continually improve, which in turn will lead to discovery of additional tools that aide with defining neuronal phenotypes. This, in essence, is a positive feedback loop with the rate of discovering novel toxins positively linked to the rate of categorizing neurons. At some critical point, both processes should accelerate significantly, and once that point is achieved the challenge of screening thousands of agents on *Conus* venoms will cease to be daunting.

In order to illustrate the applicability of constellation pharmacology for screening, experiments are currently being performed to screen for conantokin peptides that inhibit NMDA responses from cerebellar neurons. Based on what we currently know of NMDA receptor composition in mouse cerebellum, at least three possibilities exist for the results of these screens. 1) Discovery of an NR2B-selective conantokin, 2) discovery of novel NR2C-selective conantokins, or 3) discovery of conantokins that may be selective for triheteromeric $NR1_2$-NR2B-NR2C NMDARs. The latter two possibilities present the most exciting potential outcomes for two reasons: no NR2C selective conantokins have been discovered date, and it is unknown whether conantokins can specifically target triheteromeric receptors.

Looking forward, as additional regions of the brain are characterized with constellation pharmacology and conantokin peptides, it is likely we will encounter cells that express NMDAR combinations that have not yet been appreciated. As the NMDARs in these cells are characterized, these cells can be used to screen for conantokins with unique NMDAR selectivity. Even if agents with high NMDAR selectivity are not found in *Conus* venoms, these techniques can be extended to screen any animal venom or natural product

source (e.g., spider venoms, wasp venoms, sea anemones). Furthermore, similar approaches can be used to identify ligands for many of the non-NMDAR ion channels found in mammalian neurons. Thus, it is an exciting time for neurobiologists who incorporate calcium imaging and constellation pharmacology techniques.

Perspectives on the future of neuroscience

This dissertation has presented scientific results spanning many orders of magnitude. From the atomic details of conantokin peptides to the use of conantokin peptides in understanding NMDARs of mammalian neurons, the ideas presented here begin to connect the molecular level with the cellular level of the nervous system. To inclusively understand nervous system function, future scientists will need to combine ideas taken from the many levels at which nervous systems can be studied. Studying atoms, proteins, protein complexes, organelles, cells, synapses, and neuronal networks has value, yet singular studies limit the ability to develop comprehensive models of nervous system function. Combining results from various disciplines and levels of study may one day unveil how nonsentient physical objects organize to create sentient networks via molecular and cellular interactions. Clearly, *Conus* venoms harbor tools that can be used to bridge many levels of nervous system organization, and I am optimistic that conotoxins will contribute significantly to our scientific understanding of the molecules, cells, and networks that make us human.

References

1 Gowd, K. H. *et al.* Conantokins derived from the Asprella clade impart conRl-B, an N-methyl d-aspartate receptor antagonist with a unique selectivity profile for NR2B subunits. *Biochemistry* **51**, 4685-4692 (2012).

2 Karakas, E. & Furukawa, H. Crystal structure of a heterotetrameric NMDA receptor ion channel. *Science* **344**, 992-997 (2014).

3 Watanabe, M., Inoue, Y., Sakimura, K. & Mishina, M. Developmental changes in distribution of NMDA receptor channel subunit mRNAs. *Neuroreport* **3**, 1138-1140 (1992).

4 Watanabe, M., Mishina, M. & Inoue, Y. Distinct spatiotemporal expressions of five NMDA receptor channel subunit mRNAs in the cerebellum. *Journal of Comparative Neurology* **343**, 513-519 (1994).

5 Akazawa, C., Shigemoto, R., Bessho, Y., Nakanishi, S. & Mizuno, N. Differential expression of five N-methyl-D-aspartate receptor subunit mRNAs in the cerebellum of developing and adult rats. *The Journal of Comparative Neurology* **347**, 150-160 (1994).

6 Farrant, M., Feldmeyer, D., Takahashi, T. & Cull-Candy, S. G. NMDA-receptor channel diversity in the developing cerebellum. *Nature* **368**, 335-339 (1994).

7 Brickley, S. G., Misra, C., Mok, M. H. S., Mishina, M. & Cull-Candy, S. G. NR2B and NR2D subunits coassemble in cerebellar Golgi cells to form a distinct NMDA receptor subtype restricted to extrasynaptic sites. *Journal of Neuroscience* **23**, 4958-4966 (2003).

8 Jones, S. & Gibb, A. J. Functional NR2B- and NR2D-containing NMDA receptor channels in rat substantia nigra dopaminergic neurones. *The Journal of Physiology* **569**, 209-221 (2005).

9 Rauner, C. & Köhr, G. Triheteromeric NR1/NR2A/NR2B receptors constitute the major N-methyl-D-aspartate receptor population in adult hippocampal synapses. *Journal of Biological Chemistry* **286**, 7558-7566 (2011).

10 Ikonomidou, C. & Turski, L. Why did NMDA receptor antagonists fail clinical trials for stroke and traumatic brain injury? *Lancet Neurology* **1**, 383-386 (2002).

11 Lipton, S. A. Failures and successes of NMDA receptor antagonists: molecular basis for the use of open-channel blockers like memantine in the treatment of acute and chronic neurologic insults. *NeuroRX* **1**, 101-110 (2004).

12 Hoyte, L., Barber, P., Buchan, A. & Hill, M. The rise and fall of NMDA antagonists for ischemic stroke. *Current Molecular Medicine* **4**, 131-136 (2004).

13 Kalia, L. V., Kalia, S. K. & Salter, M. W. NMDA receptors in clinical neurology: excitatory times ahead. *The Lancet Neurology* **7**, 742-755 (2008).

14 Bulaj, G. Integrating the discovery pipeline for novel compounds targeting ion channels. *Current Opinion in Chemical Biology* **12**, 441-447 (2008).

15 Olivera, B. M. & Teichert, R. W. Diversity of the neurotoxic *Conus* peptides: a model for concerted pharmacological discovery. *Molecular Interventions* **7**, 251-260 (2007).

16 Olivera, B. M. *Conus* peptides: biodiversity-based discovery and exogenomics. *Journal of Biological Chemistry* **281**, 31173-31177 (2006).

17 Grienberger, C. & Konnerth, A. Imaging calcium in neurons. *Neuron* **73**, 862-885 (2012).

18 Sugimori, M. & Llinás, R. R. Real-time imaging of calcium influx in mammalian cerebellar Purkinje cells in vitro. *Proceedings of the National Academy of Sciences* **87**, 5084-5088 (1990).

19 Williams, D. A., Fogarty, K. E., Tsien, R. Y. & Fay, F. S. Calcium gradients in single smooth muscle cells revealed by the digital imaging microscope using Fura-2. *Nature* **318**, 558-561 (1985).

20 Haack, J. A., Parks, T. N. & Olivera, B. M. Conantokin-G antagonism of the NMDA receptor subtype expressed in cultured cerebellar granule cells. *Neuroscience Letters* **163**, 63-66 (1993).

21 Teichert, R. W., Memon, T., Aman, J. W. & Olivera, B. M. Using constellation pharmacology to define comprehensively a somatosensory neuronal subclass. *Proceedings of the National Academy of Sciences* **111**, 2319-2324 (2014).

22 Teichert, R. W. *et al.* Characterization of two neuronal subclasses through constellation pharmacology. *Proceedings of the National Academy of Sciences* **109**, 12758-12763 (2012).

23 Raghuraman, S. *et al.* Defining modulatory inputs into CNS neuronal subclasses by functional pharmacological profiling. *Proceedings of the National Academy of Sciences* **111**, 6449-6454 (2014).

24 Monyer, H., Burnashev, N., Laurie, D. J., Sakmann, B. & Seeburg, P. H. Developmental and regional expression in the rat brain and functional properties of four NMDA receptors. *Neuron* **12**, 529-540 (1994).

25 Petralia, R. S., Wang, Y. X. & Wenthold, R. J. The NMDA receptor subunits NR2A and NR2B show histological and ultrastructural localization patterns similar to those of NR1. *The Journal of Neuroscience* **14**, 6102-6120 (1994).

26 Sheng, M., Cummings, J., Roldan, L. A., Jan, Y. N. & Jan, L. Y. Changing subunit composition of heteromeric NMDA receptors during development of rat cortex. *Nature* **368**, 144-147 (1994).

27 Watanabe, M., Mishina, M. & Inoue, Y. Distinct distributions of five NMDA receptor channel subunit mRNAs in the brainstem. *Journal of Comparative Neurology* **343**, 520-531 (1994).

28 Malenka, R. C. & Nicoll, R. A. NMDA-receptor-dependent synaptic plasticity: multiple forms and mechanisms. *Trends in Neurosciences* **16**, 521-527 (1993).

29 Rossi, B. & Collin, T. Presynaptic NMDA receptors act as local high-gain glutamate detector in developing cerebellar molecular layer interneurons. *Journal of Neurochemistry* **126**, 47-57 (2013).

30 Turecek, J. *et al.* NMDA receptor activation strengthens weak electrical coupling in mammalian brain. *Neuron* **81**, 1375-1388 (2014).